Development of Novel Form-Stable Composite Phase Change Materials and Integration in Building for Thermal Regulation

By

Md Jaynul Abden

A thesis submitted in total fulfilment of the requirements for the degree of

Doctor of Philosophy

Centre for Infrastructure Engineering

Western Sydney University, Australia

March, 2021

Abstract

The integration of phase change materials (PCMs) into building components has attracted increasing interest in stabilising indoor temperatures by enhancing the thermal energy storage (TES) capacity and decreasing temperature swings, which lead to an improvement in buildings' thermal comfort and energy efficiency. Gypsum board, with the advantages of low cost and ease of placement, has wide applications for ceiling or wall covering. Thus, PCMs have great potential to be incorporated into gypsum board to improve the energy performance of buildings. However, the application of PCMs has been remarkably restrained by their poor shape stability during the phase change process. Accordingly, a challenge to practical application is that the PCM leak from the building materials. Moreover, due to its low thermal conductivity, the low heat transfer rate of normal PCM also acts as a block upon the wide utilisation of its enormous TES capacity benefits. As yet, very little research has been conducted to study the performance and benefits of using PCMs in real houses, especially in combination with thermal insulation.

This study aims to overcome the above issues by containing PCM in porous diatomite material to develop form-stable composite PCM (FSPCM) and study the influence of using FSPCM in maximising the TES capacity of gypsum board for improving the thermal performance of houses. Test results showed that the produced FSPCM with 48.7 wt.% of diatomite enhanced the thermal conductivity of PCM by 63.7% and eliminated the leakage issue above the PCM melting point. Experimental studies were conducted to develop an energy storage gypsum board by incorporating 40 wt.% of FSPCM in the board. The physical, mechanical, and thermal properties of the FSPCM board were then studied, and the thermal and energy performance of the FSPCM board for use in buildings was assessed by experimental and numerical studies. The experimental test performed on small chambers in real environment conditions demonstrated that the use of FSPCM board in ceilings is economically feasible with cooling load savings of 16.2% and a payback period of 1.7 years.

An experimental study and a numerical investigation were conducted to investigate the feasibility of using the FSPCM board as a retrofitting solution to a model house in Sydney, Australia. FSPCM board with a melting temperature of 26 °C was installed in different locations, including the (i) walls, (ii) ceiling, and (iii) both walls and ceiling of the model house. The experimental results showed a reduction of up to 5.8 °C in the peak indoor air temperature and a shift of 71 min for the peak load to the off-peak period when the FSPCM board was used to retrofit the walls and ceiling. A simulation model was developed using EnergyPlus and validated by experimental test data. A parametric analysis was conducted to study the effect of the PCM's melting temperature, board thickness, and natural ventilation on the thermal performance of the house.

Furthermore, the effectiveness of the combined use of FSPCM board and thermal insulation in improving the energy efficiency of residential houses was investigated. Simulations were conducted to find out the optimised PCM melting temperature and FSPCM board thickness coupled with thermal insulation in three Australian cities (Darwin, Alice Springs, and Sydney). It was found that the combined use of FSPCM board with thermal insulation in building envelopes has great potential to improve the energy efficiency of houses while reducing/avoiding overheating. Depending on climate conditions, the optimum combination of FSPCM board and thermal insulation resulted in energy-related life cycle savings of AU$39.7-167.0/$m^2$ and an increase of 3.5-4.3 stars energy rating of the studied house. This also shows that the combined use of FSPCM board and thermal insulation in the life cycle can generate an annual carbon credit potential of AU$4.4-9.7 /$m^2$ and the payback periods are 2.2-7.5 years for the renovation, depending on climate conditions. Finally, the design of the studied residential house in the Sydney climatic conditions was further optimised. The energy efficiency of the optimised house was then investigated, which further confirmed the benefits of the combined use of FSPCM board and thermal insulation.

Declaration

I, Md Jaynul Abden, hereby declare that this thesis titled “Development of Novel Form-Stable Composite Phase Change Materials and Integration in Building for Thermal Regulation” is my work and has not been submitted, in whole or in part, in respect of any academic award. No material, to the best of my knowledge, was previously published in any form by another person except where due reference is made in the text of the thesis.

Md Jaynul Abden

March 2021

List of Publications

Published Journal Papers

1. Md Jaynul Abden, Zhong Tao, Zhu Pan, Laurel George, Richard Wuhrer, Inclusion of methyl stearate/diatomite composite in gypsum board ceiling for building energy conservation, Applied Energy 259 (2020) Article ID 114113.

Journal papers under preparation

1. Md Jaynul Abden , Zhong Tao, Mohammad A. Alim, Zhu Pan , Ali Hellany, Richard Wuhrer, Experimental and numerical study of thermal management for form-stable PCM enhanced board used in building envelopes,
2. Md Jaynul Abden, Zhong Tao, Zhu Pan, Laurel George, Richard Wuhrer, Combined use of phase change material and thermal insulation to improve energy efficiency of residential buildings,

Acknowledgement

It is an immense pleasure to finally submit my PhD work. I am grateful to Almighty Allah for helping me and guiding me to travel this exhausting journey.

I would like to express my sincere gratitude and appreciation to my supervisor, Professor Zhong Tao for providing invaluable supervision throughout my way to the completion of this research work. This thesis would not have been possible without his invaluable guidance and research support. I am very grateful to him for keeping me on track towards this fatiguing journey. It has been a pleasure working with him on this project and I look forward to future collaborations together.

I would like to express my sincere thanks and deepest gratitude to my supervisors Dr. Zhu Pan, Dr. Richard Wuhrer, and Dr. Md Kamrul Hassan for their constant encouragement and motivation, throughout my study. I would like to express deep thanks to Professor Bijan Samali, Director, Centre for Infrastructure Engineering (CIE) for all support during the years. I would like to express my appreciation to all my colleagues, academic and administrative staff of CIE. I would like to acknowledge the technical staffs of the Advanced Materials Characterization (AMCF) and Structural Research and Testing Laboratory for their technical support and help in conducting the experiments. Special thanks go to Laurel George for her continuous support during the experiments.

Finally, I would like to express my gratitude to my family, parents, wife and daughter for their unconditional support, patience and love.

Table of Contents

List of Figures

List of Tables

Abbreviations

PCM	Phase change material
TES	Thermal energy storage
FSPCM	Form-stable composite PCM
DTS	Dynamic thermal simulations
SHS	Sensible heat storage
LHS	Latent heat storage
THS	Thermochemical heat storages
MD	Molecular dynamics
SSPCM	Shape stabilised PCM
LDPE	Low-density polyethylene styrene
HDPE	high-density polyethylene
SBS	Styrene-butadiene-styrene
PP	Polypropylene
LA	Lauric acid
BES	Building energy simulation
DOE	Department of Energy
EMS	Energy management system
ConFD	Conduction finite-difference
SEM	Scanning Electron Microscopy
FTIR	Fourier Transform Infrared Spectroscopy
XRD	X-ray Diffraction
DSC	Differential Scanning Calorimeter
TGA	Thermo-Gravimetric Analysis
EDS	Energy dispersive X-ray spectroscopy
SSA	Specific surface area
DTG	Derivative of the curve
TPS	Transient plane source
DFT	Density functional theory
CSH	Calcium sulphate hemihydrate

CHTC	Convection heat transfer coefficient
ACH	Air changes per hour
FSF	Energy saving fraction
LCCA	Life-cycle cost analysis
PWF	Present worth factor
ERS	Energy-related savings
EPS	Expanded polystyrene
FV	Fluctuation variance
PRMSE	Percentage of root-mean-square error
NV	Natural ventilation
RMY	Representative Meteorological Years
EC	Economic cost
ESC	Energy-saving cost
TEC	Total energy consumption
PP	Payback period
ITD	Intensity of thermal discomfort
LCS	Life cycle saving
SC	Shading coefficient
VT	Visible transmittance
SHGC	Solar heat gain coefficient

Nomenclature

Symbol	Description
ΔQ	Latent heat storage [J/kg]
ΔH_r	Heat of reaction [kj/mol]
T	Temperature [°C or K]
T_i	Temperature computed at time t_i [°C or K]
T_f	Temperature computed at time t_f [°C or K]
Q	Sensible heat stored [J/kg.K]
m	Mass [kg]
c_p	Specific heat capacity [J/kg.K]
ρ	Density [kg/m^3]
V	Volume [m^3]
ΔH_F	Latent heat [J/kg]
T_m	Melting temperature [°C or K]
T_s	Solidifying temperature [°C or K]
a_m	Melt fusion [J/g]
ΔH_m	Melting latent heat [J/kg]
ΔH_s	Solidifying latent heat [J/kg]
B	Mass fraction [%]
F_c	Crystallisation fraction [%]
ΔT	Degree of supercooling [°C]
q_{conv}	Convective heat flux [W/m^2]
h_{natural}	Convection heat transfer coefficient [W/m^2·K]
U_i	Heat transfer coefficient [W/m^2·K]
A_i	Area of the i^{th} element [m^2]
Q_{Ref}	Energy consumptions of the reference chamber [kWh]
Q_{FSPCM}	Energy consumptions of the FSPCM chamber [kWh]
I	Interest rate [%]
Φ	Inflation rate [%]
N	Life-time [year]

C_{Ref}	Annual cooling costs of the reference chamber [$]
C_{FSPCM}	Annual cooling costs of the FSPCM chamber [$]
C_{e}	Cost of electricity [$]
τ	Factor
t_p	Indoor peak temperature [°C]
t_0	Indoor minimum temperature [°C]
H	Enthalpy [J / kg]
K	Thermal conductivity [W/m·K]
Δt	Time step
Δx	Finite difference layer thickness
C_i	Initial cost [$/m^3]
χ	Material volume [m^3]
C_{E}	Energy cost [$]
C_{T}	Total cost [$]
P	Period over which the integration is performed
$T_{\mathrm{op}}(\tau)$	Indoor operative temperature [°C]
T_{over}	Upper limit of comfort temperature [°C]
t_{b}	FSPCM board thickness [mm]
t_{EPS}	EPS insulation thickness [mm]
E_{savings}	Energy savings [%]
CO_2	Carbon dioxide
ϕ_{CO_2}	CO_2 savings [kg/m^2]
R	Resistance [m^2.K/W]
T_{set}	Set point temperature [°C]

CHAPTER 1

Introduction

1.1. General

This first chapter presents the background and motivation relevant to this research and identifies latent heat thermal energy storage (TES) potential value using phase change material (PCM). An overview is given of the research aim and objectives, and finally a short summary of the thesis structure is also presented.

1.2. Research background

With an ever-expanding global economy and growing population, the rise in energy consumption derived from non-renewable resources has led to a significant environmental crisis. Nowadays, refined fossil fuels (i.e., petroleum, natural gas, and coal) are an overriding energy source contributing to intensive environmental pollution and global warming. Buildings today account for ~40% of the world's energy use and related CO_2 emissions, making it crucial to decrease energy use in houses to reach national energy efficiency performance and environmental hurdles [1, 2]. The major area of energy use in buildings is space conditioning — heating and cooling demands in developed countries account for more than 50% [3]. In Australia, electricity contributes 45% of total residential energy and is responsible for 83% of CO_2 emissions because of the dominant high greenhouse intensity coal-fired electricity production [4]. The solar heat gain from outdoor environments is one of the foremost issues that impact the energy used for heating and cooling. This energy results from outdoor ambient heat flow into indoor spaces through the building envelope – the boundary between the conditioned interior of the building and the outdoors – which directly increases buildings' overall energy consumption. Building envelope with improved thermal performance plays a predominant role in limiting outdoor heat from entering the building, so that the indoor temperature can be kept as close as possible to a comfortable temperature. Hence, improving the thermal performance of building

envelopes can potentially save energy in the building sector [5, 6]. To ensure large scale energy conservation and simultaneously to use renewable energy in an optimum method, the development of integrated, smart technologies for building envelopes is needed.

In the past, many efforts have been made to develop different technologies to improve the energy performance of houses by cutting energy demand for both heating and cooling [7]. Using insulation materials is the most common way to improve energy efficiency. Insulation materials with high thermal resistance can reduce heat gain or loss through the envelope, such as ceiling and walls. It is reported that if a home is insulated based on the Australian Standard AS 2627 [8], heat loss through the ceiling and walls can be reduced by 30-40% and 20-30%, respectively [9]. However, the use of conventional insulation, such as expanded polystyrene (EPS) or mineral wools, in low-energy buildings is not always the most cost-effective solution to achieve the best energy performance [10]. This is because a highly insulated and air-tight envelope may lead to overheating in summer, which increases cooling energy demand and thus induces extra costs for occupants in passively designed houses [11]. To cope with this issue, TES is a useful technique for integrating building envelopes to improve buildings' energy efficiency [6, 12]. The potential of TES implementation in construction is to recycle excess energy as a peak load shifting approach or minimize the energy gap between demand and supply. This, in turn, also decreases the environmental problems related to energy consumption.

Among the various techniques studied, dynamic thermal masses such as phase change material (PCM) can be seen as a promising technique to attain massive TES capacity in buildings [12]. PCM is intended to store a substantial amount of thermal energy in the form of latent heat at a fixed temperature point during their phase change process [13]. The major advantage of using PCM is substantially boosting TES capacity without adding much to a building’s mass. This is due to the intrinsic properties of PCM, such as high volumetric heat capacity, low temperature variation, and small volume variation during the phase transition process [14, 15]. PCMs absorb unwanted heat in the daytime and release it back to the buildings in night. Therefore, they can decrease the frequency of indoor temperature swings and cut down related peak cooling or heating loads [16, 17]. This idea,

marked with the increase of energy efficiency in buildings utilising PCM in passive manners, has directed researchers in recent years to develop composite materials and make use of them in building envelopes [17-19].

1.3. Research motivation

The motivation of this research is to decrease the variations of the temperature inside building spaces to get comfortable living environments for the occupants. PCM use in different parts of the houses, such as walls and ceilings, has received much attention in building thermal energy management. Many researchers have tried different types of PCMs in building envelopes for this purpose [17-19]. At the same time, combining PCM with cementitious materials such as cement mortar and concrete holds great potential for their use in building envelopes [20]. However, these PCM-enhanced materials are more suitable for constructing new buildings than retrofitting existing buildings [21]. Unlike concrete and mortar, gypsum board is widely accepted as an internal finishing material in walls or ceilings for such purposes. Gypsum board-based TES systems fabricated by incorporating PCMs have documented high cost-effective energy storage and saving potential in houses.

Unfortunately, the low thermal conductivity and instability or leakage of PCM with a gypsum matrix adversely affects the developed PCM-enhanced gypsum board's mechanical and thermal performance, limiting their practical application in buildings [22]. Therefore, it is crucial to incorporate PCM into the gypsum board without the risk of leakage. The issues above are foreseen to be addressed with wrapping technology, such as encapsulation or shape stabilisation, to develop form-stable composite PCM either in a liquid or solid-state [23]. The arduous PCM encapsulation process with polymer or inorganic materials not only habitually upsurges the synthesis cost but also affects thermal instability and significantly decreases the structural strength of the construction material [15]. The ‘Achilles heel’ of encapsulated PCMs issues entail a policy change to fabricate form-stable composite PCMs (FSPCMs) by incorporating porous structure materials. Nevertheless, including a rock-solid matrix of porous insets decreases the operative volume of the PCMs for latent

heat storage and acts as a fence for the fluid current movement for natural convection. Thus, there is a limit to the quantity of porous inset which can be used for a specific application to evade PCM volume reduction and lower natural convection heat transfer performance. The use of open-pore types of highly absorbent material can confirm the small volume reduction of PCM. Several studies have also reported the thermal enhancement of PCM only inside a porous medium [24, 25]. For instance, Zhao et al. [24] reported that a porous medium improves the melting and solidification process. In another study, Lafdi et al. [25] observed that porous materials with lower porosity promote the conduction mechanism while higher porosity assists the convection mechanism. Therefore, porous supporting materials' porosity and pore size significantly influence the phase change process, thereby affecting the efficiency of such FSPCM in thermal management applications.

Among the various porous materials [26], diatomite is more favourable as a supporting material to prepare FSPCM because of its highly porous (80-90%) three-dimensional structure and unique pore size distribution of mesopores to open macropores, which significantly improve the heat transfer behaviour (heat storage/release rates) of PCMs in TES materials for thermal management applications [22]. Diatom’s skeletons are honeycomb silica structures that give useful characteristics of high surface area and the resulting ability to absorb and retain up to 2-3 times their weight in liquids. Recent studies on the enhancement of mechanical properties of the composite have focused on the use of diatomite as a filler [27-30]. Considering the issues above, this study has focused on developing FSPCMs by using diatomite as a supporting material. Moreover, experimental studies on energy efficiency improvement in houses applied with an FSPCM integrated gypsum board (FSPCM board) also help determine PCM's actual effects in places, rarely detailed in the open literature. Hence, a methodical experimental investigation is vital to overwhelm the issues discussed above to successfully use the resultant FSPCM board in houses.

Dynamic thermal simulations (DTS) would help assess the impacts of PCM and its thermo-physical properties on the thermal behaviour and compute the expected energy consumption of a house following different boundary conditions Though various criteria exist for assessing PCMs’

thermal performance in places, proper guidelines to optimise the energy efficiency performance of houses incorporated with the FSPCM board are still lacking [12, 13]. The issues mentioned above have been addressed by developing a novel FSPCM board that involves a novel FSPCM incorporated into the gypsum board. The present study uses experimental and numerical investigations on the new FSPCM and the so-called FSPCM board. Besides this, the house's existing conditions regarding its thermal behaviour and energy demand are analysed to predict the corresponding results of a parametric study by installing an FSPCM board with thermal insulation material. By simulating various scenarios of solutions using DTS, the energy efficiency of the houses will be optimised.

1.4. Research questions

The research questions are as follows:

- What is the most appropriate technique to integrate PCM into building materials such as gypsum board while preventing PCM instability and improving thermal performance?
- What is the proposed use of FSPCM-enhanced gypsum board (FSPCM board) in houses? What is the efficiency of the developed FSPCM board in improving houses' thermal performance?
- What are the benefits of using FSPCM board combined with thermal insulation to improve the energy performance of houses?
- What are different design variables and construction parameters that need to be optimised for a high energy-efficient house?

1.5. Aim and objectives

Based on the above research questions, this study aims to evaluate the feasibility of incorporating diatomite-based FSPCM into gypsum boards for employment in buildings to enhance TES capacity and promote energy efficiency. The objectives of this study are as follows:

- Develop a novel form-stable PCM composite by containing PCM in porous diatomite material and evaluating structural and thermal performances to check its suitability for TES application in buildings.
- Evaluate the feasibility of incorporating FSPCM into gypsum board and preventing PCM leakage by developing new diatomite-based FSPCM that are more stable.
- Examine the thermal-physical and mechanical performance of FSPCM integrated gypsum-based building material (FSPCM board).
- Investigate the thermal performance of a small-scale test chamber and house model prepared with FSPCM board to reduce temperature fluctuations through experimental study. Assess the energy performance of the FSPCM board in buildings by conducting a parametric study through a numerical model and then assessing their application's economic feasibility in building envelopes.
- Assess the benefits of using an FSPCM board with insulation materials to improve the energy rating of a typical standalone house in Australia through life-cycle cost analysis and optimise the energy efficiency performance by conducting parametric study.

1.6. Thesis outline

This thesis consists of eight chapters. The first two chapters are the introduction and literature review. The third chapter is devoted to the development of FSPCM and extensive experimental tests for TES applications. The fourth and fifth chapters are then devoted to experimental and numerical studies on the improvement of energy efficiency in houses applied with developed FSPCM-integrated gypsum board (FSPCM board). The sixth and seventh chapters check the potential benefits of the combined use of FSPCM board and thermal insulation in improving the energy efficiency of buildings. Finally, the conclusion and recommendations are compiled in chapter eight.

The detailed outlines of each chapter of this thesis are as follows:

Chapter 1 contains the introduction of this thesis. This chapter gives an overview of the background of the present research work, research motivation, research questions, research aim and objectives and the thesis's outline.

Chapter 2 provides a comprehensive literature review on the published works related to this research work. The TES systems, different types of PCM, encapsulation techniques, and dynamic thermal simulation models will all be discussed. Recent studies on PCM integrated building components are reviewed, highlighting their potential benefits in improving the building's thermal behaviour and energy performance. Chapter 2 also summarises the existing literature, identifying the problem and current research gaps then argues the motivation behind the present research work.

Chapter 3 is devoted to the development of a novel FSPCM by containing PCM (methyl stearate) in porous diatomite material. Material characterisation techniques including morphological analysis, chemical compatibility, thermal conductivity, thermal properties and thermal stability are carried out to check their feasibility for integration into building materials such as gypsum board. The leakage of the developed FSPCM is observed. Finally, the thermal performance (heat storage/release) of the FSPCM is evaluated.

Chapter 4 presents the thermal reliability (leakage) of gypsum board integrated with 40 wt% of FSPCM. The performance of the FSPCM-enhanced gypsum board for cooling load reduction in summer in real environmental conditions is investigated. A small-scale test chamber with an FSPCM-integrated gypsum board ceiling is prepared and modelled to study the thermal/energy performance. Through life cycle cost analysis an economic benefit of using the FSPCM-integrated gypsum board (FSPCM board) is also evaluated in this chapter.

Chapter 5 presents an experimental and numerical study of the thermal performance of the FSPCM board with PCM's melting point of 26 °C that can be used in the inner surface of the walls and ceiling in a small model house. A simulation model based on EnergyPlus is developed and verified by the experimental test results. This model is then used to conduct a parametric analysis to further study

the influence of PCM melting temperatures, FSPCM board thickness, and natural ventilation on the energy performance of the model house. To further understand the potential economic benefits of using the FSPCM board in each case an economic evaluation through life cycle cost analysis is also performed.

Chapter 6 conducts a numerical study to assess the performance of the combined use of FSPCM board and thermal insulation in improving the energy efficiency of a real residential house in Australia. Simulations are conducted to find out the optimised PCM melting temperature and FSPCM board thickness coupled with thermal insulation in three Australian cities (Darwin, Alice Springs, and Sydney). The influence of occupancy profile on house star rating is assessed. Finally, an economic and environmental feasibility analysis is also conducted in this chapter.

As an extended study of Chapter 6, comprehensive research is conducted in Chapter 7 to optimise the design of the studied residential house in Sydney's climatic conditions. The energy efficiency of the optimised house is then investigated, which further confirms the benefits of the combined use of FSPCM board and thermal insulation.

Finally, the conclusions of this research work are presented in Chapter 8 followed by future recommendations.

CHAPTER 2

Literature review

2.1. Overview

Building occupants are concerned with the heat flow through building envelopes. The indoor air temperature is highly related to the material properties of the building envelope, such as thermal resistance and heat capacity. Hence, an energy-efficient building envelope is crucial to ensure occupants' thermal comfort with a minimum system energy use for heating and cooling. In this regard, the thermal energy storage (TES) in the building's envelope is the main factor in achieving a high energy efficiency building, and PCMs could play a significant role in this field. The integration of PCMs provides large heat storage capacity, storing more thermal energy in the building's envelope and thus reducing the necessary energy production to achieve the energy balance. Thermal energy is generally stored in the building envelope by the sensible heat of the materials. Contrary to sensible heat storage, PCM enhanced building envelopes store heat in the form of latent heat, which provides a high heat capacity where more energy may be stored in the building's envelope at a narrow temperature range compared to sensible traditional materials. Therefore, the integration of PCM into construction materials is an initial step that requires to be considered.

Gypsum board is the most widely used material in building envelopes as an internal furnishing material, and hence has great potential to integrate PCM. However, it is essential to note that incorporating PCM into gypsum board should not be prejudicial to the developed composite material's durability and mechanical performance. An encapsulation technique relating to PCM retention into porous supporting materials such as diatomite, named as form stable PCM (FSPCM), can be one of the practical integration techniques of PCM into gypsum board. This is due to their intrinsic properties of stabilising the shape of PCM in the melting or cooling process and improving the heat transfer behaviour (heat storage/release rates) of PCM in TES materials. This chapter presents

a comprehensive literature review associated with PCM use for thermal energy storage enhancement in buildings.

2.2. Thermal energy storage system

The TES system includes the assembly of technologies that allow excess energy (heat/cold) to be stored and used when needed. In thermodynamics, we have learned that heat is absorbed (stored) in a material by the change of that material's internal energy, and that there are several ways to achieve this, such as thermo-chemical, sensible heat, and latent heat or any combination of these [31]. In all cases, energy is conserved in a storage system in the form of heat to be used in the future, which involves a single charge-storage-discharge cycle, as shown in Fig. 2.1.

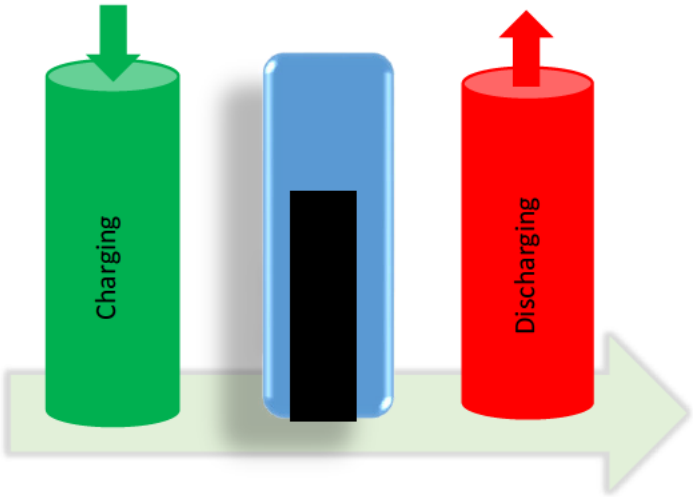

Fig. 2.1. TES complete storage cycle.

2.2.1. Thermochemical storage

Thermochemical storage is a technique for storing thermal energy by a dissociation reaction followed by a reverse reaction to recover the energy from the system, as shown in Fig. 2.2. Heat stored in the process relies on a number of factors such as (i) the amount of storage compound, (ii) the decomposition (endothermic) process and (iii) the degree of conversion [31, 32]. Although thermochemical storage systems have the advantages of higher energy density, being able to operate over a wide temperature range, and long storage life compared to other forms of TES, they are currently economically infeasible.

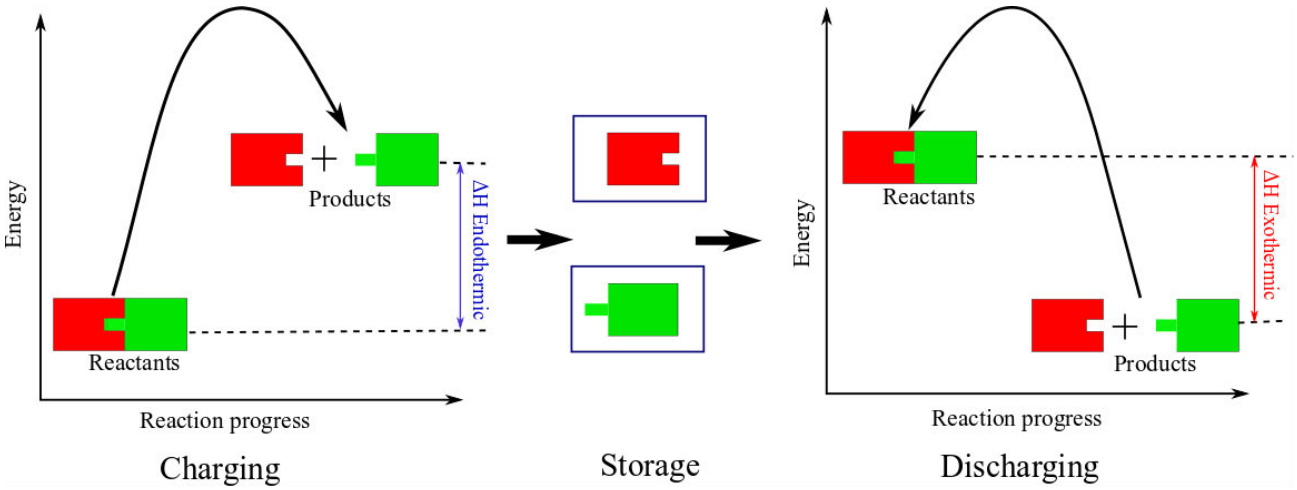

Fig. 2.2. Heat storage process with chemical reaction.

As mentioned earlier, the dissociation and reverse reactions are crucial for thermochemical energy storage, and some conditions must therefore be fulfilled in order for a reaction to be useful for heat storage [33].

- The heat of the chemical reaction should be relatively high, which does not generally occur when all the reaction components are liquid or solid.
- The products of the reaction must be storable.
- The reaction must be reversible.

As for latent heat storage, the heat stored by chemical reactions can be expressed in Eq. 2.1:

$$\Delta Q = \Delta H_r \tag{2.1}$$

where ΔH_r is the heat of reaction associated to the chemical system.

2.2.2. Sensible heat storage

Heat absorbed by raising the temperature of a material is stored as sensible heat. The sensible heat storage (SHS) technique uses specific heat and disparity in temperature through charging and discharging steps without phase change. The stored heat energy is directly proportional to the temperature, as shown in Fig. 2.3.

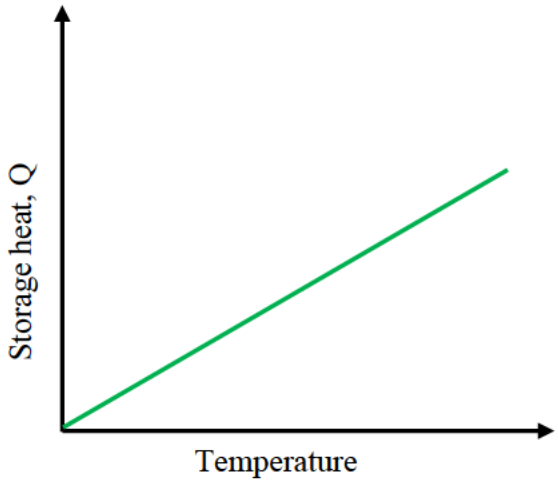

Fig. 2.3. Energy as a function of temperature, sensible heat.

The sensible heat Q stored or released by a material because of change in temperature from T_i (initial) to T_f(final) can be written as Eq. 2.2:

$$Q = \int_{T_i}^{T_f} m.C_p\, dT = V \int_{T_i}^{T_f} \rho.C_p\, dT \tag{2.2}$$

where m, C_p, ρ and V are mass, specific heat, density, and volume of the medium, respectively. As can be seen, the capacity of SHS relies on the temperature difference in specific heat, and mass of the substance. The specific heat and density of a substance determine the stored heat in a given volume. There are some other factors, however, which influence the performance of the sensible heat storage process such as (i) thermal conductivity, (ii) thermal diffusivity, (iii) temperature of operation, (iv) vapour pressure, and (v) storage material and container compatibility. Table 2.1 shows a number of common heat storage solid-liquid materials used in SHS systems [31, 33].

Table 2.1 Typical solid-liquid materials used in SHS systems.

Medium	Fluid type	Temperature (°C)	Density (kg/m^3)	Specific heat (J/kg.K)	Thermal conductivity (W/mK)
Rock	–	20	2560	879	
Brick	–	20	1600	840	0.5–0.7
Concrete	–	20	1900–2300	880	0.9–2.0
Sand	–	–	1602	830	
Water	–	0–100	1000	4190	
Glass	–	–	2710	837	
Steel	–	–	7840	465	
Castable ceramics	–	–	3500	866	1.4

2.2.3. Latent heat storage

In the LHS system, the material stores heat energy during phase change. There are several ways that the phase change can take place; however, the expected transition is the solid-liquid transition. The solid-solid transition is the second choice while liquid-gas transition is impractical. The key feature of the LHS system is that the temperature of the material remains constant even though heat is absorbed or released by the phase transition process as shown in Fig. 2.4.

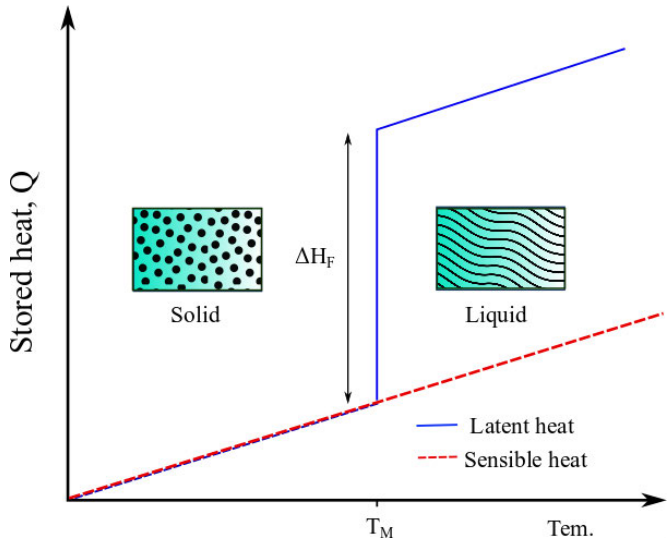

Fig. 2.4. Energy as a function of temperature, ΔH_F is the latent heat, T_M is the melting temperature.

The solid-solid transition provides greater flexibility in design and has less stringent container requirements [31]. However, the capacity of latent heat storage in this type of phase change is much lower compared to that of solid-liquid transitions, which restricts its widespread use. Moreover, solid-liquid transitions are an economically appealing choice for use in TES systems. The heat energy (Q) stored in LHS systems is given by the Eq. 2.3 [34]:

$$Q = \int_{T_i}^{T_m} m.C_p dT + ma_m \Delta H_m + \int_{T_m}^{T_f} m.C_p dT \quad (2.3)$$

where a_m is the melt fraction and ΔH_m is the melting latent heat, in J/kg. Since the melting occurs at a constant temperature, the stored thermal energy can only be determined from enthalpy difference between the solid and liquid states. The heat storage capacity mainly depends on the material's latent heat and specific heat, and thus, it is desirable to have higher values for these parameters [35].

Materials used in LHS are known as PCM. The following three components are crucial for any LHS system [36].

- The melting temperature of PCM should be in the expected range,
- A compatible container/encapsulation for the PCM, and
- An applicable heat exchange surface.

However, for building applications, there are some additional criteria, listed in Table 2.2, that have to be fulfilled by the PCM related to the thermophysical, kinetic, chemical, economic and ecological properties.

Table 2.2 Preferable properties of PCM [37, 38].

Thermal properties	-	Phase transition temperature within the range suitable to the application
	-	High latent heat per unit volume
	-	High specific heat to supply extra energy in the form of sensible heat
	-	High thermal conductivity to increase the charge/discharge rates
Physical properties	-	Small volume changes on phase change and low vapor pressure at operating temperature to minimise the containment difficulty
	-	Favourable phase equilibrium
	-	High density and congruent melting
Kinetic properties	-	High nucleation rate (to prevent supercooling)
	-	High crystal growth rate (to fulfill the needs of heat recovery from the storage system)
Chemical properties	-	Chemical stability
	-	Exclusively reversible melting/freezing process
	-	No chemical degradation after a number of melt/freeze cycles
	-	Chemically compatible with building materials
	-	Corrosion resistant to construction materials
	-	Nontoxic, nonflammable and nonexplosive to assure safety
Economic and usability	-	Large-scale availabilities with low cost
	-	Good overall environmental parameters and non-polluting during service life
	-	Easily recyclable

2.2.4. Comparison of TES technologies

A comparison among three available TES systems involving different technical aspects is presented in Table 2.3. As can be seen, latent TES is applicable for greater temperature range compared to its counterparts. It is also evident that despite having the highest heat storage density, thermochemical TES has not yet been tested for practical implementation. In addition, safety concerns for thermochemical TES are much higher compared to latent TES though the two have a similar efficiency output.

Table 2.3 Comparison between sensible, latent and thermochemical system [39].

Category	Sensible TES	Latent TES	Thermochemical TES
Temperature (˚C)	0–1200	–100–1000	180–2500
Power (kW)	1–10000	1–1000	10–1000
Efficiency (%)	50–90	75–90	75–100
Capacity (kWh/t)	10–50	50–150	120–250
Storage density (kWh/m^3)	50	100	500
Storage period	Limited	Limited	Unlimited
Technology status	Industrial scale	Pilot scale	Laboratory scale
Safety issues	No	Depends on materials used, but usually limited	Higher concern
Technical complexity	Low	Medium	High
Environmental impact	Negligible	Negligible	Negligible
Corrosion issue	Mild	Medium-high	High
Flexibility (regulation, partial charge/discharge etc.)	High	Medium	Low

Sensible storage is commercially available on a large scale due to its easy construction features. However, the low energy density and short-term storage limit its applicability. Latent heat storage with PCM provides a higher energy density. The application of PCMs is often limited by their low thermal conductivity and degradation over cycling. Thermochemical heat storage (THS) offers a much higher energy density and being able to store for a long period of time without degradation. THS is able to provide efficient intersessional storage without significant heat loss. However, the complex arrangement of the system has caused its application to be restricted mostly to laboratory scales. There are several issues such as uncertainty about the reliability, system lifetime, safety concerns, potential toxicity, a relatively high cost and recyclability that have to be tackled in order to make this technology more practical. LHS with PCMs is, therefore, the most promising approach

among TES technologies for real-world application considering its high energy storage density, typically 5 to 14 times when compared to SHS [40]. Higher energy storage density may lead to a significant size reduction which will ultimately lead to cost minimisation.

2.3. Phase change material

PCM is a substance which melts and freezes at certain temperatures and can absorb and release a considerable amount of thermal energy in the form of latent heat. There is no unique classification of PCMs, however, several models can be found in the available literature. One of the most general classifications, which will be considered as reference, is schematically represented in Fig. 2.5 [36].

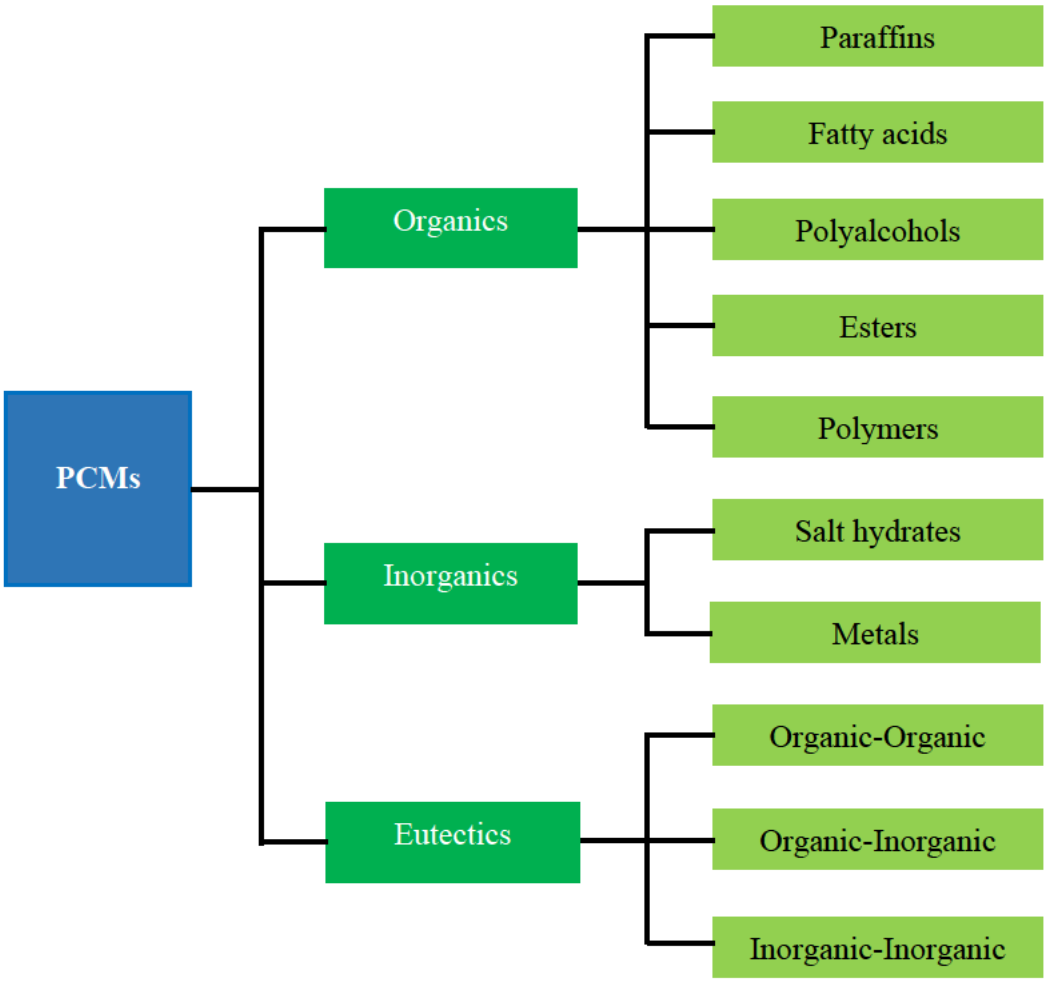

Fig. 2.5. Classification of PCMs.

The following subsections will present a general overview on properties of different classes of PCMs with a focus on the recent research progress. At the end, an evaluation of various types of these materials will be presented.

2.3.1. Organic PCM

Organic PCMs are classified into two categories: paraffin and non-paraffin. All these materials are both physically and chemically stable, and therefore the complexity associated with incorporating stabilisers or additives can be avoided. The most promising feature of organic PCM is the congruent phase transition, meaning no segregation or consequent degradation after multiple melting and freezing cycles. Other attractive features are minimal corrosiveness when coming in contact with metal and recycling potential. On the contrary, drawbacks include low thermal conductivity, greater volume expansion in the phase change process, low density, flammability, and a high cost [41, 42].

2.3.1.1. Paraffin

Among organic PCMs, a significant category for storage of solar and low-grade waste heat is those of paraffin, a mixture of mostly straight chain n-alkanes (C_nH_{2n+2}) with *n* value ranging between 20 and 40. They show a small change in volume on phase transition and have low vapor pressure in the form of melt state. Even though they are non-corrosive, non-toxic and melt congruently during phase transition, the application of paraffin is often limited by their high flammability nature (low ignition resistance) and low thermal conductivity (0.1-0.3 W/m.K). The melting point (operating temperature of a PCM) and latent heat can be increased with the chain length or creating mixtures of different hydrocarbons [31]. The availability across the board range of temperature and having high latent heat of fusion make paraffin suitable as a TES system for building applications. The lowest purity paraffin, however, may only be used as PCM in LHS systems with regard to the cost and expenses [43].

2.3.1.2. Non-paraffin

The non-paraffin organic PCMs consist of a broad range of fatty acids, esters, alcohols, and glycols which show considerably distinct properties.

(a) Fatty acids:

Fatty acids (i.e., carboxylic acids) are organic compounds with chemical formula $CH_3(CH_2)_{2n}COOH$, derived from animal or vegetable sources, which makes them biodegradable and

non-toxic. They have high latent heat close to that of paraffin's and also show good stability during repetitive cycles with little or no supercooling effect. The main disadvantage however, is the cost, being 2-2.5 times higher than that of paraffin [44]. Besides, the corrosive nature of these materials is also limiting their application to some extent [44]. Above and beyond, they are more combustible than paraffin, and therefore exposure to high temperatures, fires or oxidising agents should be avoided [42, 45]. At large, the latent heat and phase change temperature of fatty acids can be increased with increasing the size of the carbon chain. The melting temperature of fatty acids is usually ≤70 °C and they are thus employed mostly for low-grade heat storage such as buildings [46, 47]. However, their use as TES materials mostly depends on their thermophysical properties such as specific heat, density and thermal conductivity.

(b) Polyalcohols:

Polyalcohols have been introduced as storage materials at moderate temperatures (90-200°C) for a long time since they have high storage density, are non-toxic, reasonably low cost and hold non-corrosive properties [42]. Although some polyalcohol has volumetric latent energy storage capacity as much as twice that of other organic PCMs, the higher melting temperature restricts their use for building thermal storage applications. Beside this, some studies have reported a high degree of supercooling, which can seriously compromise their useful application for thermal storage [48]. Polyalcohol has various crystalline forms, each one with distinct features. This is a result of different preparation methods employed and additives used [49, 50].

(c) Esters:

Esters are formulated from acids in which hydroxyl group (–OH) is substituted by the alkoxy group (R–O) of alcohol. The fatty acid esters are manufactured by direct esterification of fatty acids separated from vegetable oils (i.e., soybean, coconut, or palm oils) and fats that are environmentally friendly. These bio-based PCMs have the potential to absorb, store, and release enormous amounts of heat with no or insignificant supercooling. They are widely available at an affordable cost, possess excellent chemical stability and their surface tension is considerably high (27−32.1 mN/m) [12]. The

melting temperature of fatty acid esters is usually lower than 60 °C, and having a high ignition resistance compared to other PCMs they are therefore mainly employed for energy saving in buildings [51]. The bio-PCMs have good stability for several years and thousands of melting-freezing cycles without any oxidation risk since they are fully hydrogenated [51, 52].

(d) Polymeric materials:

Polymeric materials are long chain molecules formed by composing many repeated subunits. They provide the opportunity for creating conspicuous physical and chemical modifications, which assist the manufacture of specific end products with 'tailor made' thermal storage properties. Among polymers, two of the most commonly used are HDPE and polyethilenglycol [42, 50].

Table 2.4 Comparison of organic, inorganic, and eutectic PCMs.

Classification	Advantages	Disadvantages
Organics	- Obtainability in a wide temperature range - Physical and chemical stability - Good thermal behaviour - Non-toxic and non-corrosive - Little or no super-cooling - No segregation - High enthalpies or latent heat - Self-nucleating properties - Adjustable transition zone	- Low thermal conductivity (~ 0.2 W/mK) - High volume change - Flammable - Volumetric heat storage capacity is low
Inorganics	- Higher energy storage density - Higher thermal conductivity (~ 0.5 W/mK) - Economically competitive - Small volume change	- Super-cooling - Phase segregation - Corrosion - Incongruent melting point
Eutectics	- Sharp melting points - High heat storage density per unit volume - No segregation during the phase transition	- Minimal data is available on their thermos-physical properties for many combinations - Few fatty eutectics have a strong aroma, and thus they are inadvisable for use as PCM

2.3.2. Inorganic PCM

Inorganic PCMs are mainly composed of salt hydrates, metals, and alloys or eutectic mixtures. They can have enthalpies per unit volume as much as two times higher than that of organic ones and cover a broader range of phase change temperatures. Other advantages are a high thermal conductivity, relatively low cost and non-flammability. These properties allow them to be used in numerous applications, expressly where corrosiveness is not a serious concern. The properties for organic, inorganic and eutectic PCMs are compared and listed in Table 2.4.

2.3.2.1. Salt hydrates

Salt hydrates are inorganic ionic compounds that absorb several water molecules to confine within their crystal lattice. The general formula of a hydrate is $A_xB_y \cdot n(H_2O)$ where n is the number of water molecules. There is no actual liquid-solid transition occurring for this type of material. When heated, salt hydrates generally transform either to their anhydrous form or shape to a hydrated salt with some water molecules as shown in Eq. (2.4) and (2.5), respectively.

Congruent dehydration:

$$A_xB_y \cdot nH_2O = A_xB_y + nH_2O \quad (2.4)$$

or semi-congruent dehydration:

$$A_xB_y \cdot nH_2O = A_xB_y \cdot mH_2O + (n\text{-}m)\ H_2O \quad (2.5)$$

The particular interest to employ salt hydrates as PCMs is due to their extraordinary latent heat of fusion, high thermal conductivity, low thermal expansion, non-toxicity, low corrosion rate and compatibility with plastics [53]. However, the behaviour of these types of PCMs during phase change is quite complicated and is affected by a wide range of factors. Salt hydrates can be categorised in three groups depending on their phase transition process:

- Congruent: if the dehydrated salt is entirely soluble in its hydration water at melting temperature.
- Incongruent: if the amount of hydration water is not sufficient to dissolve the salt crystals.

- Semi-congruent: if the liquid and solid phases are in equilibrium at different compositions due to transmutation of hydrate to a lower hydrated material through the loss of water [31].

Though a range of salt hydrates have prospective features to become effective PCMs, the incongruent or semi-congruent melting leads to segregation phenomena which results in degradation of the storage capacity. During these melting processes, the quantity of water liberated from the hydrated salt is not enough to dissolve the salt crystals, resulting in the solution becoming supersaturated and separating the solid salt. Because of the phase separation, recombination of solid salt with water is not possible in the reverse process of freezing/crystallisation. As a result, thermal effectiveness is lost in thermal cycling.

Various approaches have been considered to solve the difficulties related to incongruent melting. For example, the inclusion of a gelling material into the salt leads to creating a 3D network to inhibit sedimentation of the salt. The presence of a congealing agent raises the salt hydrate viscosity and assists in holding its molecules together [54]. Another proposed solution is the incorporation of additional water to decrease the precipitation of solids, which gives satisfactory results in terms of material stability. However, this process raises the range of melting temperatures, and as a result, the melting latent heat decreases. In addition, salt hydrates experience a great extent of supercooling, which ultimately narrows down their possible application.

2.3.2.2. Metallics

This family involves low-temperature melting metals and metal alloys. Although metallic PCMs possess high melting latent heat per unit volume, their specific heat, vapor pressure and melting latent heat per unit mass are considerably low. They comprise a broad range of melting temperatures and manifest a sharper melt transition than organic PCMs. For instance, Caesium (Cs) melts at an ambient temperature (28.65 ˚C) whereas Magnesium (Mg) melts at a very high temperature (648 ˚C). Custom metal alloys can be developed to meet the desired melting points and latent heat for particular applications. Moreover, they are the only PCMs that exhibit very high thermal conductivities, with a

magnitude of several orders when compared to other PCM materials. Aluminium (Al) shows exceptional thermal conductivity of 237 W/m.K [55] while other metals such as caesium, gallium, indium, tin, bismuth and zinc exhibits very low thermal conductivities ranging between 8 to 40 W/m.K [56]. Even though metallic PCMs previously were not considered to be useful for TES applications because of their weight disadvantages and fairly high melting temperatures, development of nanomaterials paves the way for their use in TES systems.

2.*3.3. Eutectics*

Eutectic PCM is a blend of two or more different components which form a minimum melting composition compared to its primary agents. These compositions are mainly binary and ternary mixtures of inorganic salts, salt hydrates and alkalis. The main advantage of eutectic compounds is that they invariably melt and freeze without segregation since during freezing they form a mixture of crystals. The components liquefy together in the melting process which also inhibits segregation. The primary limiting issue of these types of PCMs is their non-uniform augmentation in volume which could be damaging for the container and the internal structure. The fundamental needs for eutectic PCMs are (i) a stable solution (no segregation or degradation), (ii) no or less super-cooling and (iii) close melting and solidifying points for all compounds of the eutectic composition. Fatty acids and fatty-acid ester compositions are favourable eutectic PCMs for building applications. Their major benefits over other PCMs are superior latent heat, long-term durability and high surface tension that allows them to successfully impregnate into porous supporting mediums.

2.4. Methods of PCM integration into construction materials

PCM has been considered for the storage of thermal energy in buildings since 1980. Thermal energy storage can be achieved by implementing PCM in various building components. Once a suitable PCM has been selected for building applications, the next step is to explore how it could be integrated into the construction materials. This can be achieved by direct incorporation (immersion and direct impregnation) and indirect incorporation (encapsulation, shape-stabilisation and form-stable composite PCM) methods [26, 57].

2.4.1. Direct incorporation methods

2.4.1.1. Direct impregnation method

This is the simplest way in which liquid or solid PCM powders are directly incorporated into the building materials including cement, gypsum, mortar and concrete during construction. For effective inclusion of PCM into building materials, it should not (i) affect the paste-aggregate bond [58], (ii) interfere with the hydration process and hydration products [58], or (iii) impact on strength and durability. However, possible leakage phenomenon of PCM in direct mixing has been one of the major concerns [59] which may interfere with the hydration products and deteriorate the durability and strength of the structure. Therefore, the direct incorporation method cannot be adopted for building applications.

2.4.1.2. Immersion

In this method, building materials (plater boards, bricks and concrete slabs, etc.) are immersed into molten PCM which allows these construction materials to absorb the PCM by capillary action. Although the immersion technique can avoid some of the issues that appear in the direct incorporation method, the leakage of liquid PCM is highly likely, particularly after repeated thermal cycles [19, 20]. For example, a significant reduction in mechanical properties has been reported when PCM in powder or liquid form is directly added to the construction materials, such as concrete [60, 61]. The mechanical properties and durability of construction materials can also be affected by the interaction between the leaked PCM and cement mortars [62]. To eliminate the above discussed issues, wrapping technologies such as encapsulation or shape-stabilisation are employed to develop a form-stable composite PCM (FSPCM) either in a liquid or solid state. This technology has been studied extensively in recent years [26, 63].

2.4.2. Indirect incorporation methods

Through this method, the PCM is encapsulated prior to its inclusion in building materials. Encapsulation can be defined as a process, in which the PCM (solid particle/liquid droplets) is wrapped by a protective layer that can provide a physical barrier between the PCM and surroundings

matrix materials such as gypsum powder [64]. Therefore, the advantages to encapsulating the PCM are (i) preventing migration when it is in a liquid state and (ii) so that the PCM does not form one solid, inflexible mass as it cools. Indirect incorporation methods are classified into encapsulations, shape stabilisation, and form-stable PCM based on incorporating and supporting materials.

2.4.2.1. Encapsulation

As mentioned above, encapsulation is a process where PCM is enclosed in a capsule to form a core-shell type composite before being used in building elements. The primary reason for encapsulation is to encase the molten PCM in a shell which acts as a fence. This method not only helps in achieving thermal and mechanical stability and a good heat transfer surface [65], but also allows for its utilisation, storage, and transportation [66]. The PCM capsules consist of two parts [67]: the core (PCM) and shell (polymer or metal), as shown in Fig. 2.6 (a). The PCM capsules can be either regular or irregular shapes, having one or more cores inside the single capsule or a single core within multi-walled capsules [67, 68] as displayed in Fig. 2.6 (b). Regin et al. [69] reported that PCM capsules should (i) fulfil the requirement of thermal stability, corrosion resistance and giving mechanical integrity to the capsule when the PCM is in the liquid state, (ii) shield the PCM from unsafe interaction with the surrounding medium, (iii) have a passable surface area for efficient heat transfer, and (iv) be steady structurally while offering simplicity in handling.

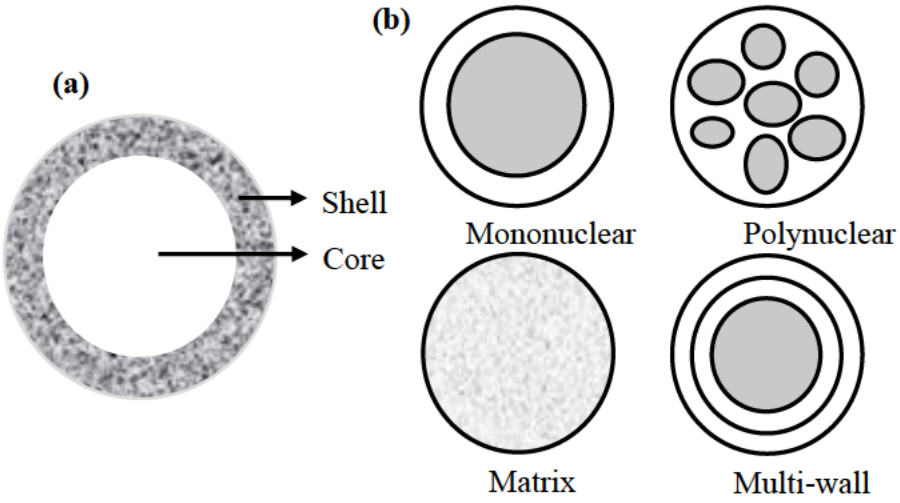

Fig. 2.6. (a) Description of capsule, (b) morphology of a capsule.

In general, there are three methods of PCM encapsulation depending on their particle size:

(a) Macro encapsulation,

(b) Micro encapsulation, and

(c) Nano encapsulation.

(a). Macro-encapsulation

Macro-encapsulation of PCM involves packing a large amount of PCM (up to several litres) in any type of container (>1 mm), those including spheres, tubes, pouches, and panels which can be integrated into construction materials which would act as heat exchangers shown in Fig. 2.7 [70, 71]. The encapsulation thickness can significantly influence the melting and freezing process of the PCM. A thick capsule may detain the PCM solidification when contrasted with a thin capsule, thereby foiling the effective heat transfer [72]. Therefore, optimum encapsulation thickness has to be determined for effective heat transfer together with thermal stability and corrosion resistance.

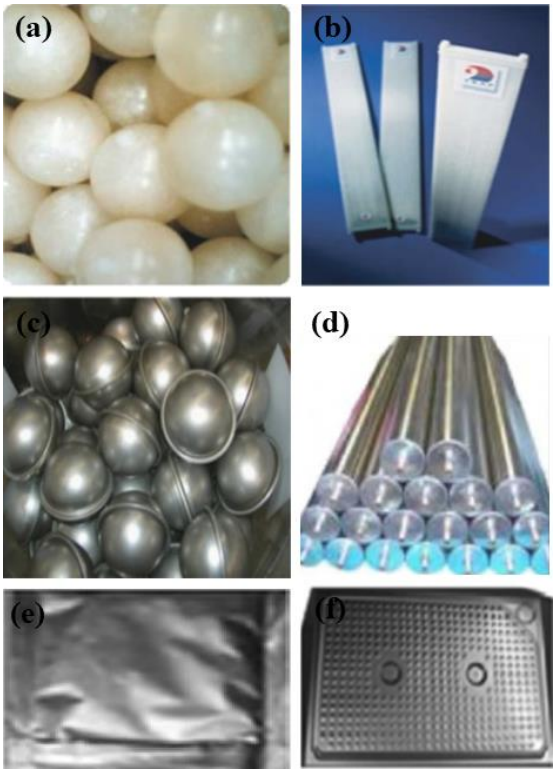

Fig. 2.7. PCM macroencapsulation, (a) polyolefin spherical capsules, (b) PCM in PVC flat panel, (c) metal ball capsules, (d) PCM tube encapsulation, (e) PCM in aluminium pouches, and (f) PCM in aluminium panels.

(b). Microencapsulation

Microencapsulation is a process in which PCM particles (solid or liquid) are enclosed or layered with a thin and solid shell of polymeric material (Fig. 2.6a) to produce a capsule size within a range between 1– 1000 µm. A PCM having phase transition temperatures ranging from -10 to 80 ˚C can be manufactured with this method [73]. Although most of the microcapsules are spherical, the fabrication method and composition of shell material mainly influence the appearance of the microcapsules. Based on the mechanism of micro-particle creation, the microencapsulation approach can be divided into three different classes: (i) chemical, (ii) physico-chemical and (iii) physico-mechanical processes [74]. Each production technique has some advantages depending on the intended characteristics of microcapsules. These comprise the microcapsule's shape and size, the thickness of the shell and their mechanical properties. The different techniques used for microencapsulation and their properties are shown in Table 2.5.

Table 2.5 The microencapsulation techniques and their advantages and disadvantages.

Methodology	Techniques	Advantages	Disadvantages
Chemical	Suspension polarisation	Reaction heat can be controlled	Limited monomers can be dissolved in water. Size ~2 to 4000 µm [75]
	Dispersion polarisation	Formation of monodisperse polymer particles in the range of micron size by a single step process	–
	Emulsion polarisation	High molecular weight polymer fast	Refine polymer from the Surfactant
	In situ polarisation	Uniform particle covering	Enormously complex process Size range 1 to 2000 µm
	Interfacial polarisation	Simple procedure and lower emphasis on the purity of monomer	The high cost of polymer monomer, time-consuming Size 2–2000 µm
Physico-chemical	Coacervation and phase separation	Allows control of the particle size and layer thickness Versatile	Agglomeration of particles Difficult to scale up
	Sol–gel encapsulation	High thermal conductive inorganic shell	Under development

	Supercritical CO_2-assisted	The low critical temperature value Cost effective process	Until now under research
Physico-mechanical	Spray-drying	Easy and low-cost commercial process Versatile	Low encapsulation efficiency and accumulation of particles
	Electrostatic encapsulation	Spherical microbeads	Only for <50 μm
	Single step method	Easy to scale-up Self-stabilisation	–

The core/shell technique is essential for the formation of microcapsules. The core holds the active material, and the shell safeguards the core. Depending on the core material and deposition process of shell material, the microcapsules are divided into four categories (Fig. 2.6b):

1. Mononuclear (core/shell): only one core covered by a continuous shell.
2. Polynuclear: several cores enclosed within a continuous shell.
3. Matrix: core materials are uniformly distributed into a continuous shell.
4. Multi-wall: a multilayered shell covers the core material.

It is important to note that particle size substantially influences the stability of PCM capsules. PCM microcapsules can easily be broken in the fluid flow process, which would increase the fluid viscosity that confine their final application. The structural stability of PCM microcapsules is needed for thermal storage. The volume shrinkage/expansion of the core material (~10%) during the thermal cycling process damages the capsule wall from the inside. The correlation between structural stability and particle size was reported by Yamagishi et al. [76], as shown in Fig. 2.8. The slurry containing PCM microcapsule particles (20 vol%) in water was circulated by a pump. The results showed that the PCM microcapsule particles within the size range of 1000–1500 μm were broken (~90%) very quickly. The damage rate was reduced by 40% when the size range was within 75–300 μm. In addition, this level of breaking was observed after 500 times more circulation cycles compared to the previous case. The microcapsules of 20–100 μm particle size was broken ~10% of the time while 5–10 μm particles were almost entirely unbroken (structurally stable) for pump circulation cycles higher

than 7000 times (Fig. 2.8). The outcomes of this study demonstrated that the structural stability of a PCM microcapsule is highly influenced by its size. Therefore, PCM nanoencapsulation is gaining interest among researchers, giving the benefits of a smaller particle size, greater heat storage aptitude, high specific surface area, and a low damage rate (around zero) during the pumping and mixing process.

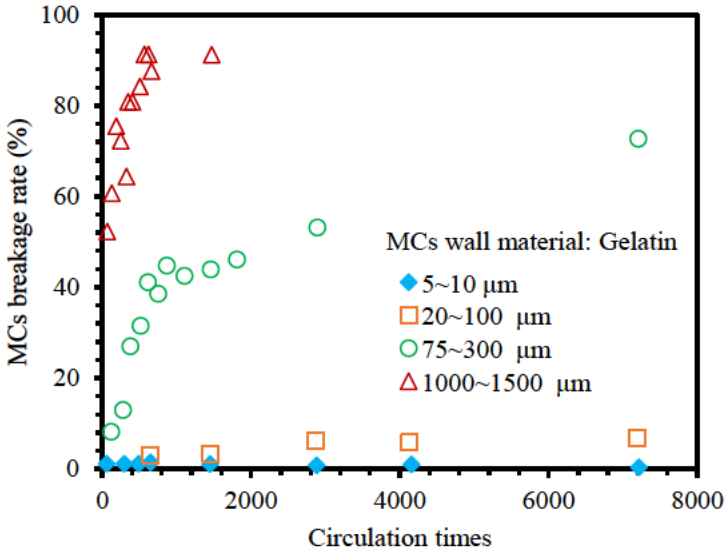

Fig. 2.8. Breakage rates of PCM microcapsules during pump circulation.

(c). Nanoencapsulation

Nanoencapsulation is a method in which microscopic PCM particles (1 nm to 1000 nm) are covered by a thin polymer layer or inorganic materials. Smaller size capsules could significantly boost the heat transfer area while keeping the mechanical properties of the composite intact. Nanoencapsulated PCM has some unique properties including the surface effect, volume effect, and macroscopic quantum tunnelling effect [68] which contribute to a steady dissemination in the thermal fluid. This confirms its effective application in thermal energy storage and transport. In recent years, molecular dynamics (MD) simulation has become an important technique for understanding the heat and mass transfer mechanisms, self-diffusion, microscopic behaviours and transport properties of encapsulated PCMs from the molecular point of view. Rao et al. [77], for example, investigated the self-diffusion coefficient of nanoencapsulated PCMs using the MD method. In their simulation they used n-octadecane (diameter 4 nm) as a core and SiO_2 as shell materials with a diameter of 5 nm to

formulate the nanoencapsulated PCM under two conditions: (i) free, and (ii) constrained shell as shown in Fig. 2.9.

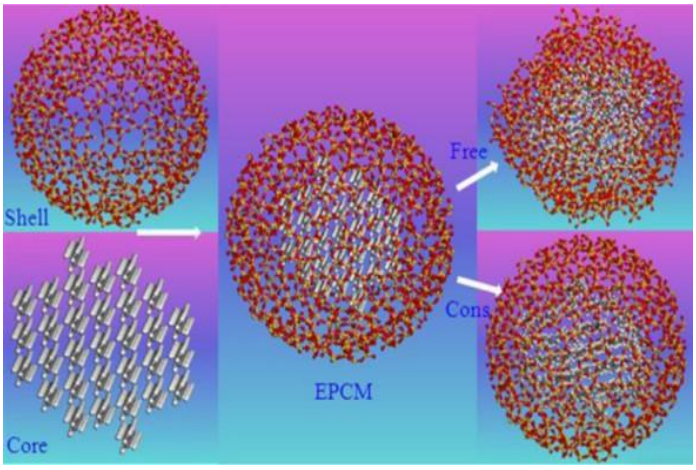

Fig. 2.9. The typical structures of encapsulated PCM.

It was revealed that the mobility and interaction of the n-octadecane molecules were restrained with the SiO_2 shell. The encapsulated PCM with restrained shell reduced the self-diffusion coefficient. The heat transfers of the whole capsule were increased by reducing the thermal interaction resistance of different capsules when the shell was free.

The most often used techniques for the formulation of PCM nanoencapsulation are interfacial polymerisation, *in situ* polymerisation, emulsion/miniemulsion polymerisation, and sol–gel. Among them, the interfacial and *in situ* polymerisation methods are simple and more reliable processes in which a polymer shell is shaped at the oil/water interface rather than within emulsion droplets. *In situ* polymerisation contains monomers in single emulsion phase while both phases of monomers exist in interfacial polymerisation. Although interfacial polymerisation has the advantage of controlling the PCM capsule size and the thickness of the polymer shell layer, only a few studies focus on this method for the synthesis of PCM capsules at nanoscale. The fabrication of nanocapsules via the *in-situ* polymerisation method has favourable morphological features and thermal properties. However, further study is required to not only make the procedure simpler, but also minimise manufacturing costs. The miniemulsion polymerisation technique is a single step, cheap, stable and eco-friendly method for the formation of nanocapsules with appropriate particle sizes by controlling the stabiliser

dosage. In this method, the principle of small nanoreactors is followed as demonstrated in Fig. 2.10. At the first step, small stable droplets, 30-500 nm, are shaped in the miniemulsification process which is polarised with keeping their originality in the second step.

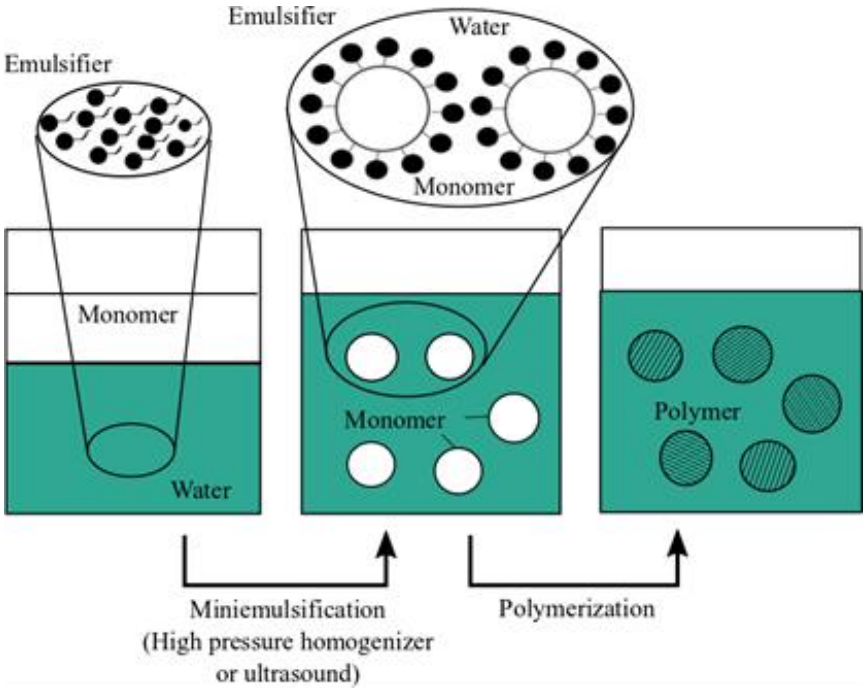

Fig. 2.10. The principle of miniemulsion polymerisation.

Several studies have reported that the most successful technique for the formulation of PCM nanocapsules with an improved thermal characteristic is the reaction of miniemulsion polymerisation [78, 79]. During the PCM nanoencapsulation process prompted by this technique, the required system higher stability and polymerisation rate can easily be met [80]. However, the additional miniemulsification operation process is time consuming, which limits the application of this technology on a commercial scale. There are some other issues with this technology such as the requirement of highly viscous organic phases and additional energy being needed for the attainment of a small droplet size and their homogenisation. Although nanocapsulated PCMs have a higher heat storage capacity, the higher degree of supercooling in the phase transition process restricts their employment in TES systems [81]. Therefore, future research may focus on how to reduce the degree of super-cooling by improving their heat transfer ability. In addition, study of fabrication of PCM nanocapsules with higher encapsulation efficiency and more homogeneous particle size distribution

can be conducted. At the same time, the manufacturing cost should be taken into consideration to determine the feasibility.

2.4.2.2. Shape-stabilised PCM

Shape stabilised PCM (SSPCM) is a composite material in which PCM and another phase of carrier matrix such as low-density polyethylene styrene (LDPE), high-density polyethylene (HDPE), styrene-butadiene-styrene (SBS), or polypropylene (PP) are mixed together at their melted states. The subsequent cooling allows the carrier matrix to solidify and encapsulate the PCM. A microscopic image of the shape-stabilised paraffin is shown in Fig. 2.11, an example in which HDPE was used as supporting material. As can be seen, the paraffin (black element) was homogenously disseminated into the netted texture of HDPE (white element), and this net-like crystal structure of HDPE is capable of stopping the seepage of molten PCM during the heat storage process [82]. The SSPCM has the advantages of (i) high apparent specific heat, (ii) good thermal reliability, (iii) suitable thermal conductivity, (iv) no need for containers and (v) the mass portion of PCM can be as high as 80%.

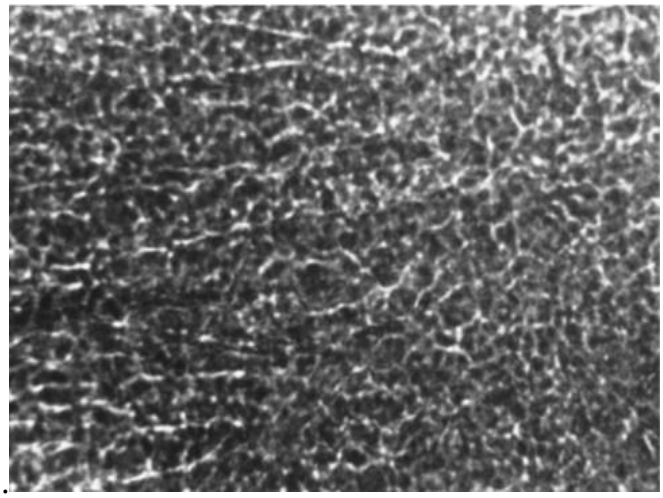

Fig. 2.11. Micrograph of shape-stabilised paraffin [82].

Many studies on thermal storage systems using SSPCM have been reported in recent years [83]. Zhang et al. [84], for instance, studied the thermal performance of SSPCM which consisted of paraffin and HDPE (Fig. 2.12), and reported that the technique simplified the TES system as it could directly encapsulate the traditional PCM without a container. In another study, Zhou et al. [85] analysed the thermal effect of SSPCM plates, used as inner facings, on the indoor air temperature of a south facing

direct gain room in Beijing, China in winter via an enthalpy model. They considered various effecting factors and the results documented that the SSPCM plates were beneficial in direct gain passive solar buildings. Although this technique can improve the thermal conductivity of PCM, the value is quite low and insufficient for any potential application in a building's thermal management system. Thus, further research is required on how the thermal conductivity can be improved. In addition, investigation on how they react in the hydration process with cement-based materials has yet to be performed.

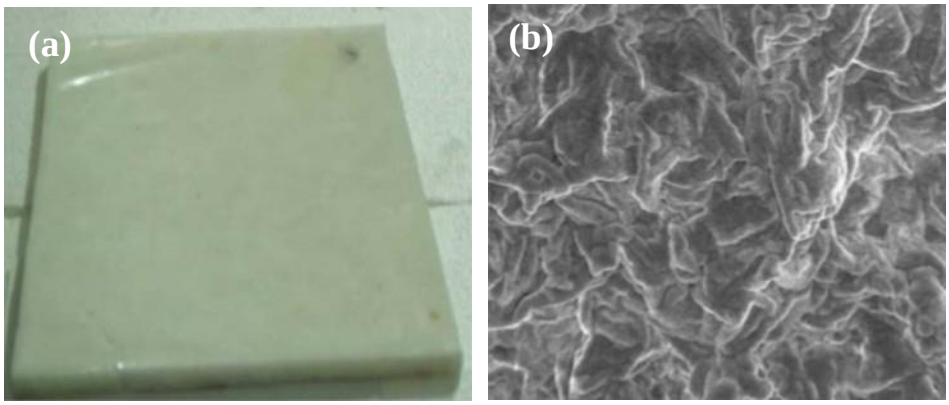

Fig. 2.12. Shape-stabilised PCM: (a) image of the PCM plate, and (b) SEM micrograph.

2.4.2.3. Form-stable composite PCM

In recent years, FSPCM has been tested for energy storage and thermal management systems. In this technique, liquid PCM is confined in porous supporting materials to form a FSPCM. In the case of FSPCM, the carrier substance does not need to be molten. The liquid PCM is retained in the pores of porous materials by surface tension and capillary action which not only stabilises the shape of the PCM but also eliminates the leakage problem during phase transition. A micrograph of form-stable lauric acid (LA) is shown in Fig. 2.13, where porous diatomite is used as supporting material. In the micrograph of porous diatomite (Fig. 2.13a), there are various gully and tunnel-like veins signifying the surface inhomogeneity and the existence of many areas which would be filled by LA (Fig. 2.13b). To improve the TES performance, it is important that the direct heat exchange between PCM and its supporting substance occurs. From this perspective, the highly porous granular phase change

composites are appealing materials since they facilitate rapid heat transfer, are non-corrosive and have a high thermal storage density.

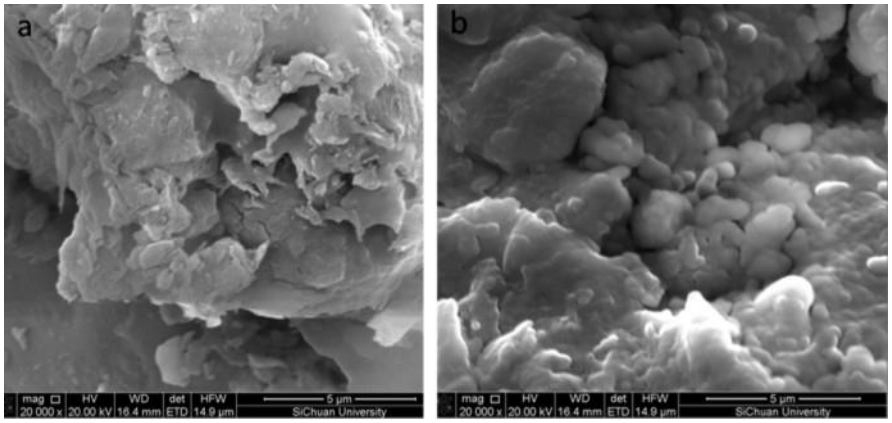

Fig. 2.13. SEM micrographs of (a) diatomite, and (b) form-stable of LA/diatomite composite PCM.

FSPCM can be fabricated by simple immersion and vacuum impregnation techniques. The PCM retaining ability of the supporting material can be enriched by a vacuum impregnation system. The FSPCM process is simple and can be adopted for large scale industrial level production. It has been reported that the thermal conductivity and pore structure of carrier substances have a substantial impact on the phase changing behaviour of the composites [86]. Porous geometry has a significant impact on the thermal conductivity of the composite. For instance, Zhao et al. [87] reported that the use of a porous medium enriches the melting and solidification process faster than pure PCMs without a porous medium. It is important to note that most available studies have focused on the formation of FSPCM by using different supporting materials including diatomite, vermiculite and expanded perlite. However, what happens when these types of substances are mixed with cementitious materials and their interaction with the hydration process has yet to be determined.

2.5. Thermal conductivity enrichment of PCM

The key concern that needs more attention is that PCMs have very low thermal conductivity which leads to inefficient heat transfer and thus, prolonged charging/discharging time [88]. Therefore, a number of approaches have been proposed [20, 35], including (i) developing FSPCM by using high conductive porous supporting material; (ii) dispersing conductive particles such as graphite, copper, aluminium, silver etc. with PCM; (iii) packing PCM in a container (lesser rings, metal fins and metal

beads); and (iv) encapsulating PCM to improve the rate of heat transfer in the LHS system. As we have discussed previously the incorporation of high thermal conductive materials with PCM enhances the heat transfer performance; however, the integration would also cause a decline in overall heat storage capacity. Thus, this technology cannot be adopted for practical application. It was also discussed in the previous section that integration of PCMs with building materials such as gypsum boards, plaster, and concrete would have insignificant influence on heat transfer [89]. The only option left is for FSPCM which has promising features to be considered as construction materials, described in subsection 2.4.2.3. It can be argued that in-depth study on thermal conductivity enhancement of FSPCM could make these materials practically feasible for building thermal management applications.

2.6. PCM in building envelopes

The building envelope is a key element in a building for controlling the interior thermal environment regardless of outdoor conditions. Therefore, an energy efficient building envelope is a major benefit which can be achieved by using PCMs. The key reason for incorporating PCM into building components is to increase their thermal mass, which leads to reduction in interior temperature variations, ensures thermal stability inside, provides a comfortable interior environment and shifts the heating/cooling peak load to an off-peak period [90, 91]. The use of PCMs in a building's structure could potentially save up to 25–30% on annual heating and cooling energy [92-94]. The outcomes of related research are extraordinary and have influenced many researchers to turn their attention to building envelope optimisation by using PCM.

The most common and suitable way of employing PCM into buildings as yet is by incorporating it with wallboards and placing them at the inner side of the of the building envelope. In this section, recent studies concerned with the integration of PCM into wallboards and gypsum plasterboard for building envelope applications are reviewed. The wallboards with PCM have the potential to store thermal energy and deliver it when needed. However, the performance of PCM-based wallboards depends on various factors such as the PCM melting temperature, the latent heat capacity per unit

area of the wall, the manufacturing technique and alignment of the wall, conditions of solar gains (direct/indirect) and ventilation rate [90, 95-102].

The thickness of the PCM-wallboard is one of the key factors that have substantial influence on its performance. An optimisation process of PCM wallboard thickness was reported by Kuznik et al. [103] considering the effect of insulation thickness, phase difference, and indoor and outdoor air temperature swing. Their results indicated that insulation thickness and outside temperature have no effect on determining the optimal thickness of PCM, however, the internal air condition does influence the results. In another study, Kuznik et al. [104] used Dupont de Nemours PCM wallboard (Fig. 2.14) for the renovation of a lightweight tertiary building located in the south of Lyon (France) to assess their thermal performance. They monitored the thermal performance of the construction for approximately a year and concluded that the PCM wallboard was more effective when the outside air temperature was close to the phase transition temperatures of the PCM.

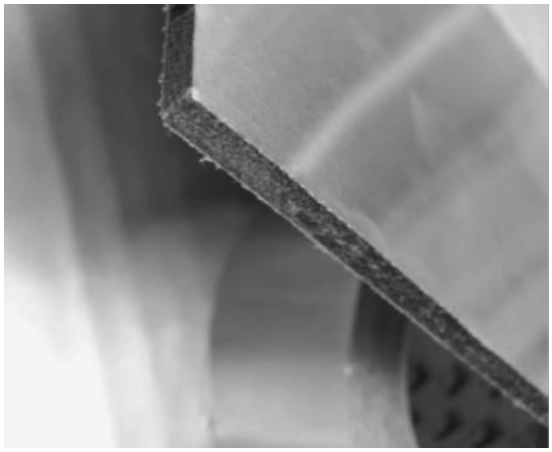

Fig. 2.14. Dupont de Nemours PCM wallboard.

Mandilaras et al. [98] introduced PCM gypsum board in a typical two-story family house and monitored the thermal response. The PCM gypsum boards were attached to all outdoor walls and inward partitions. It was observed that the decrement factor was reduced by 30–40% and the time lag increased by about 100 min. The position of PCM in a building's walls affects the phase change process, and thus, is crucial for optimal thermal performance [105].

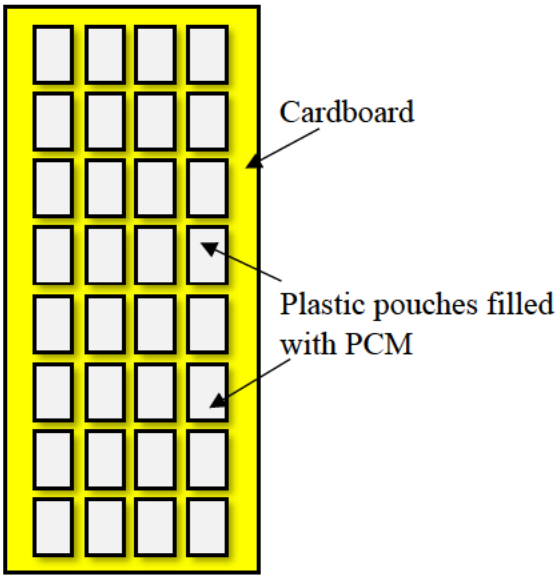

Fig. 2.15. PCM thermal shield.

Jin et al. [105] developed a PCM thermal shield prototype (Fig. 2.15) and investigated its effectiveness for three different locations within the cavity of a standard North American residential wall. As stated, the optimal location for the thermal shield was next to the interior surface of the gypsum wallboard. The peak heat flux reduction was found to be 10.7% in comparison with the traditional wall. When a PCM thermal shield was stacked between the insulation layers, it produced small impacts on the peak heat fluxes, yet almost no effect was observed when put next to the inner face of oriented strand board.

Zhou et al. [106] examined the thermal response of a non-deform laminated composite PCM gypsum board in a laboratory scale test room. They concluded that the effective temperature reduction was 5 ˚C in contrast to the typical gypsum board which resulted in only 1.8 ˚C reduction. Jeong et al. [107] put forward the concept of hybrid gypsum board by incorporating two kinds of shape-stabilised PCM. The melting temperatures of the PCMs were chosen differently in order to decrease the heating and cooling load of the building in winter and summer seasons. Singh and Bhat [108] studied the thermal performance of two layers of PCM gypsum board. PCM layers of two different melting temperatures were sandwiched into two separate gypsum boards and laminated with ply before being attached to the roof. It was found that the duel-PCM gypsum board could offer narrow indoor air temperature swings and is suitable for both hot and cold seasons.

2.7. Building energy simulation

According to the literature reviewed in the previous section, passive design using PCM is a sustainable solution for improving buildings' thermal performance. Passive PCM systems can achieve long-term energy efficiency, improve comfort quality and make substantial energy savings by stabilising indoor air temperatures. However, before employing these PCM-based innovative passive designs, their performance should be assessed by means of validated building energy simulation (BES) tools as the application of PCM needs some particular consideration to select the appropriate materials, the location and the amount of PCM [109]. Nowadays, computer-based simulation has become a conclusive, cost-effective and swift method to evaluate the effectiveness of new technologies such as thermal/energy performance of PCM on a building. Authorised BES models can facilitate alternative designs, testing and optimisation of PCM-based building materials without conducting a whole building field investigation on a real system, which is costly and time-consuming. Moreover, computer-based simulation helps researchers to make decisions and ensure long-term success. For instance, Kapetanakis et al. [110] developed thermal load predictive models of commercial buildings through the use of BES software, and there are several studies where the BES model was used to benchmark the energy performance of buildings [111]. The BES tool can be employed for evaluating the influence of different parameters or optimisation scenarios affecting the energy performance of the building. Over the past few decades, a wide variety of BES tools have been developed which are competent in facilitating dynamic energy simulation for different applications [112]. However, in the building energy field there are very limited validated whole-BES models that can simulate the influence of PCM on the energy performance of buildings. EnergyPlus [113], TRNSYS [114], and ESP-r [115] are all accepted and widely used forms of BES software that can handle PCM modelling in buildings. Table 2.6 shows the comparison of some major features and proficiencies of these building energy simulation tools.

Table 2.6 The comparison of some major features of EnergyPlus, TRNSYS and ESP-r simulation tools [112].

Features	EnergyPlus	TRNSYS	ESP-r
Interior surface convection			
• Dependent on temperature	√	√	√
• Dependent on air flow	P	E	√
• Dependent on surface heat coefficient from CFD	E		E
• User-defined coefficients (constants, equations or correlations	√	√	E
Outside surface convection algorithm			
• BLAST/TARP	√		
• DOE-2	√		
• MoWiTT	√		√
• ASHRAE simple	√		
Single zone infiltration	√	√	√
Automatic calculation of wind pressure coefficients	P		
Natural ventilation	√	O	√
Multi zone air flow	√	O	√
Displacement ventilation	√	O	√
User-configurable HVAC systems	√	√	√
Simple energy and demand charges	√	√	√
Complex energy tariffs including fixed charges, block charges, demand charges, ratchets	√	E	
Scheduled variation in all rate components	√	√	
User selectable billing dates	√	E	

√: feature or capability available and in common use; P: feature or capability partially implemented; O: optional feature or capability; E: feature or capability requires domain expertise.

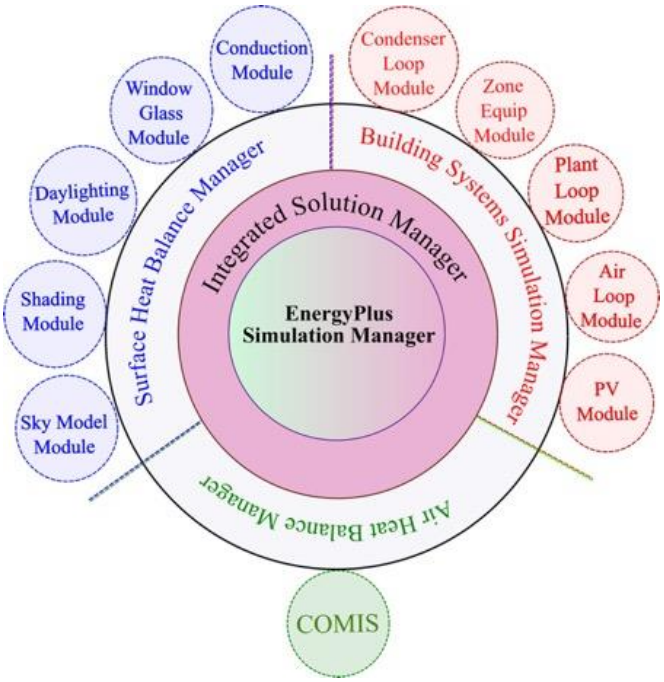

Fig. 2.16. EnergyPlus integrated simulation manager.

Comparing the tools, EnergyPlus is one of the most flexible and reliable building energy performance simulation tools. It was first realised in 1996 by the U.S. Department of Energy (DOE), building on the strength of both BLAST and DOE–2 accompanied by new capabilities. It is predominantly a simulation tool—there is no formal user interface. The structure of the EnergyPlus simulation manager is shown in Fig. 2.16.

The combined solution manager controls the surface and air heat balance units, which acts as an interface between the heat balance and the simulation module of the building systems [113]. In EnergyPlus, it is feasible to formulate original modules and/or regulate tactics and assimilate them into the program as sub-routines by an energy management system (EMS). This acts as a customised computer that can be programmed to operate each of a building's energy related schemes, for instance, ventilation, cooling, heating, internal lighting, and mechanized operations for shielding devices, actuators and windows [116]. In addition, the abilities which afford strength to this software are high-level infiltration and fenestration analysis, more realistic HVAC system controls, calculation of multizone airflow, environmental emissions and economic assessment techniques including life cycle energy and cost analysis. In the EnergyPlus tool, a PCM module is offered using an implicit conduction finite-difference (ConFD) solution algorithm that provides the opportunity to simulate based on the enthalpy-temperature curve as a material property. Recently released EnergyPlus 8.8 includes an inherent module developed by NRGSIM to simulate the PCM layer that enables the execution of thermal properties associated with hysteresis phenomena [117]. But this module can only simulate the single PCM layer in a monolayer envelope structure, and therefore in EnergyPlus version 8.9, the latest version, a custom NRGSIM module is integrated, which allows the simulation of multilayered structures that comprise a PCM layer to be implemented.

2.8. Summary and research gaps

Based on the literature review presented so far, it is clear that the TES system using PCMs has huge potential as a strategic technology to improve the energy efficiency of buildings. However, it should also be mentioned that the integration of PCM into the building materials results in an adverse

effect on their properties. This can be overcome through the selection of the proper and most suitable method of PCM incorporation. The form-stable PCM (FSPCM) showed better performance compared to the direct incorporation of PCM and other encapsulated PCM. However, what happens when FSPCMs are mixed with cementitious materials and their interaction with the hydration process has yet to be determined. Also, there is a need to conduct the thermal performance investigation of FSPCM in building envelopes. In that context, the PCM integration technique is the initial step that requires to be determined, and the first research question includes:

1. What is the appropriate technique to integrate PCM into building materials such as gypsum board while preventing PCM instability and improving thermal performance?

Among different PCM incorporation techniques discussed in section 2.4, the encapsulation regarding PCM retention into porous supporting material known as FSPCM is one of the most suitable forms that involves inclusion into building elements. However, in most of the reviewed studies, the stability of FSPCM in gypsum board has not been extensively studied. In the present study, the FSPCM based on diatomite has been extensively characterised for TES applications. The characterisations of morphological analysis, chemical compatibility, thermal stability (leakage), thermal conductivity and thermal performance (heat storage/release) of the developed FSPCM will be carried out in Chapter 3.

No research work has been found in the literature on using diatomite based FSPCM in gypsum boards. Hence, the thermal stability (leakage) of developed FSPCM in gypsum board needs to be examined for evaluating their thermal performance. The related experimental study for these characterisations is detailed in Chapter 4. Stated

It is well known that the incorporation of PCM into construction elements increases the TES capacity of buildings, helping to increase the house's energy performance and indoor thermal comfort. However, the performance study of FSPCM incorporated gypsum board in building applications was lacking. Hence, it is crucial to evaluate the thermal performance of the proposed FSPCM enhanced

gypsum board utilisation in houses, and therefore, the second research question is expressed as follows:

2. What is the proposed use of FSPCM-enhanced gypsum board (FSPCM board) in houses? What is the efficiency of the developed FSPCM board in improving houses' thermal performance?

The proposed application of FSPCM board in the building's envelope is as an interior finishing material. However, the FSPCM board needs to be examined for its thermo-physical and mechanical properties. The thermal performance studies are needed to evaluate the efficiency of FSPCM board on improving indoor thermal comfort while reducing temperature variations. This research work studies the thermal performance improvement of FSPCM board in buildings through an experimental test and numerical analyses and optimises thermal/energy performance by conducting parametric research presented in Chapter 5.

Although the improvement of indoor thermal comfort by integrating FSPCM board into building envelopes has been proved, the adoption of this technology in practice is still very limited. Of course, the combined use of PCM with thermal insulation provides a high energy efficiency building. However, the benefits of adopting this idea have not been fully justified. Therefore, the third research question is expressed as follows:

3. What are the benefits of using FSPCM board combined with thermal insulation to improve the energy efficiency performance of houses?

The combined use of FSPCM board and thermal insulation could be more effective in improving the energy efficiency of houses. Hence, energy performance studies of the building envelope composed of FSPCM board with thermal insulation should be evaluated in terms of improving the star rating of those houses. The evaluation was conducted through numerical simulation for three different Australian cities (Darwin, Alice Springs, and Sydney). To evaluate the benefits of their combined use, an economic and environmental analysis are presented in Chapter 6.

Lastly, even if various parameters are applied for optimising the energy efficiency of FSPCM board with insulation materials in houses, there is still a lack of proper design optimisation for high energy efficiency houses. Hence, the fourth research question of the present work are as follows:

4. What different design variables and construction parameters need to be optimised for a high energy efficiency building?

Previous research has mainly focused on evaluating the benefits of using FSPCM board together with thermal insulation in improving house energy efficiency for different outdoor conditions and suggested their optimum design parameter of thickness value through a life cycle cost analysis. The current study optimises some design parameters that are related to heat transfer processes in buildings. Finally, an optimised design model relating to life cycle cost and the set of design variables of a PCM-enhanced residential house in Sydney is presented in Chapter 7.

CHAPTER 3

Development of diatomite-based form-stable phase change material

3.1. Introduction

As discussed in the literature review, phase change material (PCM) has a great prospect of use in construction as an energy conservation material. PCM is a kind of material that can absorb and release a large amount of thermal energy in the form of latent heat by undergoing a phase change process [22]. PCM has a high energy storage density and shows isothermal features when energy is stored. Hence, PCM can be used in buildings to control the indoor temperature, enhance the thermal comfort and reduce the energy consumption for heating and cooling. However, pure PCM limits its usage in many thermal energy storage applications due to the low thermal conductivity and leakage issues.

To overcome these issues, form-stable composite PCM (FSPCM), made by encapsulating PCM into porous supporting materials, has been investigated recently [22, 118]. The FSPCM can keep its solid shape even when the PCM is transformed to a liquid state. In particular, the porous supporting material can make liquid PCM convenient to control and prevent PCM from adverse collisions with the surrounding materials. It should be noted that FSPCM has been developed by using various porous carrier materials, such as diatomite, perlite, expanded graphite, gelator, vermiculite and kaolinite, etc. [26]. Among them, diatomite has been widely used as a carrier material to prepare FSPCM due to its unique properties, including large specific area, highly porous three-dimensional structure (up to 80-90% porosity), low bulk density (128-320 kg/m^3), fairly low price, superior thermal stability and chemical inertness even at elevated temperatures [22]. There is no study on using methyl stearate (MeSA) as a PCM and diatomite as the supporting material to prepare the form-stable PCM for thermal energy storage applications. As a bio-based PCM, MeSA that is manufactured with reduced heat energy exhaustion than fatty acid is a favourable candidate for TES applications at mild

temperatures due to its moderate solid-liquid phase change temperature of 36.8 ºC and high heat storage capacity of 217.7 J/g.

In this chapter, the development of a novel form-stable PCM is reported by incorporating methyl stearate into porous diatomite material. The morphologies and chemical compatibility of the developed FSPCM are investigated by Scanning Electron Microscopy (SEM), Fourier Transform Infrared Spectroscopy (FT-IR) and X-ray Diffraction (XRD). The thermal properties, thermal stability, thermal conductivity and thermal reliability (leakage) of the FSPCM are determined by Differential Scanning Calorimeter (DSC), Thermo-Gravimetric Analysis (TGA), Hot-disc thermal constants analyser and thermal cycling test. Finally, the thermal performance (heat storage/release) of the FSPCM is evaluated.

3.2. Materials and methods

3.2.1. Materials

A commercial grade methyl stearate (purity: ≥96%) with a melting temperature of 36.8 ºC was obtained from Sigma Aldrich Pty. Ltd., Australia. The diatomite sample used was sourced from Mount Sylvia Pty. Ltd., Queensland, Australia.

3.2.2. Development of diatomite-based form-stable PCM

The form-stable PCM was prepared by using a direct impregnation method in which methyl stearate was used as a PCM and diatomite as the porous supporting material. A double-jacketed glass reactor as shown in Fig. 3.1 was used to prepare the FSPCM. The fabrication process of the form-stable PCM is as follows. At first, the diatomite particles were thermally treated at 120 ºC for 24 h to remove all moisture in the pores. Then, a certain amount of diatomite was placed in the glass vessel and the vessel temperature was maintained at 60 °C by using the oil bath. The solid PCM was then heated to the same temperature in a dropping funnel installed on the top of the vessel (Fig. 3.1). When the PCM was completely melted, it was added to the diatomite in a dropwise manner. During this process, a stirring electric motor was used to mix the diatomite with the PCM. The mixing process was terminated when the liquid PCM was entirely absorbed by diatomite into its porous structure.

The PCM/diatomite composite was then placed in open air below the PCM's melting temperature for 6 hours to make sure that PCM becomes solid. The PCM is retained in the porous diatomite to form the form-stable PCM (FSPCM).

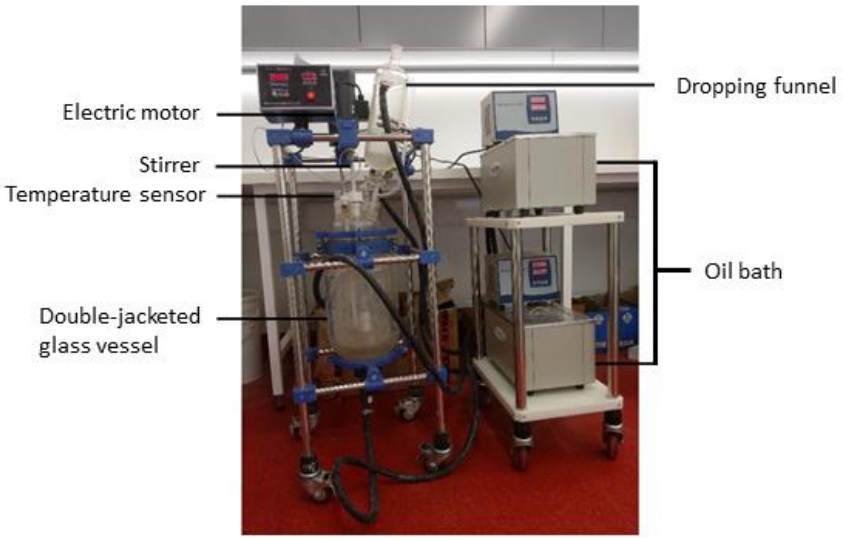

Fig. 3.1. Setup used to prepare form-stable PCM.

3.2.3. Testing methods

3.2.3.1. Morphological characterisation

The morphology and surface topology of the porous diatomite and developed FSPCM was performed by Scanning Electron Microscopy (SEM; SEM JEOL 6510 LV). The SEM requires a highly conductive sample; thus, the experiment was started with a coating of FSPCM samples with a very thin layer of gold to increase their conductivity. The SEM was operated in a low vacuum mode at 30 Pa and 15 kV. The SEM was also equipped with an energy dispersive X-ray spectroscopy (EDS) detector for elemental analysis.

3.2.3.2. Surface area analysis

The surface area and porosity of the diatomite material were determined by a physisorption analyser (ASAP 2020, Micromeritics). The Micromeritics ASAP 2020 is equipped with two vacuum systems: one for sample preparation and the other for sample analysis. Therefore, the sample preparation (de-gassing) and analysis can occur simultaneously. During the sample analysis, the sample contained in a bulb-shaped tube is evacuated and cooled to cryogenic temperatures. Then the

analysis gas (usually N_2) is introduced into the tube at precisely controlled pressures. The pressure at which adsorption equilibrium occurs is measured and the universal gas law is applied to determine the quantity of gas adsorbed. Any micropores in the material's surface are quickly filled, then the free surface becomes completely covered, and finally larger pores are filled. The process may continue to the point of bulk condensation of the analysis gas. Then, the desorption process may begin in which pressure is systematically reduced, resulting in the liberation of the adsorbed molecules. Analysis of these adsorption and desorption isotherms yields information about the surface characteristics of the material.

The tube sample holder can hold volumes from 1–20 cm^3 solid sample to be characterised. The mass of the sample needed depends upon the material density and expected specific surface area (SSA). Typically, 0.5–1.0 g for samples SSA > 100m^2/g and 1.0–8.0 g for SSA < 100m^2/g. The ASAP 2020 Operator's Manual recommends 40-120 m^2 of total surface area per sample for achieving the best surface area analysis results.

3.2.3.3. Chemical compatibility and phase analysis

The chemical compatibility of the samples was tested by Fourier transform infrared (FTIR) spectroscopy (Bruker Vertex 70). The FTIR test relies on infrared light to scan samples to measure how the molecules of a substance absorb infrared radiation, which varies based on the substance's molecular structure. The chemical identity of the FSPCM was tested by FTIR between the wavelengths of 4000 and 360 cm^{-1}.

The chemical composition of form-stable PCM was also analysed by X-ray diffraction (XRD; D8 Advance Bruker AXS, Germany). The test was performed with Cu-Kα radiation (λ=1.5406 Å) in the 2θ range 10-60° at a scan rate of 0.2 s/step. The operating current and voltage were set at 40 mA and 40 kV, respectively.

3.2.3.4. Thermal properties analysis

The thermal analysis of raw PCM and FSPCM to obtain phase transition temperatures and latent heat capacity was conducted by a differential scanning calorimetry (DSC) -Netzsch 204 F1 Phoenix.

The measurement was performed under an atmosphere of argon which was injected at a flow rate of 25 mL/min. Approximately 10 mg of the sample was precisely weighed and then encapsulated in an aluminum pan. The pan was then placed inside the DSC instrument's measurement cell along with an empty reference pan and heated at a rate of 5 °C/min in the temperature range from –20 to 60 °C and cooled at a rate of 5 °C/min. The heat flow DSC is a technique in which the difference between the heat flow rate into a sample pan and that into a reference pan is determined as a function of temperature or time. Each sample underwent three cycles of heating-cooling while the data was collected from the third cycle.

3.2.3.5. Thermal stability analysis

The thermal stability of form-stable PCM was conducted using a thermogravimetric analyser (TGA; Netzsch STA 449C Jupiter). Approximately 10 mg of the sample was precisely weighed and then encapsulated in an aluminum pan. The sample pan was then placed in the TGA along with an empty reference pan. Heating was conducted at a 10 °C/min rate up to 600 °C. The measurement was performed under an atmosphere of argon, which was injected at a flow rate of 25 mL/min. A curve of weight loss against temperature was constructed from the data obtained by the instrument. A derivative of this curve (DTG) was produced to indicate the temperatures at which maximum rates of weight loss occurred.

3.2.3.6. Thermal reliability analysis

The thermal reliability of the prepared FSPCM was evaluated concerning the change in phase change temperature and latent heat after several thermal cycles. The thermal cycling consisted of exposing the form-stable PCM to multiple melting and freezing processes. This was done by keeping the sample in a controlled environment through thermal cycler (TC-25/H, Bioer) in which the sample was heated (melting) and cooled (freezing) between 0 ºC and 50 ºC at a rate of 0.5 ºC/min. Fig. 3.2 shows the graphical representation of thermal cycling test. After 50 consecutive melting and freezing cycles, the FTIR, XRD and DSC analyses were repeated to verify the chemical and thermal stability of FSPCM.

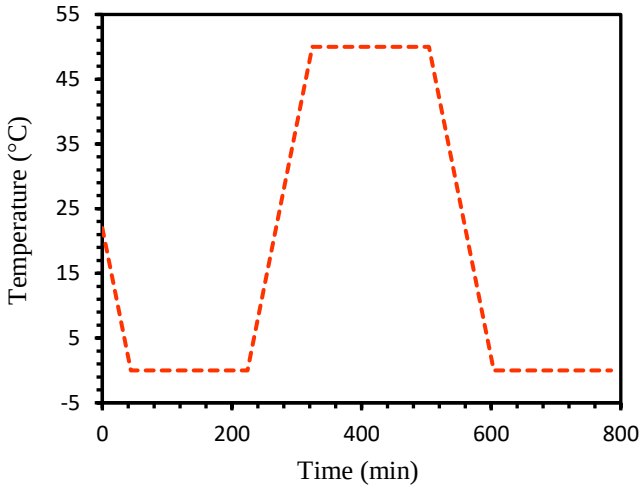

Fig. 3.2. Thermal cycling test.

3.2.3.7. Thermal conductivity measurement

A hot-disc thermal constants analyser TPS 2500 s was used to determine the thermal conductivity of the samples at room temperature. The measurement is based on the transient plane source (TPS) method. A hot-disc sensor 5465 was used with a radius of 3.189 mm. The hot disc was calibrated using fused silica (thermal conductivity 1.31-1.32 W/m.K) to check the functionality of the hot disc. The thermal conductivity measurement started by weighing the FSPCM in a beaker, and water was then added with a water/FSPCM ratio of 0.4. The mixture was blended for 2 min to produce FSPCM slurry. Finally, the FSPCM slurry was poured into a mould (diameter of 20 mm and a thickness of 10 mm) and heated at 90 °C for 24 h. For pure PCM, the PCM was melted at 60 °C before pouring into the mould and cooling for 24 h. For this measurement, the sensor was placed between two layers of samples with a diameter of 20 mm and a thickness of 10 mm.

3.2.3.8. Thermal performance analysis

To inspect the thermal performance of the prepared FSPCM for practical applications, the heat storage and release periods of the pure PCM and FSPCM were examined by measuring the temperatures with respect to time during the melting and solidifying processes. The experimental setup is depicted in Fig. 3.3. Two glass tubes were loaded with 15 g of pure PCM and FSPCM, respectively. A thermometer with an accuracy of ±0.1 °C was placed in the centre of each tube. The glass tubes were then put into a water-filled glass beaker and the temperature was recorded once every

1 min during the melting process from 25.5 to 45 °C, and then during the subsequent solidification process back to room temperature.

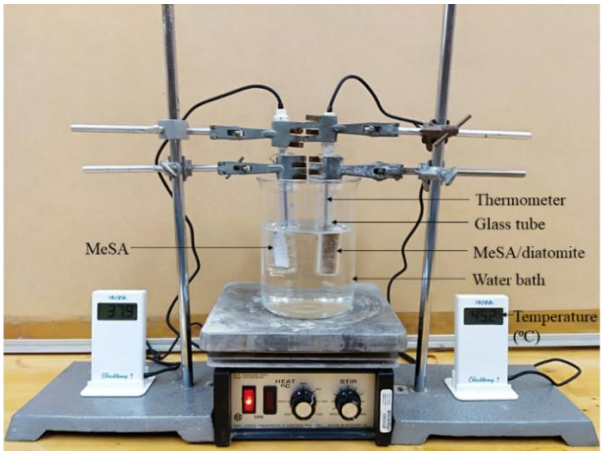

Fig. 3.3. Test setup for thermal performance measurement.

3.3. Results and discussion

3.3.1. Morphology of diatomite

The morphology and microstructure of diatomite investigated via SEM analysis are shown in Fig. 3.4. As shown in Fig. 3.4(a-d), the isolated diatomite particles, in the order of microns, are mainly in a disc and cylindrical forms with extremely porous and hollow centres. Numerous macropores (300-400 nm in diameter) are uniformly distributed, signifying the diatomite's large specific surface area as expected. They also have two different 3D cylindrical porous structures: one is full frustule with both ends entirely closed (Fig. 3.4b), and the other is half frustule with one end half open and the other end closed (Fig. 3.4c). The length of a typical diatomite particle is found to be 8-12 μm, with a diameter of 5-8 μm. Diatomite has a smooth surface with various open pores, cavities and channels. It is interesting to note that all diatomite particles show a similar hierarchical porosity characteristic. The open cavities in diatomite are responsible for absorbing liquid PCM. As the used diatomite has high purity, only a few pores are blocked by visible impurities. The more pores are accessible, the more PCM can be loaded in the diatomite.

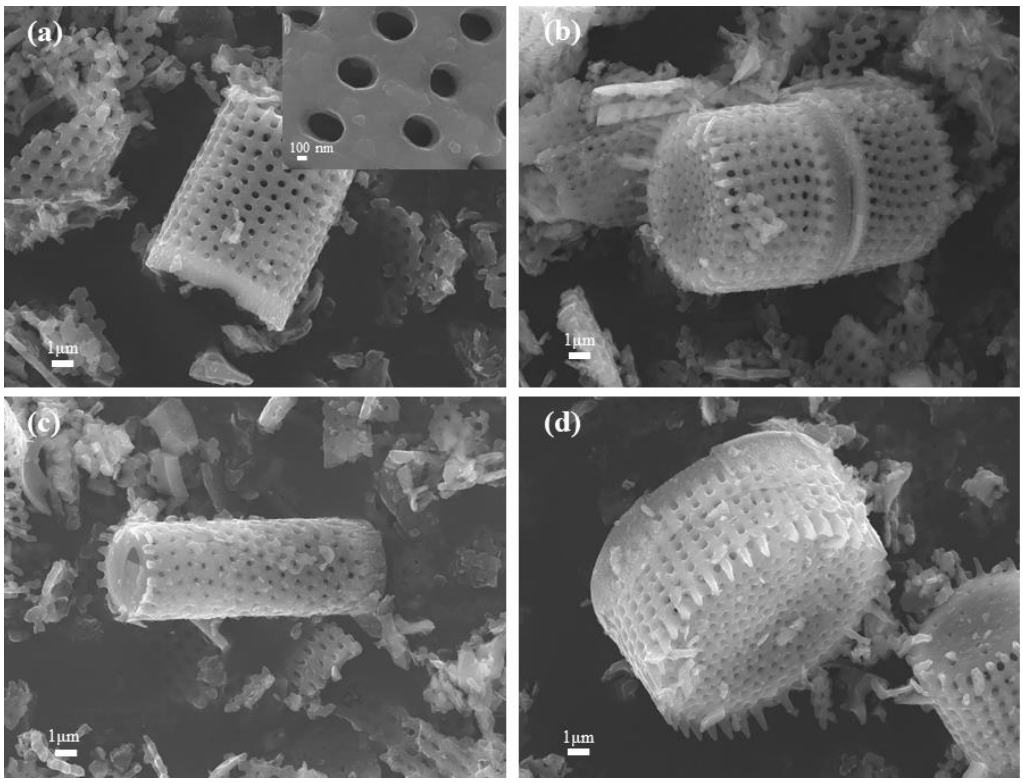

Fig. 3.4. SEM morphologies: (a-c) cylindrical shape, and (d) disc shape.

The elemental characterisation of diatomite was determined through EDS analysis and is shown in Table 3.1, which shows that the diatomite particle is mainly composed of SiO_2 (92.5%) and a small amount of Al_2O_3 (4.8%). This indicates that the diatomite can potentially combine with inorganic construction materials such as cementitious materials well even after absorbing PCM [119-121].

Table 3.1 Chemical composition of diatomite.

Compound	SiO_2	Al_2O_3	MgO	Fe_2O_3	CaO	Na_2O	TiO_2
Ratio (%)	92.5	4.8	0.7	1.2	0.5	0.2	0.1

3.3.2. Surface properties of diatomite

The surface area and porosity properties of the thermally treated diatomite were analysed by nitrogen adsorption measurements. Fig. 3.5a shows the resulting adsorption-desorption isotherm and Fig. 3.5b demonstrates the corresponding density functional theory (DFT) pore size distribution graph of the thermally treated material. The isotherms feature an adsorption-desorption hysteresis loop in the relative pressure range of 0.45-0.96. It can be observed from Fig. 3.5a that the isotherm of the diatomite sample resembles a type II isotherm, as there is no plateau when it approaches the p/p_0 ratio

of 1, where p and p_0 are the condensation pressure and saturated pressure of the bulk fluid, respectively.

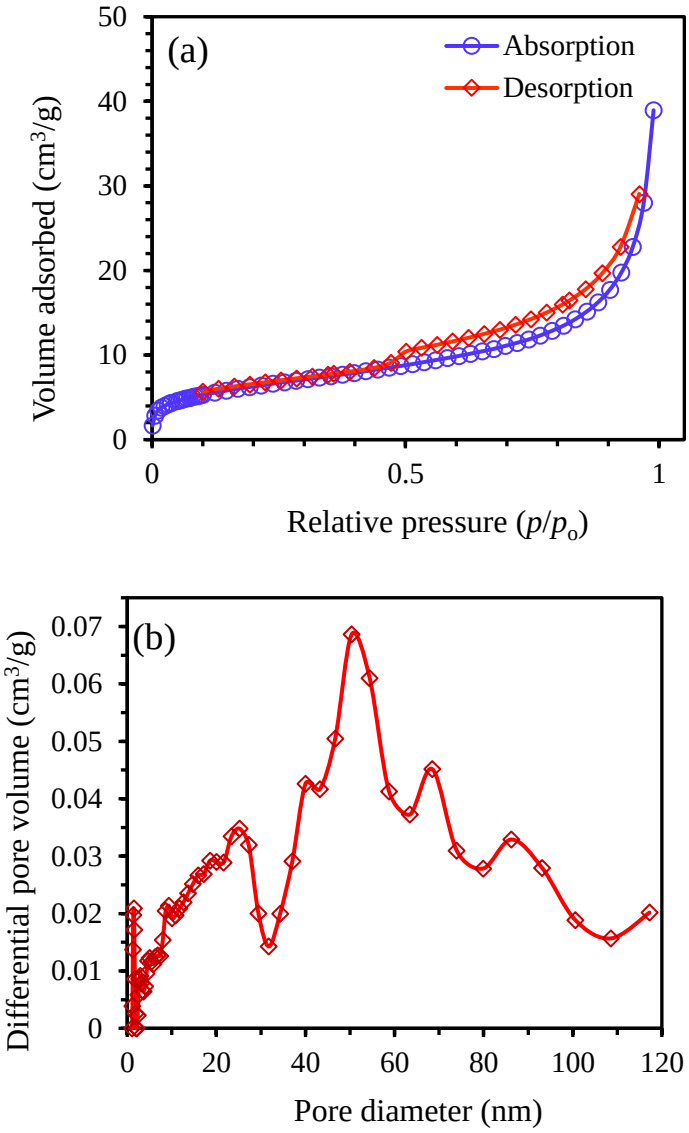

Fig. 3.5. Thermally treated porous diatomite material: (a) N_2 adsorption-desorption isotherms, and (b) DFT pore size distribution.

According to IUPAC nomenclature [122], macropores are defined as pores with diameters greater than 50 nm, mesopores 2-50 nm, and micropores less than 2 nm. The presence of macropores was confirmed by the pore sizes observed in the SEM images shown in Fig. 3.4. However, the existence of a small amount of uptake at low relative pressure could suggest the filling of micropores. Also, present is a hysteresis loop ($0.5 < p/p_0 < 0.9$), which seems to have attributes similar to both an H3 hysteresis (the absorption capacity rises steeply at a higher relative pressure > 0.95) and H4

hysteresis (shows some micropore filling at low relative pressures). These hysteresis types could indicate macropores that have not been filled with pore condensate, or the existence of some mesopores. It is highly likely that this porous diatomite material possesses a microstructure with an array of pore sizes, including micro-, meso- and macropores. The higher specific surface areas attributable to the mesopores are projected to influence interfacial processes.

The BET surface area and pore structure characteristics are key factors in selecting porous carrier materials for wrapping PCM. The diatomite has a BET surface area of 22.69 m^2/g and DFT pore volume of 0.04362 cm^3/g, respectively. Due to the nature of the experiment, it should be noted that this pore volume only includes pores with diameters up to 120 nm (i.e., those shown in the DFT plot in Fig. 3.5b). The large surface area and pore volume explain the high absorption capacity of diatomite due to capillary and surface tension forces, making it suitable for PCM encapsulation.

3.3.3. Morphology of form-stable PCM

The morphology of the form-stable PCM is shown in Fig. 3.6. As shown in Fig. 3.6a, form-stable PCM has a light grey colour. Compared with the empty pores observed in the SEM images of the pure diatomite (Fig. 3.4), there are no visible pores left after PCM impregnation (Fig. 3.6b), indicating that PCM has been impregnated into diatomite pores in the FSPCM.

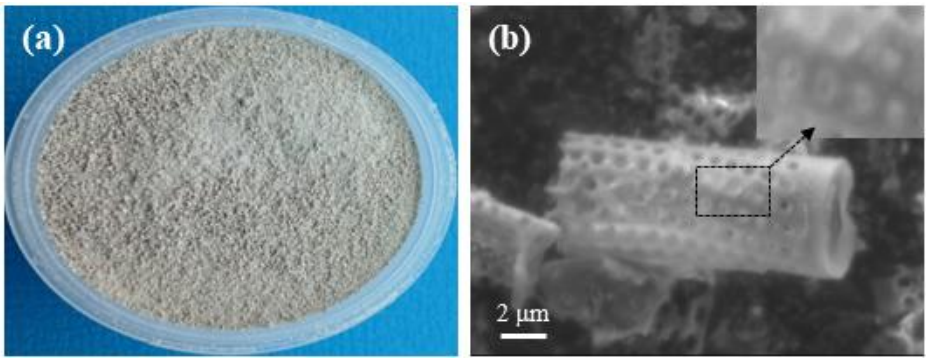

Fig. 3.6. Prepared form-stable PCM: (a) normal appearance, (b) SEM micrograph.

3.3.4. Chemical compatibility of form-stable PCM

The chemical compatibility between PCM and diatomite was determined by using the FTIR spectroscopy analysis method. Fig. 3.7 shows the FTIR spectrums of pure PCM, diatomite and form-stable PCM. The raw diatomite possesses three strong absorption peaks at 454, 780 and 1062 cm^{-1}.

The characteristic peak at 454 cm^{-1} belongs to the Si-O bending vibration. The band at 780 cm^{-1} ascribes to the silanol (SiO-H) groups and 1062 cm^{-1} signifies the siloxane (Si-O-Si) stretching vibration group. All these characteristic peaks belong to SiO_2. In the pristine PCM spectrum, the absorption bands at 2848 and 2915 cm^{-1} are attributed to the symmetric and asymmetric stretching vibrations of $–CH_2$ group. The stretching vibration of $–CH_3$ is found at 2951 cm^{-1}. The stretching vibration of the C=O group is detected at 1739 cm^{-1}. The peaks at 1169 and 1107 cm^{-1} can be assigned to C-O asymmetric and symmetric vibrations. In addition, the peaks at 1462 cm^{-1} and 723 cm^{-1} are caused by the CH_2 or CH_3 deformation vibration and $(–CH_2–)n$ ($n \geq 4$) rocking vibration. In the form-stable spectrum, all typical absorption bands of both PCM and diatomite are still visible as expected. Moreover, no new peaks have appeared in the composite PCM spectrum, suggesting that no chemical interaction takes place between the pore confined PCM and diatomite.

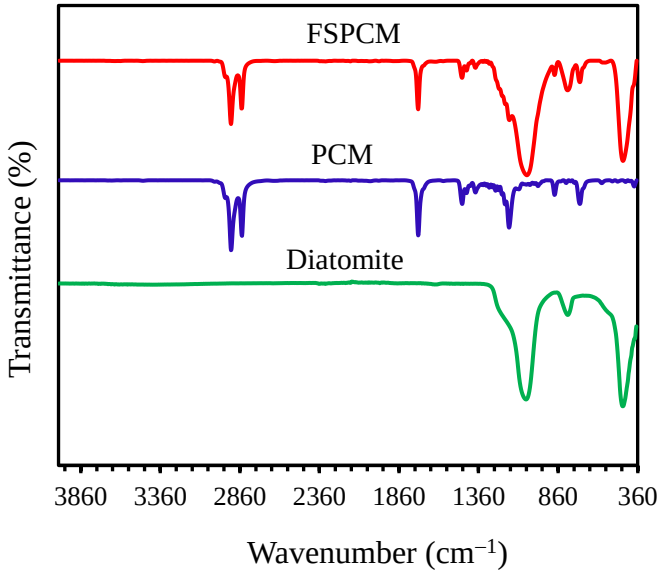

Fig. 3.7. FTIR spectra of diatomite, PCM and form-stable PCM.

Table 3.2 shows the characteristic FTIR peaks of the diatomite, PCM and FSPCM. It seems that some FTIR peaks of the FSPCM have shifted slightly in comparison with those of pure PCM and diatomite. These shifts may be because of the weak physical interactions between PCM and the supporting diatomite material. The physical interactions induce capillary and surface tension forces, arresting the liquid PCM from leaking out during the phase transformation process [123]. The FTIR

results shown in Table 3.2 indicate excellent chemical compatibility between PCM and the diatomite matrix.

Table 3.2 FTIR characteristic peaks of diatomite, PCM and FSPCM.

Sample	Si–O	$–CH_2$	SiO–H	Si–O–Si	C–O		C=O	$–CH_2$ and $–CH_3$			
Diatomite	454	–	780	1062	–	–	–	–	–	–	–
PCM	–	723	–	–	1107	1169	1739	1462	2848	2915	2951
FSPCM	452	723	779	1056	1106	1165	1740	1462	2848	2916	2951

To further characterise the diatomite, pure PCM and FSPCM, X-ray diffraction (XRD) investigation was performed and the spectra are shown in Fig. 3.8. The broad diffraction peak found in the diatomite spectrum spanning a range of approximately 20–25° can be ascribed to the non-crystalline silica (SiO_2), whereas the strong peak centred at 26.7° can be assigned to the (101) reflection of quartz crystal. In the PCM spectrum, the appearance of peaks at 11.1, 14.8, 19.9, 20.6, 21.8 and 24.1° confirms the formation of highly crystalline PCM with a monoclinic system.

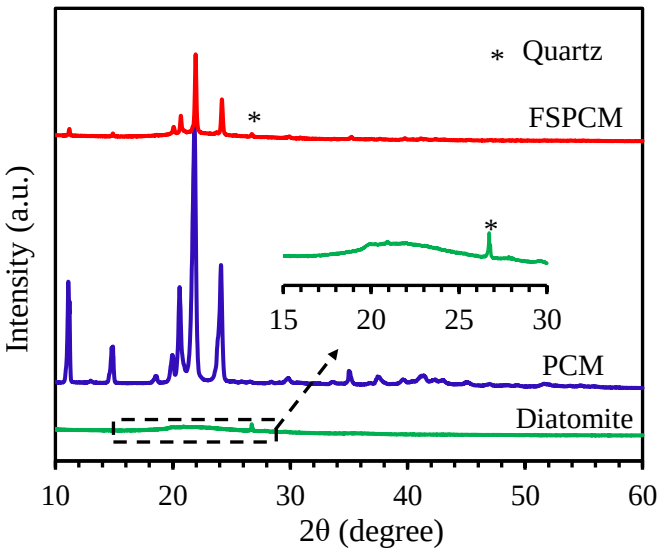

Fig. 3.8. XRD spectra of diatomite, PCM and FSPCM.

It can be seen that the main diffraction peak of PCM appears in the XRD pattern of FSPCM without appreciable shifting of the 2θ angle. Meanwhile, there is no new peak appearance. This supports that the PCM segment of the composite has a similar crystal structure as the pure PCM, without chemical interactions taking place between the PCM and diatomite during the impregnation process.

3.3.5. Thermal properties of form-stable PCM

Thermal properties such as melting and freezing temperatures and latent heat capacity are the most important parameters for thermal energy storage system. The phase change properties of PCM and FSPCM were determined by DSC tests. Fig. 3.9 shows the typical DSC curves of the raw PCM and form-stable PCM and the resultant data of thermal properties are summarised in Table 3.3.

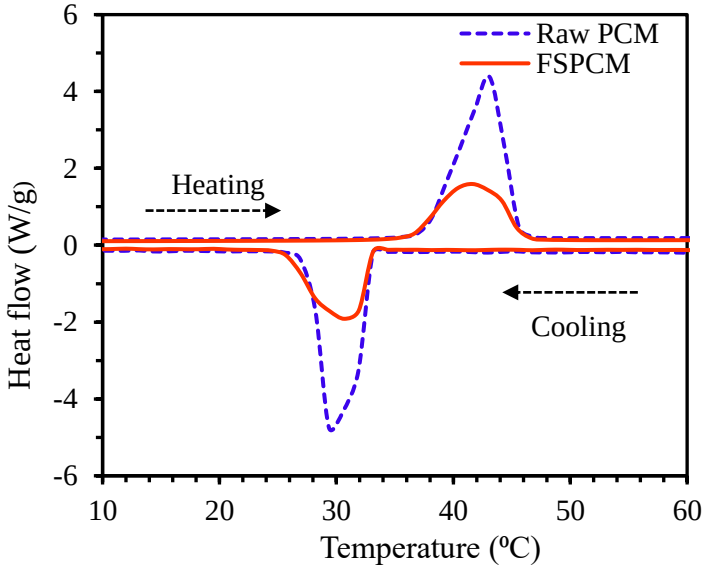

Fig. 3.9. Measured DSC curves of raw PCM and FSPCM.

Both the raw PCM and FSPCM display only one peak in the endothermic and exothermic DSC curves, corresponding to the latent heat storage of PCM during melting and solidifying processes. As shown in Fig. 3.9, the raw PCM displays sharp and strong endothermic and exothermic peaks with an onset melting temperature (T_m) of 36.8 °C and an onset solidifying temperature (T_s) of 32.7 °C, giving a total temperature range of approximately 26–46 °C. Conversely, the FSPCM has broader and blunt endothermic and exothermic peaks with a negligible change of phase change temperatures (T_m of 36.5 °C and T_s of 33.1 °C) in comparison with raw PCM. The raw PCM has peak melting ($T_{m,p}$) and solidifying ($T_{s,p}$) temperatures of 43.1 °C and 29.4 °C, respectively, while for FSPCM, the corresponding values are 41.7 °C and 30.7 °C. Heatwaves in Australia are becoming hotter, longer and more frequent. For example, Penrith, a suburb of Sydney, is frequently hit by heat waves and has a temperature record of 47.3 °C reached in January 2018. It has been reported that the temperature in a roof attic could be even 15–20 °C higher than the outdoor air temperature [124]. Therefore, the

FSPCM with a relatively high melting temperature is suitable for roof ceiling applications in Australian residential houses**.**

Table 3.3 Thermal properties of raw PCM and FSPCM.

Sample	Heating cycle			Cooling cycle			Extent of supercooling ($\Delta T = T_m - T_s$) (°C)
	T_m (°C)	$T_{m,p}$ (°C)	ΔH_m (J/g)	T_s (°C)	$T_{s,p}$ (°C)	ΔH_s (J/g)	
Raw PCM	36.8	43.1	217.7	32.7	29.4	219.6	4.1
FSPCM	36.5	41.7	111.8	33.1	30.7	110.6	3.4

The phase change latent heat of the PCM and FSPCM is calculated by the area under the endothermic and exothermic peaks. The melting (ΔH_m) and solidifying (ΔH_s) latent heats of raw PCM are determined to be 217.7 and 219.6 J/g, respectively. The melting and solidifying latent heats for FSPCM are 111.8 and 110.6 J/g, respectively. Tests were also conducted to measure their specific heat capacity by using the DSC and the results are shown in Fig. 3.10. Accordingly, the specific heat capacity of raw PCM and FSPCM at ambient temperature (25 °C) are about 1.84 and 1.32 J/g·K, respectively.

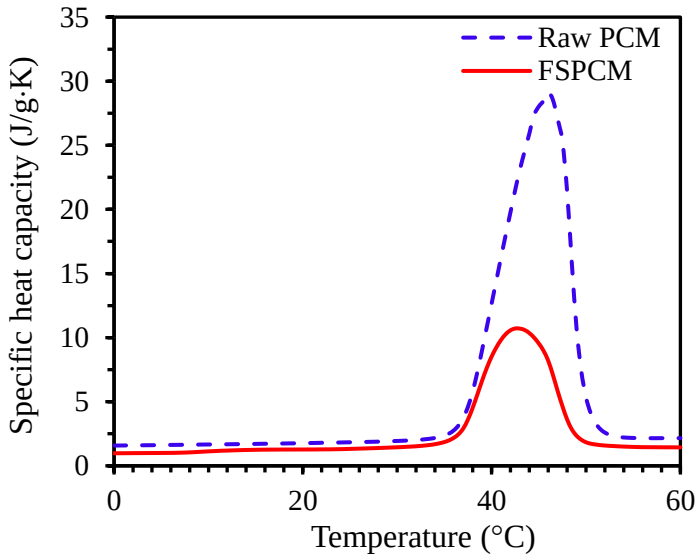

Fig. 3.10. Specific heat capacity of raw PCN and FSPCM.

For form-stable PCM, it is important to ensure the highest amount of PCM absorption at a minimum loss of the latent heat, since carrier materials do not undergo phase change. Evidently, the latent heat and specific heat capacity of the FSPCM decrease in the presence of a carrier material.

Therefore, the mass fraction of PCM is important for understanding the thermal performance of the prepared FSPCM. The mass fraction (β) of PCM in the FSPCM can be calculated by Eq. (3.1) [125]:

$$\beta \text{ (PCM \%)} = \frac{\Delta H_{\mathrm{m,FSPCM}}}{\Delta H_{\mathrm{m,PCM}}} \times 100\% \tag{3.1}$$

where $\Delta H_{\mathrm{m,PCM}}$ and $\Delta H_{\mathrm{m,FSPCM}}$ represent the melting latent heats of the raw PCM and FSPCM, respectively.

The β-ratio of PCM in the FSPCM is found to be 51.3%. However, the reduction in latent heat for the FSPCM in comparison with raw PCM not be ascribed only to the lower fraction of PCM in the FSPCM. The interaction between the PCM and porous diatomite could be another reason leading to the reduction in phase change latent heat of the FSPCM. These interactions could be reflected by crystallisation fraction (F_c) in the composite FSPCM [126]. The parameter F_c is represented by Eq. (3.2):

$$F_c = \frac{\Delta H_{\mathrm{FSPCM}}}{\Delta H_{\mathrm{PCM}}\beta} \times 100\% \tag{3.2}$$

where ΔH_{PCM} and $\Delta H_{\mathrm{FSPCM}}$ are the crystallisation latent heats of the raw PCM and FSPCM, respectively.

The variable F_c corrects the mass depletion effect owing to the addition of porous diatomite and may assist to evaluate the interaction between the PCM and the carrier material. A greater value of F_c implies higher conservation of crystalline phase and thus signifies a weaker interaction. In the current study, a high F_c value of ~98% for the FSPCM suggests high preservation of crystallinity and a very weak interaction between the PCM and diatomite material. It is well known that supercooling of PCM is a key issue from the point of practical applications. A high supercooling degree is associated with low effective heat capacity. As a result, the stored energy during the crystallisation process reduces, which is not desirable. Therefore, the control of supercooling degree of a PCM is fundamental for TES applications. The degree of supercooling (ΔT) can be evaluated by Eq. (3.3):

$$\Delta T = T_{\mathrm{m}} - T_{\mathrm{s}} \tag{3.3}$$

where ΔT is the degree of supercooling; and T_m and T_s denote the onset melting and solidification temperatures, respectively. The degree of supercooling of the FSPCM is displayed in Fig. 3.11, where the temperatures of T_m and T_s are given in Table 3.3. The phase transformation temperature of PCM in the FSPCM is influenced by the supporting diatomite material.

As shown in Fig. 3.11, the T_m value of the FSPCM decreases, but on the contrary T_s increases, hence minimising the degree of supercooling of the FSPCM to a great extent. This result is consistent with previously reported studies on polyethylene glycol/polymethyl methacrylate composite PCMs [127]. The heterogeneous nucleation effect of diatomite pores is liable for the decline of T_m. However, the crystallisation-promoting effect of the diatomite pores would cause an increase of T_s. As seen in Table 3.3, the supercooling degree of the FSPCM decreases by 0.7 °C (~17%) compared with that of raw PCM. This result indicates that employing diatomite as a supporting material has a favourable influence on reducing the supercooling degree of PCM.

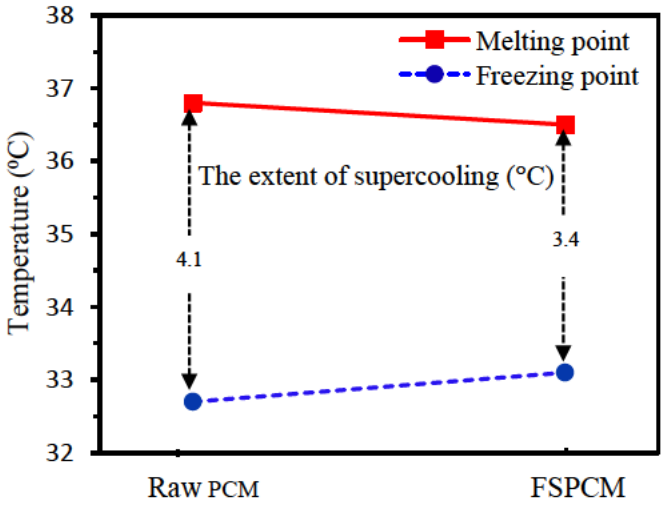

Fig. 3.11. Phase transition temperatures and degree of super-cooling of FSPCM.

Table 3.4 presents the comparison of thermal properties between the MeSA/diatomite FSPCM prepared in the present study and other composite PCMs reported in the literature [102, 128-135]. It is worth noting that the current FSPCM has significantly higher phase change latent heat (>110 J/g) compared with other composite PCMs (60–90 J/g). This is due to a significant amount of PCM with a high latent heat of 217.7 J/g is absorbed by the porous diatomite. Hence, the developed MeSA/diatomite composite is a promising PCM material to be used in solar heat storage systems.

Table 3.4 Comparison of thermal properties between the current FSPCM and those reported in the literature.

Composite PCM	Maximum PCM ratio (%)	Melting process		Freezing process		Reference
		T_m (°C)	H_m (J/g)	T_s (°C)	H_s (J/g)	
Paraffin/diatomite	47.3	27.1	89.4	26.5	89.9	[129]
Capric-stearic acid/perlite	50	29.6	82.1	17.4	82.6	[131]
Dodecanol/bentonite	32	22.6	67.6	21.1	62.3	[134]
PEG/diatomite	50	27.7	87.1	–	–	[128]
Paraffin/vermiculite	38.5	27.0	77.6	25.1	71.5	[132]
Paraffin/perlite	–	27.6	67.1	23.6	69.1	[102]
Capric-palmitic acid/pumice	35	23.1	56.5	21.7	55.4	[133]
Lauric acid/kaolinite	48.0	43.7	72.5	39.3	70.9	[130]
Capric-lauric acid/diatomite [a]	53.6	23.6	87.3	22.5	86.9	[135]
Methyl stearate/diatomite	51.3	36.5	111.8	33.1	110.6	This work

[a] Vacuum impregnation method

3.3.6. Thermal stability of form-stable PCM

Thermal stability is critical for a FSPCM to be used in thermal regulation. TGA and derivative TG (DTG) analyses were conducted to investigate the thermal stability of raw PCM and FSPCM, and the results are given in Fig. 3.12. Both raw PCM and FSPCM show only one-step degradation (Fig. 3.12a). The sharp mass loss of the raw PCM and the FSPCM (Fig. 3.12b) occurred at around 346 and 318 °C, respectively. The mass loss can be attributed to the decomposition of organic matter, namely the breaking of the PCM chains. The earlier mass loss in the FSPCM compared to that of the raw PCM may be due to the change of physical behaviour of the pore confined PCM. But no decomposition and mass loss are detected for FSPCM at temperatures below 220 °C, suggesting that the thermal stability of this prepared FSPCM is high in its temperature range of phase change. The total mass loss of FSPCM is 52% (Fig. 3.12a). This mass fraction of PCM in the FSPCM generally agrees with the measured mass fraction value of 51.3% found from DSC analysis in previous section.

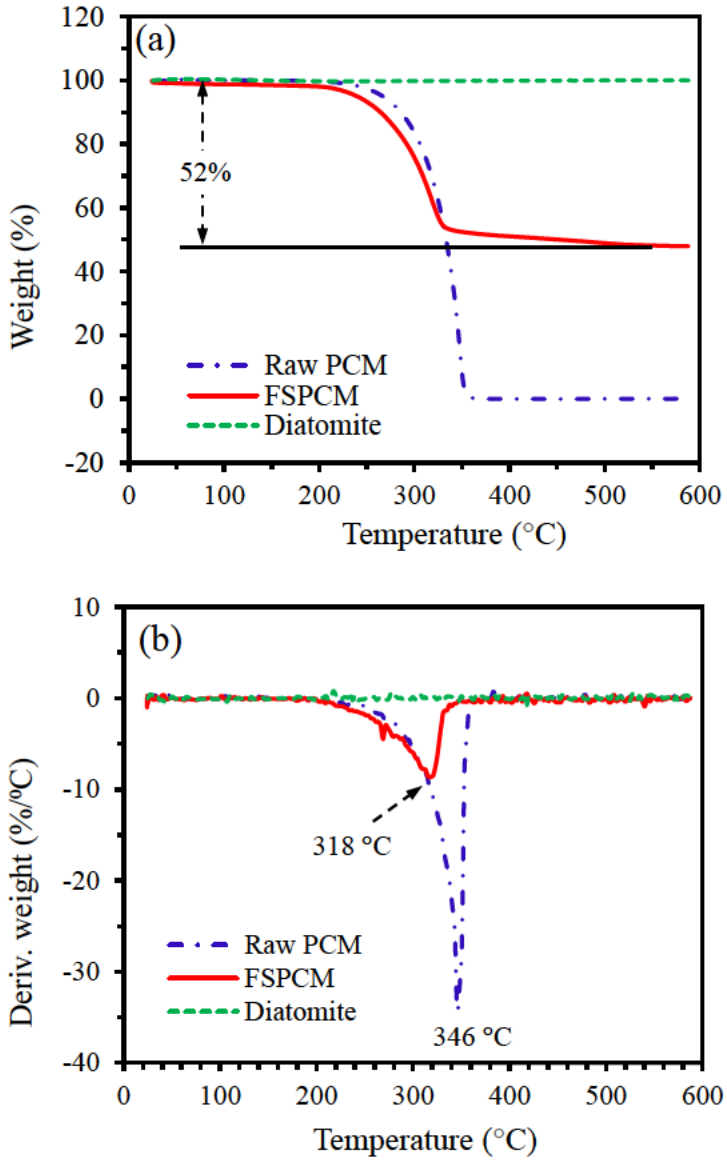

Fig. 3.12. Diatomite, raw PCM and FSPCM: (a) TGA and (b) DTG curves.

3.3.7. Thermal reliability of form-stable PCM

Thermal reliability is a key parameter for evaluating the durability of a FSPCM. To verify the reversibility of FSPCM, solid-liquid phase change cycling tests were performed. Samples were characterised before and after 50 cycle tests. The resulting DSC curves in Fig. 3.13 show that the phase transition temperatures for melting and solidification after 50 thermal cycles are 36.7 and 33.5 °C respectively, with the corresponding latent heats found to be 112.0 and 110.2 J/g, respectively.

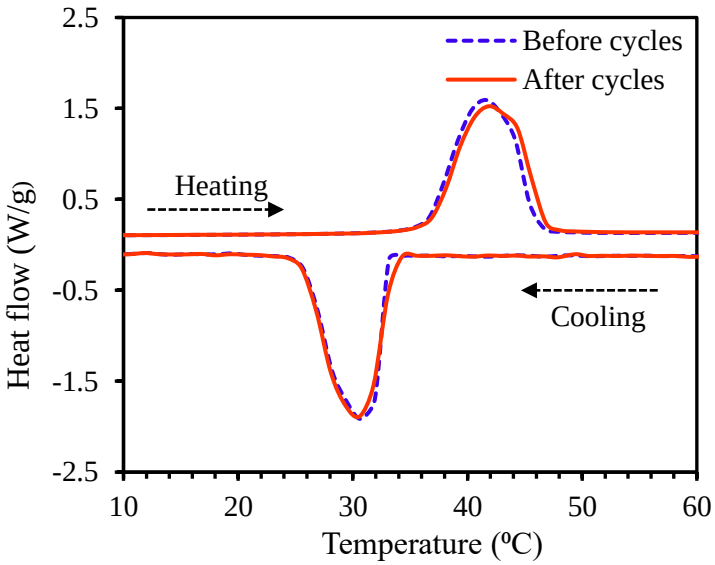

Fig. 3.13. DSC curves of FSPCM before and after 50 thermal cycles.

As compared to those values measured before the thermal cycles, the melting and solidifying temperatures of the FSPCM were shifted by 0.57% and 1.3%, respectively, whereas the latent heats for the melting and solidification processes changed by 0.18% and –0.36%, respectively (Table 3.5). The phase change temperatures and latent heat values for both melting and solidification processes of FSPCM after thermal cycling exhibited a negligible change, suggesting very good thermal reliability.

Table 3.5 DSC data of the FSPCM before and after 50 thermal cycles.

Sample	PCM (%)	Heating cycle		Cooling cycle	
		T_m (°C)	ΔH_m (J/g)	T_s (°C)	ΔH_s (J/g)
Before cycles	51.3	36.50	111.8	33.10	110.6
After cycles	51.4	36.71	112.0	33.54	110.2

The XRD pattern after thermal cycles is presented in Fig. 3.14. It is observed that the peak position of raw PCM in the FSPCM remains similar to that before 50 melting/solidifying cycles. The β (mass fraction of PCM) value is also nearly the same as the original value (Table 3.5), which indicates a retention of crystalline phase of PCM in the FSPCM after numerous melting-freezing cycles. Besides, no leakage of the PCM is found by weighing the composite (Table 3.5) before and after 50 thermal cycles, signifying excellent thermal reliability and stability. It seems that the multi-

porous structure of the diatomite arrested the seepage of melted PCM from the FSPCM by capillary action and surface tension forces.

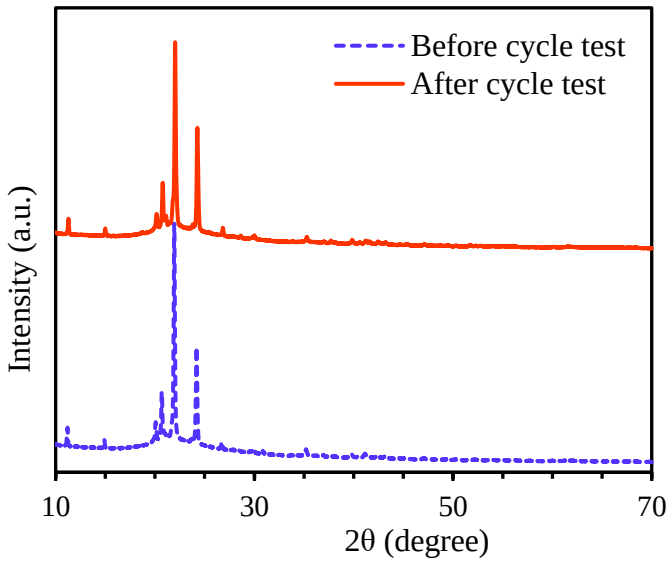

Fig. 3.14. XRD spectra of FSPCM before and after 50 thermal cycles.

In addition, the FTIR spectra (Fig. 3.15) of the FSPCM confirm that no changes of the shape and frequency values of major peaks occurred and no new peaks appeared after thermal cycles. These results again confirm that after 50 melting/solidification cycles, the chemical structure of the FSPCM is not affected. The thermal reliability and chemical stability of the prepared FSPCM thus meet the latent heat storage application requirements.

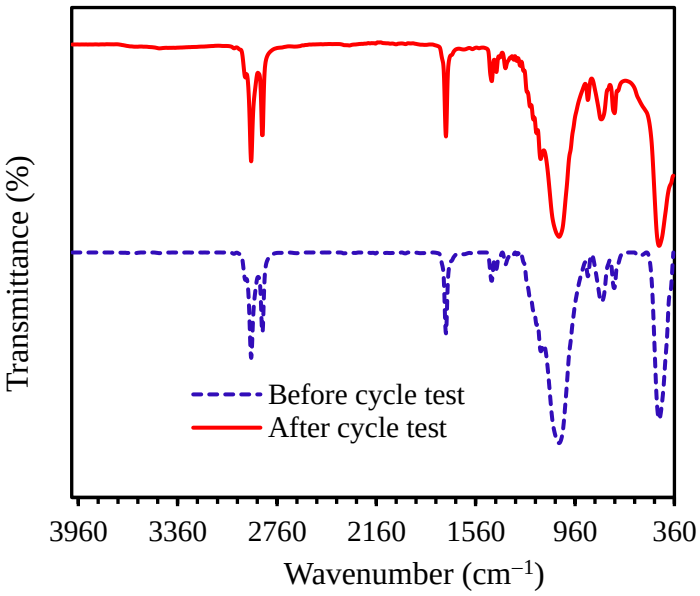

Fig. 3.15. FTIR spectra of FSPCM before and after 50 thermal cycles.

3.3.8. Thermal behaviour of form-stable PCM

Thermal storage and release rates are also important for practical applications of PCM. It is favourable for PCM to have relatively high thermal storage/release rates. Thermal storage and release processes of raw PCM and FSPCM were studied by the same custom-designed experimental system shown in Fig. 3.3. Fig. 3.16 shows the curves of temperature versus time of the raw PCM and FSPCM samples during the heating and cooling processes. It is notable that both PCM and FSPCM have an obvious temperature plateau during the heating and cooling processes because of the phase transition. However, the FSPCM displays much higher heat storage/release rates than those of the raw PCM.

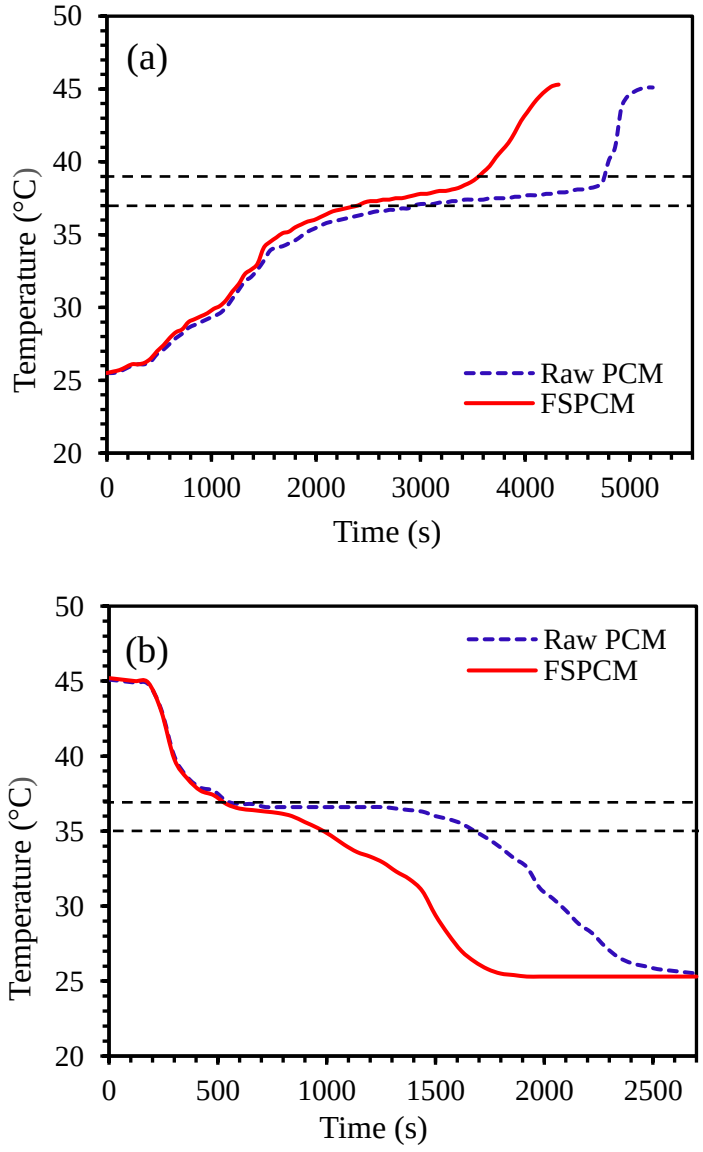

Fig. 3.16. Temperature versus time curves of raw PCM and FSPCM: (a) melting process and (b) freezing process.

In the melting process (Fig. 3.16a), for example, the times required to raise the temperature from 37 to 39 °C are 1815 and 1550 s for the raw PCM and FSPCM, respectively. In the freezing process, times of 1140 and 470 s are needed to drop the temperature from 37 to 35 °C (Fig. 3.16b) for the raw PCM and FSPCM, respectively. The results indicate that the melting and solidification times of FSPCM decrease by 14.6% and 58.8%, respectively, in comparison with those of the raw PCM. These results demonstrate the beneficial effect of the diatomite on the PCM's heat storage/release performance for practical applications.

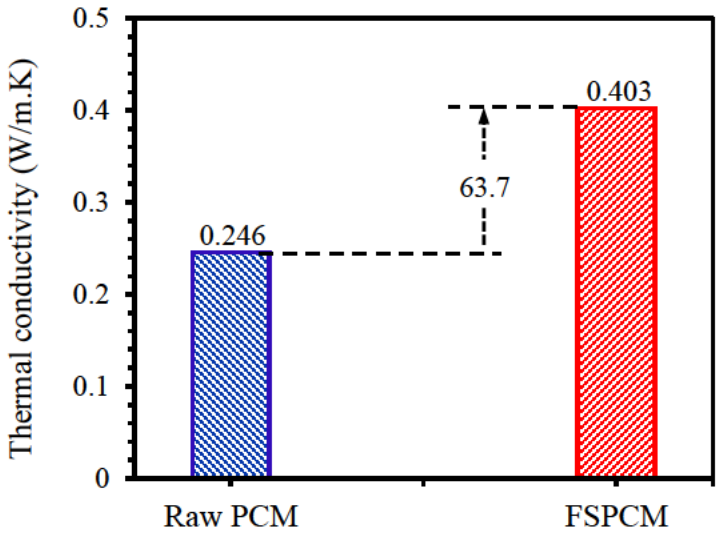

Fig. 3.17. Thermal conductivities of raw PCM and FSPCM.

The enhanced heat storage/release rates can be attributed to the higher thermal conductivity of the FSPCM compared to the raw PCM, which can be seen from the comparison of thermal conductivity in Fig. 3.17. In comparison with the raw PCM, the thermal conductivity of the FSPCM is considerably enhanced from 0.246 W/m.K to 0.403 W/m.K, which is a good agreement with the result reported by Han et al. [136]. The improvement of thermal conductivity ~63.7% by impregnating PCM into diatomite pores is due to the relatively high thermal conductivity of diatomite itself [137]. This suggests that the use of diatomite could enhance the thermal conductivity of PCM, which is beneficial for thermal management applications.

3.4. Concluding remarks

This chapter addressed the first research question of this research by investigating the PCM leakage and thermal conductivity of form-stable composite PCM, where methyl stearate was incorporated into diatomite. The FSPCM was developed by a simple direct impregnation method and its thermal performance (storage/release) was evaluated for building applications. Based on the experimental research, the following conclusions can be drawn:

1. The fabrication of form-stable PCM using diatomite as a supporting material resulted in a large absorption ratio of PCM (51.3 wt.%) in the composite. The SEM results indicated that PCM was well incorporated into the diatomite pores.
2. The developed FSPCM showed good chemical compatibility, thermal stability and excellent phase change properties. The interaction between PCM and diatomite is purely physical and a high crystallisation fraction value of ~98% for the FSPCM confirms a weak interaction between them.
3. The thermal properties showed that FSPCM had a large operating temperature range from 24 °C to 48 °C. The corresponding latent heat capacities for melting and freezing cycles are 111.8 J/g and 110.6 J/g. Using diatomite as a supporting material could reduce the degree of supercooling by around 17% for FSPCM compared to raw PCM.
4. The thermal cycling tests proved that the FSPCM has good structural stability and thermal reliability without any PCM leakage even after 50 melt-freeze cycles. During the cycling test, the deviation in the melting and freezing temperatures were found to be 0.57% and 1.3% and in the latent heats of 0.18% and -0.36%, respectively.
5. The thermal conductivity of FSPCM is found to increase compared with pure PCM. An enhancement of 63.7% in thermal conductivity was seen in the case of the FSPCM compared to raw PCM. The increase in thermal conductivity of the FSPCM was also confirmed by comparing their melting and freezing times with those of the raw PCM.

From this research, it was concluded that the FSPCM based on diatomite material could be considered as a promising candidate for the preparation of energy-storing building materials such as gypsum board that could reduce the indoor temperature fluctuation and also reduce energy consumption. Thus, further studies should be conducted to integrate the developed FSPCM into gypsum board and evaluate its thermal performance in a small-scale test chamber.

CHAPTER 4

Inclusion of FSPCM into gypsum board for building energy conservation

4.1. Introduction

In the previous chapter, the preparation of diatomite based FSPCM and characterisation of its thermal conductivity and structural stability by thermal cycling (melting/cooling) tests were introduced. Based on the work in Chapter 3, an experimental study was further conducted in this chapter (Chapter 4) to evaluate the potential inclusion of FSPCM into gypsum board for building energy conservation. Previous studies studied the thermal performance of FSPCM-integrated prototype building materials through heating/cooling thermal cycle tests either by a solar simulator [121, 138, 139] or in a laboratory-scale small chamber [62, 140-144]. However, the actual performance of FSPCM-integrated building materials in a real environment is absent. In particular, no experimental work has been conducted in the literature on using PCM/diatomite composite FSPCM-integrated gypsum board for building energy conservation. In this chapter, the performance of FSPCM-enhanced gypsum board for cooling load reduction in summer in real environmental conditions was investigated. A small-scale test chamber with an FSPCM-integrated gypsum board ceiling was prepared and modelled to study the thermal/energy performance. To further understand the potential economic benefits of using the FSPCM-integrated gypsum board, an economic evaluation through life cycle cost analysis was also performed in this chapter.

4.2. Methodology

4.2.1. Preparation of FSPCM gypsum board

The FSPCM described in Chapter 3 was incorporated into foamed gypsum board for latent heat storage. Gypsum is mainly composed of calcium sulphate hemihydrate (CSH). To reduce the density of gypsum board, foam bubbles were introduced into CSH slurry in the laboratory. The mix

proportions for gypsum board with 40 wt.% of FSPCM or without FSPCM are given in Table 4.1. A slurry was prepared by combining CSH, 0.225% accelerator (potassium sulfate), 0.65% glass fibres, 0.015% retardant (polyacrylic acid), 0.065% foaming agent (alkyl sulfate oligomers) and sufficient water to produce gypsum board with a water/CSH ratio of 0.86. It should be noted that all additives were measured in solid form as a percentage of the weight of CSH. The experimental process started by weighing the CSH and FSPCM (if any) in a beaker, and the water and retardant were then added and weighed in a mixer cup. The CSH/FSPCM was then poured into the mixer cup and blended for 30 s to produce a gypsum slurry. Then, foam was generated separately by the inclusion of potassium sulfate before adding into the gypsum slurry. The mixture was blended for 30 s to produce foamed gypsum. Finally, the foamed gypsum was poured into a mould of 250 × 200 ×13 mm and cured at 90 °C for 48 h.

Table 4.1 Mix proportions of gypsum board with or without PCM.

Sample	CSH (g)	FSPCM (g)	Water (ml)		Non-water components (g)			
			Gauge water	Foam water	Accelerator [a]	Glass fibres	Retardant [b]	Foaming agent [c]
Gypsum board	715	–	257	358	1.61	4.6	0.11	0.46
FSPCM board	511	204	184	256	1.15	3.3	0.08	0.33

[a] Potassium sulfate; [b] Polyacrylic acid; [c] Alkyl sulfate oligomers.

4.2.2. Stability of FSPCM in CSH composites

The FSPCM incorporated CSH composites were produced by mixing FSPCM with CSH and water, as presented in section 4.2.1. No other additives were used so that the stability of the FSPCM/CSH composite would be examined in a relatively simple system. The CSH to FSPCM ratio was chosen to be 2.5, and the water to CSH ratio was 0.86, according to Table 4.1. The stability of FSPCM in CSH was first assessed by visual examination of PCM leakage in FSPCM incorporated CSH composite stored in clear cylindrical vessels. This presented a qualitative analysis of PCM leakage for FSPCM integrated CSH composite. The exudation stability of FSPCM/CSH composite was also studied by diffusion-oozing circle testing [62], in which filter paper was used to determine PCM exudation from the FSPCM. To evaluate the leakage, the hardened FSPCM/CSH composite

with dimensions of $50 \times 50 \times 40$ mm was placed on the centre of the filter paper. The composite was then placed in an oven as shown in Fig. 4.1 and heated for 6 h above the PCM's melting temperature (40 or 70 °C), then any PCM leakage could be observed from stains on the filter paper.

Fig. 4.1. Specimens subjected to leakage testing at 40 and 70 °C.

4.2.3. Thermal performance of FSPCM gypsum board

The produced gypsum board without PCM is shown in Fig. 4.2a and the one with FSPCM is shown in Fig. 4.2b. To evaluate the thermal/energy performance of gypsum board, a test setup as shown in Fig. 4.2c and 4.2d was used. The experimental design consists of two similar chambers with an external dimension of 290 × 240 × 20 mm and an internal dimension of 230 × 180 × 165 mm. The walls and floors of the chambers were made from expanded polystyrene insulating material. The gypsum board with FSPCM was used as the cover of one chamber to check its thermal regulating performance as a ceiling. For comparison purposes, the other gypsum board without PCM was used to cover the other chamber. The two chambers were placed outside from 26 to 28 January 2019 (summer season in Sydney) and exposed to natural solar heating and cooling processes during day and night time. Two T-type thermocouples were used to measure the temperature variations at two different locations in a chamber (internal surface of the gypsum board and centre of the chamber), and the temperatures were recorded every 10 s by using a data logger (PCE-T 1200).

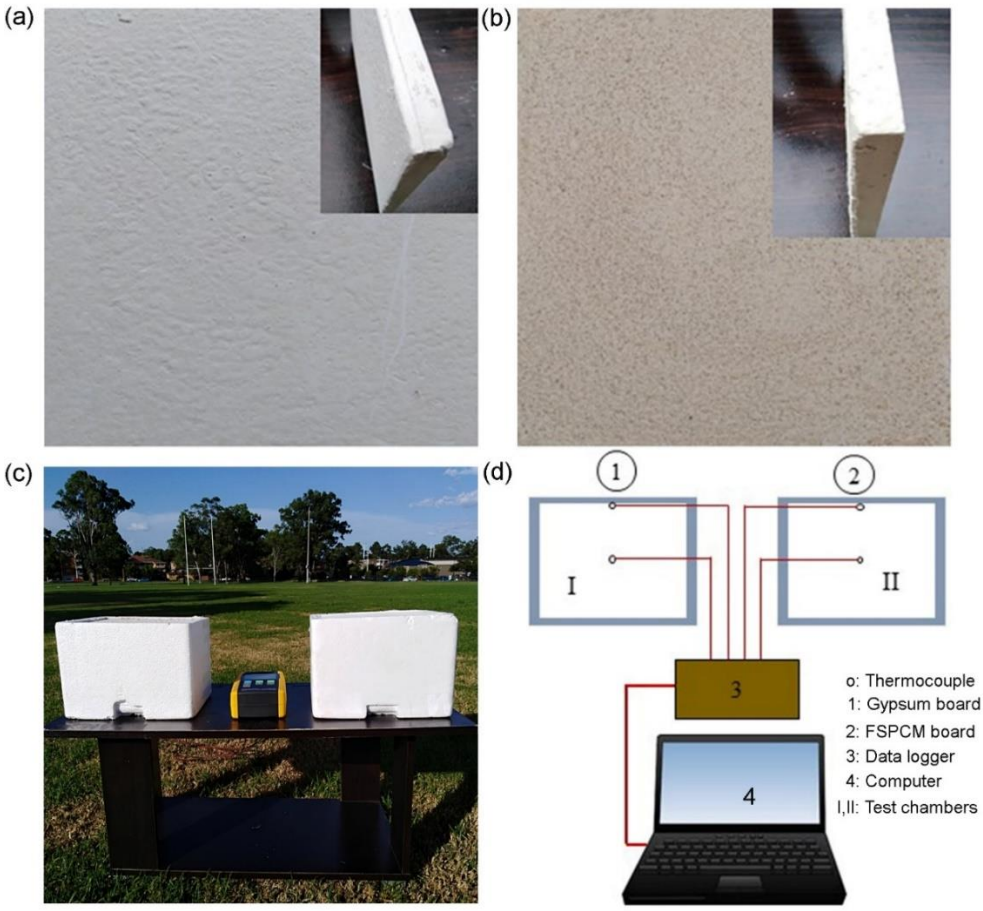

Fig. 4.2. Produced gypsum board and test setup for thermal/energy performance evaluation: (a) gypsum board; (b) gypsum board with FSPCM; (c) photo of test setup; and (d) sketch of test setup.

To analyse the effect of the FSPCM-enhanced gypsum board on test chambers' thermal and energy performance, three performance parameters based on the experimental data are quantified: heat flux by the FSPCM gypsum board ceilings, the energy consumption of the test chamber and energy-saving fraction.

4.2.3.1. The heat flux of FSPCM gypsum board

The heat is mainly transferred from the internal surface of the ceiling to the indoor air of the test chamber through natural convection. The convective heat flux of the interior surface of the gypsum board ceiling can be calculated using Eq. (4.1) [145]:

$$q_{\text{conv}} = h_{\text{natural}}(T_{\text{s}} - T_{\text{a}}) \tag{4.1}$$

where q_{conv} is the convective heat flux (W/m^2); T_{s} and T_{a} (in °C) are the internal surface temperature of the gypsum board and the inside air temperature of the test chamber, respectively; and h_{natural} is

the convection heat transfer coefficient (CHTC) of the ceiling. The value of CHTC is highly dependent on the surface to air temperature difference [146]. An average CHTC value of 4.8 W/m^{2}K was determined for ceilings with a surface to air temperature difference between 0.5 and 5 ℃ [147]. Therefore, the h_{natural} value is taken as 4.8 W/m^{2}K in this paper as the surface to air temperature difference of the chamber is in this range.

4.2.3.2. The energy consumption of the test chambers

The energy consumption of the test chamber is evaluated with empirical formulas [130, 148]. The cooling energy consumption of the test chamber can be calculated by Eq. (4.2) [130].

$$Q = \sum_{j=1}^{n} \frac{(U_i A_i + 0.33NV)}{\eta} \frac{24}{1000} (T_j - T_i) \text{ if } T_j > T_i \quad (4.2)$$

where U_i and A_i are the heat transfer coefficient (W/m^2.K) and area of the i^{th} element of the building envelope (m^2), respectively; N is the air changes per hour (ACH) in h^{-1}, taking as 0.25 h^{-1}; V is the volume of the house (m^3), η is the efficiency of the cooling system, taking as 2.5 [145], T_j is the mean daily indoor temperature (°C) in day j and T_i is the designed indoor air temperature in summer, taking as 26 ℃. In the calculation, the U-values are taken as 0.86 W/m^{2}K for the expanded polystyrene wall, 4.25 W/m^{2}K for the gypsum board ceiling, and 3.89 W/m^{2}K for the FSPCM gypsum board ceiling [130].

4.2.3.3. The energy saving fraction

The energy saving fraction (ESF) can then be determined from Eq. (4.3).

$$ESF\ (\%) = \left(1 - \frac{Q_{\text{FSPCM}}}{Q_{\text{Ref}}}\right) \times 100 \quad (4.3)$$

where Q_{Ref} and Q_{FSPCM} are the energy consumptions of the reference and FSPCM chambers, respectively.

4.2.4. Economic feasibility of FSPCM gypsum board

A life-cycle cost analysis (LCCA) is conducted to evaluate the economic feasibility of FSPCM gypsum board to be used as building false ceiling [149]. The interest rate (i), inflation rate (φ) and life-time (n) of gypsum board are considered in the analysis, where the present value is adjusted based

on the method proposed by Cuce et al. [150] to account for the interest and inflation rates. The LCCA is conducted following the procedure adopted by Daouas et al. [151].

The annual cooling cost for a test chamber is calculated by Eq. (4.4).

$$C_{\text{Ref}} = C_{\text{e}} D\ Q_{\text{Ref}} \quad \text{for reference chamber} \tag{4.4a}$$

$$C_{\text{FSPCM}} = C_{\text{e}} D\ Q_{\text{FSPCM}} \quad \text{for FSPCM chamber} \tag{4.4b}$$

where C_{Ref} and C_{FSPCM} are the annual cooling costs of the reference and FSPCM chambers, respectively; C_{e} is the cost of electricity in AUD$/kWh, taking as 33.33 c/kWh [152]; *D* is the number of hot days every year to operate an air conditioning system for cooling a building interior, taking as 120 days in view of the climatic conditions in Penrith, Australia [126]; and Q_{Ref} and Q_{FSPCM} are the daily energy consumptions of the reference and FSPCM chambers, respectively, determined by Eq. (4.2).

To convert the total cooling cost over a life-time of *n* years into present value, the present worth factor (*PWF*) needs to be calculated using Eq. (4.5) [150].

$$PWF = \frac{(1+\tau)^n - 1}{\tau(1+\tau)^n} \tag{4.5}$$

where *n* is the lifetime of ceiling board, taking as 10 years; and τ is a factor related to the interest rate (i) and inflation rate (φ), taking as 1.5% and 2.25%, respectively [52]. According to Cuce et al. [150], the τ–factor is given by Eq. (4.6).

$$\tau = \frac{i-\varphi}{1+\varphi} \quad (\text{if } i > \varphi) \tag{4.6a}$$

$$\tau = \frac{\varphi-i}{1+i} \quad (\text{if } i \le \varphi) \tag{4.6b}$$

The life cycle cost of cooling (C_{T}) for a chamber is given by Eq. (4.7).

$$C_{\text{T,Ref}} = C_{\text{i,Ref}} + C_{\text{Ref}} \times PWF \quad \text{for reference chamber} \tag{4.7a}$$

$$C_{\text{T,FSPCM}} = C_{\text{i,FSPCM}} + C_{\text{FSPCM}} \times PWF \quad \text{for FSPCM chamber} \tag{4.7b}$$

where $C_{\text{i,Ref}}$ and $C_{\text{i,FSPCM}}$ are the capital costs of gypsum board without and with FSPCM, respectively. In this study, $C_{\text{i,Ref}}$ and $C_{\text{i,FSPCM}}$ are taken as $4.00 and $9.00 per m^2 respectively, which are estimated based on the wholesale material prices obtained from the suppliers.

Hence, the energy-related savings (*ERS*) for using FSPCM gypsum board are calculated from Eq. (4.8).

$$ERS = (C_{\mathrm{T,Ref}} - C_{\mathrm{T,FSPCM}}) \tag{4.8}$$

Finally, the payback period defined as the required time length to repay the cost of the FSPCM investment can be calculated from Eq. (4.9) [150].

$$\text{Payback period} = \left(\frac{C_{\mathrm{i,FSPCM}} - C_{\mathrm{i,Ref}}}{ERS}\right) \times PWF \tag{4.9}$$

4.3. Results and discussion

4.3.1. Stability of PCM and FSPCM in CSH composites

The stability of pure PCM and FSPCM in the calcium sulphate hemihydrate (CSH) mixture was characterised through leakage tests, where PCM (Fig. 4.3b) or FSPCM (Fig. 4.3c) was mixed with CSH (Fig. 4.3a) and a suitable amount of water. In the fresh slurry, a layer of liquid PCM appeared on the top of the mixture, as shown in Fig. 4.3d. However, no leakage of PCM was found when FSPCM was used, as evidenced in Fig. 4.3e.

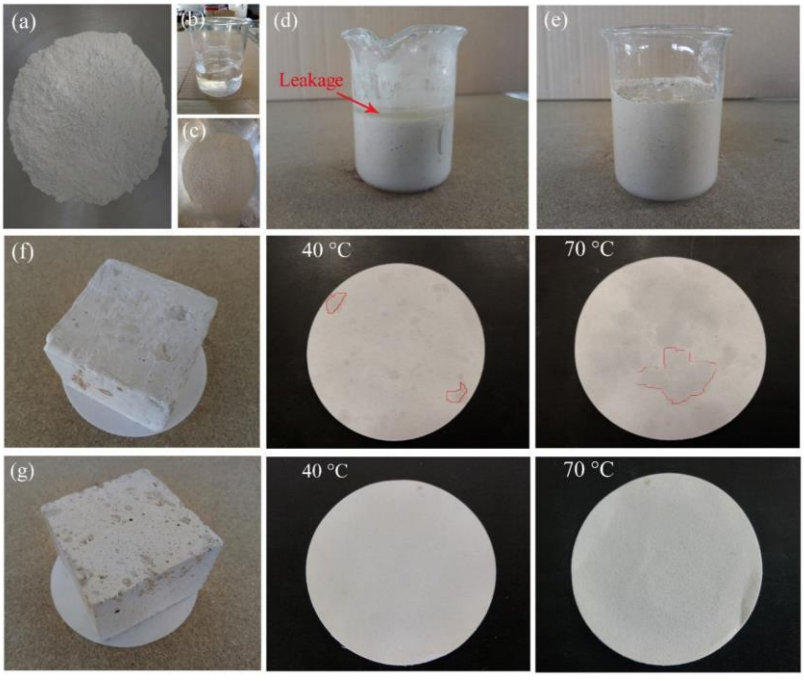

Fig. 4.3. Stability of form-stable PCM composites in gypsum board: (a) CSH, (b) liquid PCM, (c) FSPCM, (d) fresh slurry with pure PCM, (e) fresh slurry with FSPCM, (f) hardened sample with pure PCM, and (g) hardened sample with FSPCM.

PCM leakage also occur in hardened gypsum board during the phase change process. To prove this, hardened samples with pure PCM (Fig. 4.3f) and FSPCM (Fig. 4.3g) were placed on filter paper and put in an oven. The samples were kept in the oven for 6 h at a temperature of 40 or 70 °C (Fig. 4.1), which is above the melting temperature of the PCM. Any leakage of PCM would leave oily stains on the filter paper. After the testing, it was found that PCM leakage occurred for the sample containing pure PCM, as can be seen in Fig. 4.3f. To clearly show the PCM leakage, some stained areas were marked in the subfigure. In contrast, no visible trace of PCM leakage was found for the sample with FSPCM (Fig. 4.3g). It is also confirmed that there is no weight difference of the filter paper before and after the test. From the experiments, it can be concluded that the use of diatomite can eliminate leakage of PCM in gypsum board.

4.3.2. Thermal regulating performance of FSPCM gypsum board

The thermal performance of the gypsum board with or without FSPCM was evaluated by examining the indoor air temperatures of the miniaturised test chambers for three consecutive days (26–28 January 2019). The environmental temperatures are depicted in Fig. 4.4a and the measurement started at 12:00 am (midnight) on 26 January 2019. As day 1 was clear, day 2 partly cloudy, and day 3 overcast, the measured peak temperature decreased from 46.3 °C in day 1 to 38.7 °C in day 3. The variations in the interior surface temperature of the ceiling and the indoor air temperature of the test chamber are presented in Fig. 4.4b and 4.4c, respectively. As can be seen from Fig. 4.4b, the peak temperatures of the inside surface of the FSPCM ceiling are significantly lower than those of the reference ceiling without PCM. The differences are 8.9, 8.8 and 3.4 °C in days 1, 2 and 3, respectively. Meanwhile, as shown in Fig. 4.4c, the peak air temperature inside the chamber with a FSPCM ceiling is also reduced by an average of 3.5 °C in three days and a maximum of 4.9 °C in day 1 when compared with the chamber with normal gypsum board ceiling. As day 3 was overcast and the maximum temperature was only 38.7 °C, the PCM could not be fully activated. However, the temperatures for day 1 and day 2 exceeded the PCM's peak temperature. So, the PCM was fully activated in both days. Therefore, comparing with day 1 and day 2, the performance of the

FSPCM board is insignificant in day 3. The results indicate that the use of FSPCM ceiling is advantageous for building space cooling, thus keeping a comfortable indoor thermal environment. This is consistent with previous studies on PCM gypsum board. For example, Sari et al. [153] examined the thermal response of gypsum board with eutectic mixture of capric acid and stearic acid in a laboratory scale test room, and reported that the peak indoor temperature was reduced by 1.3 °C. In another study, a reduction of 3.1 °C in the peak indoor temperature was reported by Karaipekli et al. [154]. Compared with test results reported in the literature, it seems that the current gypsum board with FSPCM is more effective for building space cooling, which may be due to its high phase change latent heat (>110 J/g) and the high environmental temperatures.

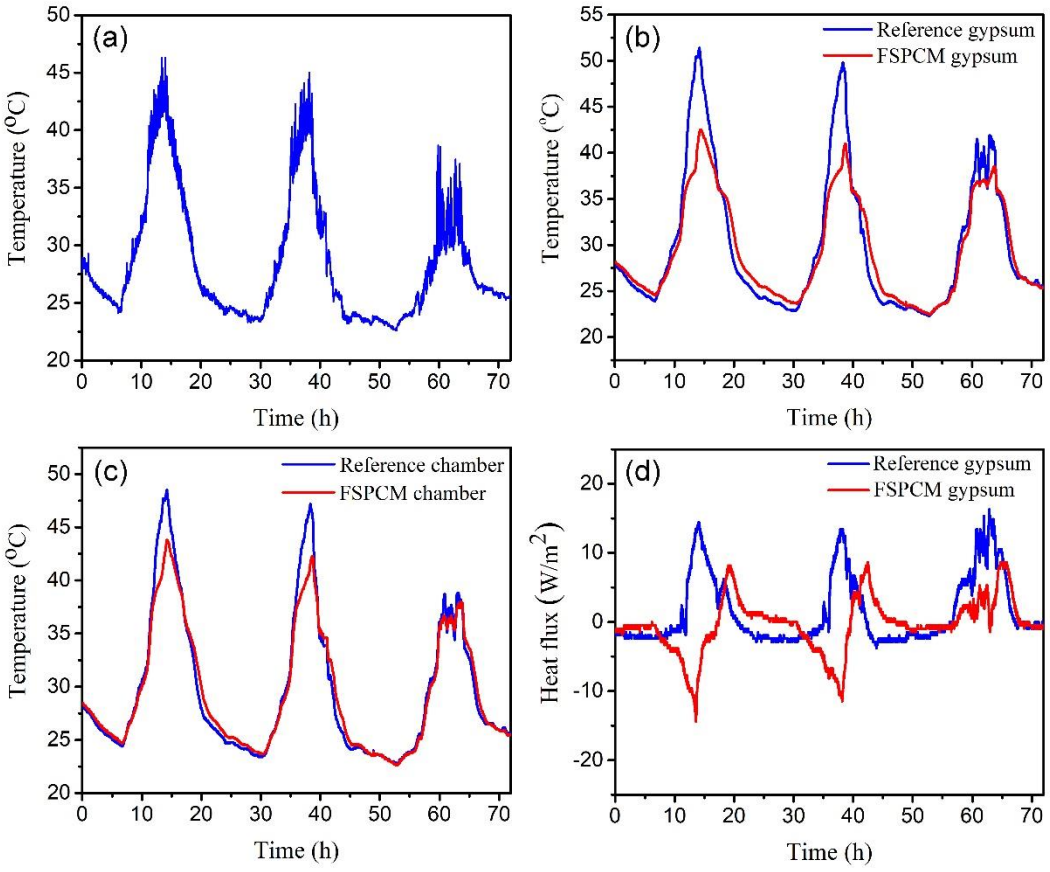

Fig. 4.4. Measured data for gypsum board roof ceiling: (a) environmental temperatures from 26–28 January 2019, (b) inner surface temperatures of gypsum board, (c) inside air temperatures of the test chamber, and (d) heat flux of inner surface of gypsum board ceiling.

The influence of FSPCM on the calculated convective heat flux of the interior surface of the gypsum board ceiling is shown in Fig. 4.4d. The FSPCM gypsum board has sharp negative and

positive heat flux peaks while the normal board only has positive peaks. Meanwhile, a reduction in the positive heat flux fluctuation amplitude and a delay in the heat flux peak are evident for the FSPCM gypsum board. The results suggest that the FSPCM absorbed solar radiation and converted the radiation into thermal energy to improve the indoor thermal environment.

4.3.3. Effect of FSPCM on cooling load

The application of FSPCM gypsum board as ceiling of a building can reduce the energy consumption for cooling in hot summer periods. To determine the possible energy saving for using FSPCM gypsum board ceiling, the energy consumption to cool the test chamber is compared with that to cool the other chamber with reference gypsum board. The evaluation is conducted based on the three-day weather conditions shown in Fig. 4.4a, as they represent hot and sunny days, hot and partly cloudy days and overcast days. As shown in Fig. 4.4c, the inside air temperatures were used to calculate the cooling energy consumptions for reference and FSPCM chambers.

The saving in energy with respect to the space cooling of the test chambers can be clearly seen in Table 4.2. The total amount of energy consumed to cool the internal space of the reference chamber is 0.0790 kWh during the three days. However, the energy consumption is reduced to 0.0662 kWh if FSPCM gypsum board is used. Therefore, the net energy saving is 0.0043 kWh/day, or a saving of 16.2% in cooling energy for the use of FSPCM gypsum board ceiling.

Table 4.2 Energy consumption and energy saving fraction.

Day	Energy consumption (kWh)		Energy saving/day (kWh)	Average energy saving/day (kWh)	ESF (%)
	Reference chamber	FSPCM chamber			
1st day	0.0267	0.0214	0.0053		
2nd day	0.0312	0.0251	0.0061	0.0043	16.2
3rd day	0.0211	0.0197	0.0014		

4.3.4. Economic feasibility of FSPCM gypsum board

A shorter payback period is usually more desirable for any investment, as it is the main determining factor for investment. The results of the life-cycle cost analysis are given in Table 4.3. According to the evaluation, the payback period by the inclusion of FSPCM is only 1.7 years. This is relatively short due to the effectiveness and low cost of the developed FSPCM.

Li et al. [145] also conducted small chamber tests to assess the feasibility of incorporating PCM in glazed roof, where PCM (about 1.8 kg) was poured into the closed cavity between two panes of glass. They reported that the PCM melting temperature has a great influence on energy saving and payback period. Through an economic feasibility analysis, they found that the annual energy cost saving increases from CNY 5 to CNY 67 and the corresponding payback period decreases from 6.2 to 3.3 years, when the PCM melting temperature changes from 18 to 32 °C. As can be seen, the PCM payback period (a minimum of 3.3 years) in [145] is longer than the payback period (1.7 years) of the FSPCM developed in this study. Since the environmental temperatures and uses of PCM are different, it is difficult to make a direct comparison on payback period. However, two reasons may be primarily responsible for the lower payback period of the FSPCM gypsum board in this study: (1) The paraffin wax used in [145] is much more expensive (~AUD $6.43/kg) than most other types of PCM [155]. In contrast, PCM used in this study is much cheaper, which is AUD $2.1/kg on a wholesale basis; and has a higher melting temperature and larger latent heat than those of the PCM used in [145].

Table 4.3 Results of life-cycle cost analysis.

Item	Capital cost (AUD$)	Total life-cycle cost (AUD$)	Net ERS (AUD$)	Payback period (year)
Reference gypsum board	0.20	10.33	1.4	1.7
FSPCM gypsum board	0.45	8.93		

4.4. Concluding remarks

This chapter reported the development of a foamed gypsum board by incorporating 40 wt% of FSPCM for potential application in building ceiling. The FSPCM was first characterized for thermal stability in CSH. This was followed by the development of FSPCM-enhanced gypsum board and the study of its thermal storage performance compared to the control gypsum board (without FSPCM). The FSPCM gypsum board's efficiency for cooling load reduction in summer was evaluated in a miniaturized test chamber. Based on the experimental study, the following conclusions can be drawn:

(i) The FSPCM showed good thermal stability in CSH. A significant amount of PCM leakage was observed when pure PCM was incorporated into CSH, while no trace of PCM leakage was observed for FSPCM.

(ii) The thermal performance test results show that the peak air temperature inside the chamber with a FSPCM ceiling was reduced by a maximum of 4.9 °C in the first day and an average of 3.5 °C in three days compared to the results of the chamber with a typical gypsum board ceiling.

(iii) The use of FSPCM in gypsum board ceiling is economically feasible with cooling load savings of 16.2% and a payback period of 1.7 years.

The gypsum board containing FSPCM can easily replace typical building false ceiling for energy conservation in real buildings. It should be noted that this study only used a small-scale test chamber to evaluate the performance of the FSPCM gypsum board. Undoubtedly, the test chamber results provide useful information for assessing the FSPCM's performance in real buildings. However, successful use of the FSPCM in real buildings depends on many factors, such as properties and amount of FSPCM used, location of the FSPCM, building ventilation conditions, building design and orientation, local climate, and occupants' behaviour, etc. [156]. Further studies should be conducted to integrate the FSPCM into real buildings' envelope for energy conservation and evaluate the building performance under various conditions. Analysis can then be undertaken to assess the life-cycle cost and energy savings of using FSPCM in real buildings.

CHAPTER 5

Experimental and numerical study of thermal management for form-stable PCM enhanced board used in building envelopes

5.1. Introduction

In the previous chapter, the thermal energy storage technology using FSPCM-integrated gypsum board (FSPCM board) with a melting temperature of 36.8 °C fitted into ceilings was presented as one of the more promising solutions to decrease the energy demand of houses by improving their indoor thermal comfort. Due to its high melting temperature, this FSPCM board is not suitable for the houses' interior finishing applications. The FSPCM-enhanced gypsum board (FSPCM board) was experimentally tested in a small-chamber in Chapter 4; in contrast, the FSPCM board was applied as an internal furnishing material to the walls and ceiling in a model house in this chapter (Chapter 5). This study deals with an experimental and numerical study of the thermal efficiency performance of a new FSPCM board containing PCMs' melting temperature at 26 °C, that can be used for the inner surface of the walls and ceiling. The FSPCM boards applied to the inside of the walls and ceiling were field-tested to assess the thermal performance of the test houses. One test house without FSPCM board was used as a control. A simulation model based on EnergyPlus was developed and verified by the experimental test results. This model was then used to conduct the parametric analysis to further study the influence of PCM melting temperatures, FSPCM board thickness, and natural ventilation on the thermal/energy performance of the model house. The economic benefits of using the FSPCM board in each case through a life cycle cost analysis is also evaluated in this chapter.

5.2. Experimental investigation

5.2.1 Test program

The experimental study was performed using two identical fully instrumented steel framed model houses with dimensions of 940 mm × 690 mm × 450 mm and designed to operate separately. The

model houses were built by lightweight materials and each with an east facing single-pane window with dimensions of 300 mm× 300 mm as well as a west facing door with dimensions of 300 mm × 390 mm. The steel plate sandwich expanded polystyrene (EPS) with a thickness of 50 mm was used on the vertical walls, floor and roof of the houses. The thickness of the steel sheet was 0.6 mm. A 35 mm thick EPS was also used in the ceiling of the houses. The schematic of the steel plate sandwich EPS and reference house are shown in Fig. 5.1. The physical properties of EPS and steel are shown in Table 5.1.

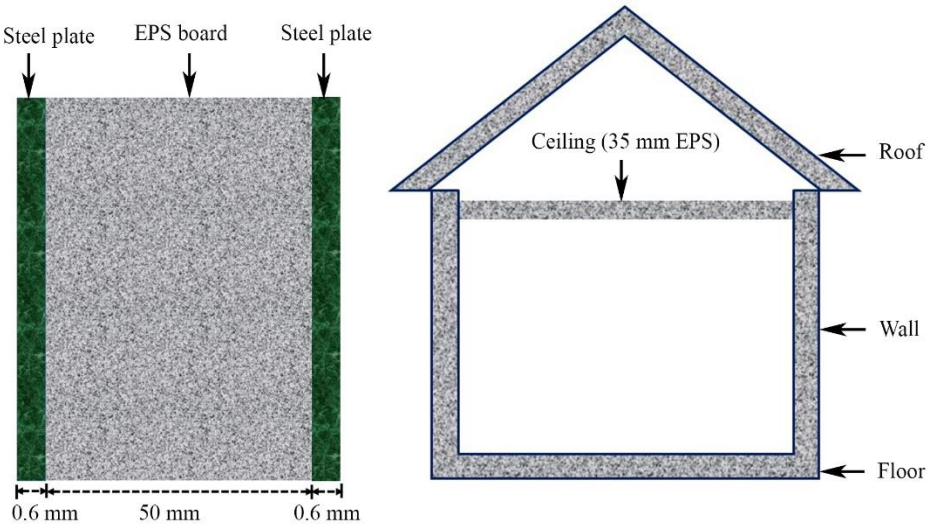

Fig. 5.1. The schematic of: (a) steel plate sandwich EPS, and (b) reference house.

Table 5.1 The physical properties of EPS and steel.

Material	Thickness (mm)	Density (kg/m^3)	Thermal conductivity (W/mK)	Specific heat capacity (J/kgK)
EPS insulation[a]	50	25	0.035	1400
Steel[b]	0.6	7850	46.6	452

Value suggested in [a][157] and [b][158]

The test house, referred to as 'PCM house' in this study, added FSPCM board inside the walls and ceiling. The other house, referred to as 'reference house,' is used as the base case without installing the boards. In our published article [22], PCM with a melting point of 36.8 °C was used to develop the FSPCM board for roof ceiling application. Due to the high melting temperature, this FSPCM board is not suitable for interior finishing applications. The roof attic is a good place to install this FSPCM board because it is a major source of heat gain, as the temperature in the attic could be

even 15–20 °C higher than the outdoor air temperature [22]. FSPCM board with a phase change temperature of 36.8 °C could then adequately reduce the temperature of the upper floors of a house. Hence, in the present study, the RT-26 with a melting temperature of 26 °C supplied by APACI Pty Ltd, Australia was used to prepare the FSPCM board for interior walls and ceiling finishing applications. In developing the FSPCM, diatomite was used as the supporting material. Detailed descriptions for the development of form stable PCM and their incorporation into gypsum board can be seen in our previous Chapter. The phase change properties of pure PCM and FSPCM were determined by DSC tests. The DSC measurement was conducted in an inert Ar gas atmosphere at a flow rate of 25 mL/min and a heating-cooling rate of 5 °C/min. Fig. 5.2 shows the DSC curves of the pure PCM (RT-26) and FSPCM and the obtained thermal properties are summarised in Table 5.2.

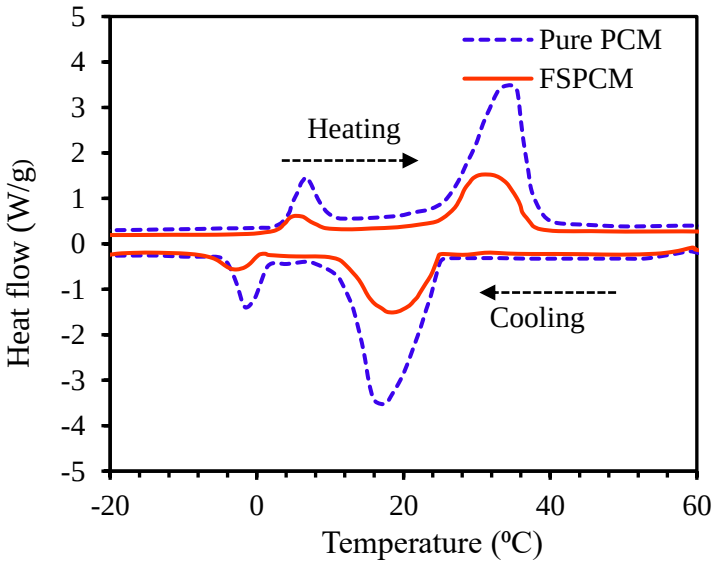

Fig. 5.2. Measured DSC curves of pure PCM (RT-26) and FSPCM.

As shown in Table 5.2, the PCM exhibits sharp endothermic and exothermic peaks with an onset melting temperature (T_m) of 26.1 °C and an onset solidifying temperature (T_s) of 25.6 °C. The FSPCM shows a negligible change of phase change temperatures (T_m of 26.2 °C and T_s of 25.5 °C) in comparison with the raw PCM. The melting and solidifying latent heats of the raw PCM are determined to be 184.5 and 184.1 J/g, respectively, while the corresponding values for FSPCM are 78.8 and 78.6 J/g. Therefore, the mass fraction of PCM in the FSPCM is found to be ~ 42.7%.

Table 5.2 Thermal properties of pure PCM (RT-26) and FSPCM.

Sample	Heating cycle		Cooling cycle	
	T_m (°C)	ΔH_m (J/g)	T_s (°C)	ΔH_s (J/g)
Pure PCM	26.1	184.5	25.6	184.1
FSPCM	26.2	78.8	25.5	78.6

Gypsum boards with 40 wt% of FSPCM were tested to measure the thermo-physical and mechanical properties, and the results are shown in Table 5.3. The morphology of the FSPCM board was examined by a scanning electron microscope (SEM JEOL 6510 LV). Fig. 5.3 shows the SEM photographs of FSPCM boards. The morphology of FSPCM is clearly observed in the boards. In Fig. 5.3(a,b), the FSPCM is uniformly dispersed and has interacted to form an FSPCM network in the boards. This means that heat can be transmitted from the outside to the inside of the boards through FSPCM, which leads to a quicker phase change.

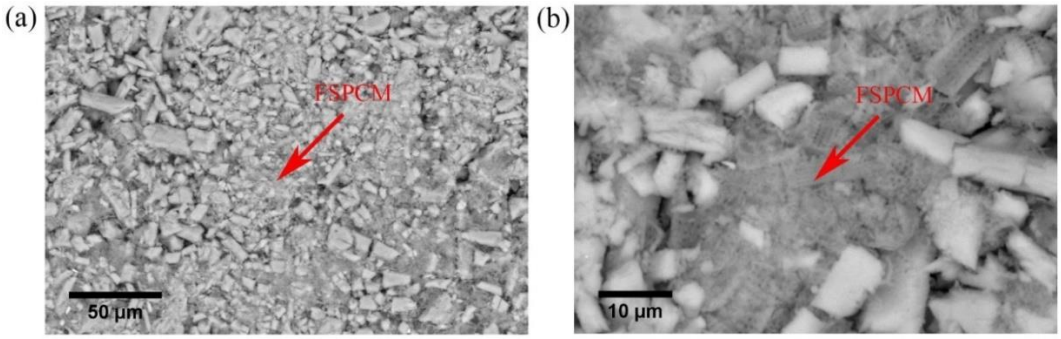

Fig. 5.3. SEM micrograph of FSPCM board: (a) low (left), and (b) high magnification (right).

The specific heat capacity and latent heat of the FSPCM board were determined by DSC test. The thermal conductivity was measured by a hot-disc thermal constant analyser (TPS 2500 S). The compressive strength was measured at the universal testing machine at a cross-head speed of 0.5 mm/min [159].

Table 5.3 Thermo-physical and mechanical properties of FSPCM board.

Thickness	15 mm
Density	530 kg/m^3
Heat storage capacity	19.9 J/g
Specific heat capacity	1984 J/kg.K
Thermal conductivity	0.43 W/m.K
Compressive strength	3.9 MPa

The test houses sit around 2 m apart from each other as shown in Fig. 5.4(a). The developed FSPCM boards were installed on the inner surface of the walls and ceiling, as shown in Fig. 5.4(b). The experimental tests that have been conducted for three selected cases to evaluate the effect of FSPCM boards on peak load shifting/reduction compared to the base case are as follows:

- Base/reference case: No FSPCM board
- Wall case: FSPCM board only used inside the walls
- Ceiling case: FSPCM board only used inside the ceilings
- Combined case: FSPCM board used inside both walls and ceilings

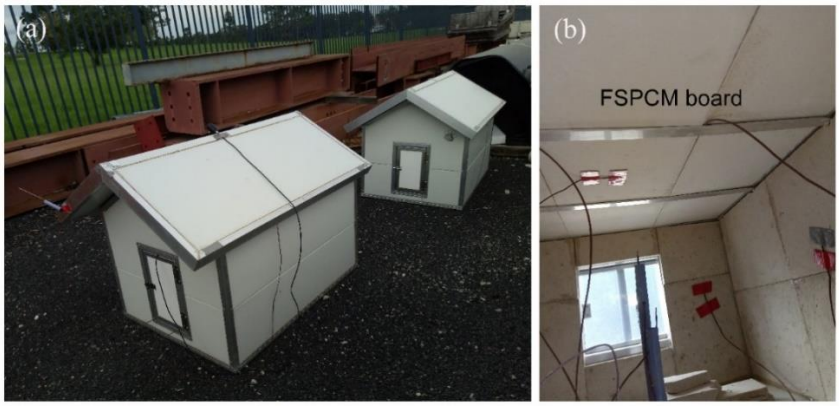

Fig. 5.4. The appearance of the model house and installation of FSPCM boards: (a) model house appearance, (b) FSPCM board installation on the walls and ceilings.

During the experiment, T-type thermocouples (accuracy ≤ ±0.5 °C) were used to continuously measure the outdoor temperature and indoor air temperature at the centre of a model house. A data logger (PCE-T 1200) was used to collect and record the temperature data every 60 s. Aside from this, a pyranometer together with data logger (HOBO Rx3000) was used for recording solar radiation data. The experiments were conducted on 24 February 2020 for the walls case, 18 March 2020 for the ceiling case, and 13 March 2020 for the combined case, respectively, in the Penrith Campus, Western Sydney University, Australia. The door and window always remained closed during the tests.

5.2.2. Test results analysis

The indoor air temperature of the model house with and without the FSPCM board, along with the ambient temperature, is shown in Fig. 5.5. It was observed that the reference house (without an

FSPCM board) showed large indoor temperature variations, and its maximum temperature values were over the ambient temperature. However, the house equipped with the FSPCM board had a narrow temperature variation and varied according to the FSPCM board's location, as reported in section 5.2.1 for each experiment. It is important to mention that in comparison to the reference house, the temperature curve for the house with FSPCM boards are right shifted. Compared to the reference house, the peak indoor air temperature is reduced by 4.2, 3.4, and 5.8 °C respectively in this study when FSPCM board has been placed on the walls, ceiling, and both walls and ceiling. Conversely, the minimum indoor temperatures of the house with FSPCM board are 0.8, 1.4 and 2.4 °C higher than that of the non-FSPCM board house. These phenomena indicate that the gypsum board incorporated with the FSPCM did fulfill their function of narrowing the indoor temperature swing.

As shown in Fig. 5.5, the indoor temperature changes in the house with the FSPCM board during the heating process showed a two-step behaviour. At the first step, when the temperature went through the phase transition temperature range (~26 °C), the PCM started to melt and stored solar energy in the form of latent heat. This resulted in decreasing the temperature's rising rate and reducing the heat from the FSPCM board integrated house in the daytime. After the PCM was fully melted, the indoor temperature rose at a faster rate, indicating an increasing solar heat gain for the indoor space. However, the heating peak lowered and shifted to a later time when compared to the reference house. A delay on the maximum peak temperature was observed in the PCM house by around 30, 64, and 71 min for the wall, ceiling, and combined cases compared to the reference house. During the cooling process, the opposite manner was noticed as the PCM released the stored heat through the phase transition process. The indoor air temperature in the PCM house decreased slower compared to that of the reference house. Hence, the former is always higher during the nighttime. These results indicate that the latent heat storage of the PCM reduces indoor air temperature fluctuation and improves thermal comfort. From these experimental results, it is observed that the integrated FSPCM in the gypsum board is appropriately working, storing the heat from peak hours during daytime and releasing it later once the temperature is dropping.

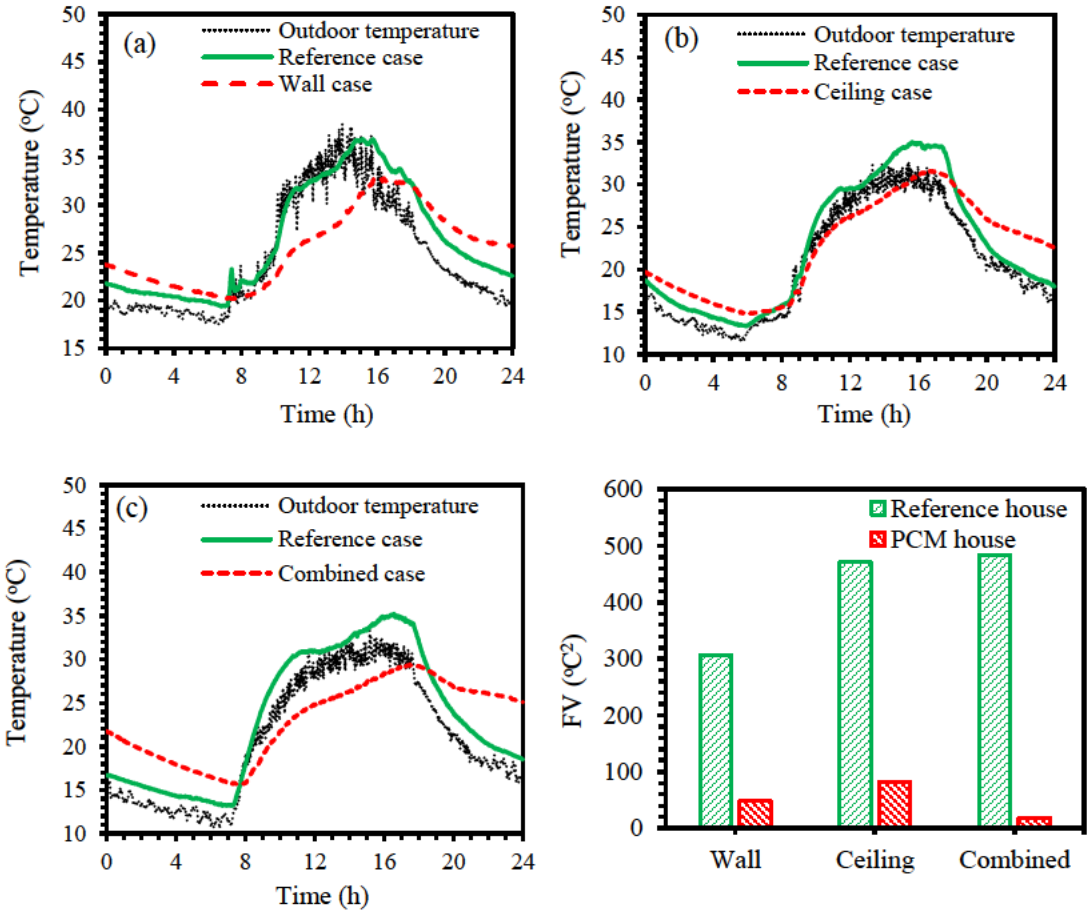

Fig. 5.5. Variation of indoor air temperatures of the houses for both the PCM case and base case: (a) walls case (24 February 2020), (b) ceilings case (18 March 2020), and (c) combined case (13 March 2020); (d) the indoor temperature fluctuation variations.

The results of this study have been compared with those previous studies reported in the literature [160-168], and a comparison of peak temperature reduction and shifting results is shown in Table 5.4. A significant impact is observed by applying the FSPCM board in both walls and ceilings, providing a decrease of peak indoor air temperature of 5.8 °C, which is much higher than that of the reported values in the literature as shown in Table 5.4. This is due to the open-pore type supporting diatomite materials' porosity and pore size influencing the PCM melting and solidification processes [169, 170] as shown in Chapter 3, which significantly improves the efficiency of the FSPCM board.

Table 5.4 The peak temperature reduction and shifting –literature review.

Object configurations and PCM type		Peak temperature reduction (°C)	Peak shifting (min)	Reference
Two 1.83 m ×1.83 m × 1.22 m test rooms. Macro-encapsulated PCM frame walls (90 mm, T_m = 25 °C, 20% of macro-encapsulated PCM).		0.46	60	[164]
An outdoor test room with a dimension of 2.82 m × 2.22 m × 2.24 m. The PCM–gypsum board attached on the vertical walls of the room (13 mm, T_m = 17-22 °C, 25% of PCM).		4.0	-	[162]
Test room 3.9 m × 3.3m × 2.7 m. The PCM-gypsum board attached inside of the walls and ceiling (30 mm, T_m = 21 °C, 25% of PCM).		1.0	-	[163]
Two 1.7 m × 1.7 m × 2.1 m test rooms. The shape-stabilised PCM (SSPCM) based wallboard attached inside of the walls and ceiling (20 mm, T_m = 25.22 °C, 95% of SSPCM).		2.8	80	[167]
Bricks cubicle 2.4 m × 2.4 m × 2.4 m. The PCM panels attached between the bricks and polyurethane in the southern and western walls and the roof (T_m = 28 °C, RT-27 PCM).		1.0	-	[166]
A test room with a dimension of 3.9 m × 3.3 m × 2.7 m. The SSPCM plates are attached to inner surfaces of four walls and the ceiling as linings (20 mm, T_m = 26 °C, 80% of PCM).		2.0	-	[165]
Concrete cubicles with a dimension of 2.0 m × 2.0 m × 2.0 m. Micro-encapsulated PCM incorporated concrete wall panels (12.0 mm, T_m = 26 °C, 5% of microencapsulated PCM).		3.0	120	[161]
Brick wall test rooms with a dimension of 2.0 m × 2.0 m × 2.4 m. Aluminium plates sandwiched PCM panels on the inside surface of the walls and roofs (11 mm, T_m = 26.5 °C)		2.3	180	[160]
Two concrete cubicles have the same dimensions of 2.4 m × 2.4 m × 2.4 m. Microencapsulated PCM integrated concrete wall panels (12 mm, T_m = 26 °C, 5% of microencapsulated PCM).		2.0	-	[168]
Two identical model houses with a 940 mm × 690 mm × 450 mm. The FSPCM board are attached on the inner sides of:	(i) the walls	4.2	30	Present work
	(ii) the ceiling	3.4	64	Present work
	(iii) the walls and ceiling	5.8	71	Present work

A large indoor air temperature fluctuation can reduce indoor thermal comfort of residents. The results obtained in this study demonstrate a smaller daily indoor temperature fluctuation of the FSPCM house than the reference house in all cases. Therefore, the use of FSPCM board has the potential to improve the residents' indoor thermal comfort. The fluctuation variance (*FV*) of indoor temperature is used to evaluate the indoor temperature fluctuation, as shown in Eq. (5.1) [102]:

$$FV\ (°C^2) = \{(t_p - t_0)^2\} \tag{5.1}$$

where *FV* is the variance ($°C^2$), t_p and t_0 are the indoor peak temperature and the minimum temperature the following day at 12:00 AM in °C, respectively. Taking these days, as mentioned in section 5.2.1 for example, the *FV* results in the reference and PCM house for three different cases are shown in Fig. 5.5(d). The *FV* value of the PCM house is much lower than that of the reference house. Compared to the reference house, the *FV* in the PCM house is reduced by 84.0, 82.8, and 96.2% for the wall, ceiling, and combined cases. Hence, it is concluded that the FSPCM board had a significant thermal performance in reducing indoor temperature fluctuation and improved thermal comfort.

5.3. Numerical simulation

As demonstrated in section 5.2.2, using the FSPCM board can reduce the peak indoor air temperature in hot summer days and improve the indoor thermal comfort. Thus, the FSPCM board has the potential to reduce energy consumption for indoor applications. However, the experimental optimisation of the FSPCM board through parametric analysis in the houses is time-consuming, relatively expensive and often impractical. Therefore, a simulation model based on EnergyPlus was developed, verified by experimental results, and used to conduct the parametric analysis.

5.3.1. Numerical model

The model house described in section 5.2.1 was considered as a case study and EnergyPlus software was used to model the test house. EnergyPlus is one of the most flexible and reliable building energy simulation tools, first released in April 2001 by the U.S. Department of Energy. It is a highly accredited software that has been widely used to assess the thermal performance of houses integrated

with PCM [20]. The EnergyPlus PCM model simulation was performed using a one-dimensional conduction finite-difference (CondFD) solution algorithm. To avoid errors, the time step of the simulation was set to 180 seconds, as recommended by Tabares-Velasco et al. [171]. The inside and outside surface convective heat transfer algorithms were considered from EnergyPlus TARP and DOE-2, respectively. For the PCM model, the CondFD algorithm was combined with the enthalpy-temperature function shown in Eq. (5.2) that the user would input to estimate the enthalpy changing during phase change. The enthalpy-temperature function was used to create an equivalent specific heat (C_p) at each time step, according to Eq. (5.3).

$$h = h(T) \tag{5.2}$$

$$C_p(T) = \frac{h_i^j - h_i^{j-1}}{T_i^j - T_i^{j-1}} \tag{5.3}$$

where C_p (T) is the specific heat as a function of temperature, h and T are the enthalpy node and temperature node. The enthalpy–temperature graph for the FSPCM gypsum board for this study is shown in Fig. 5.6.

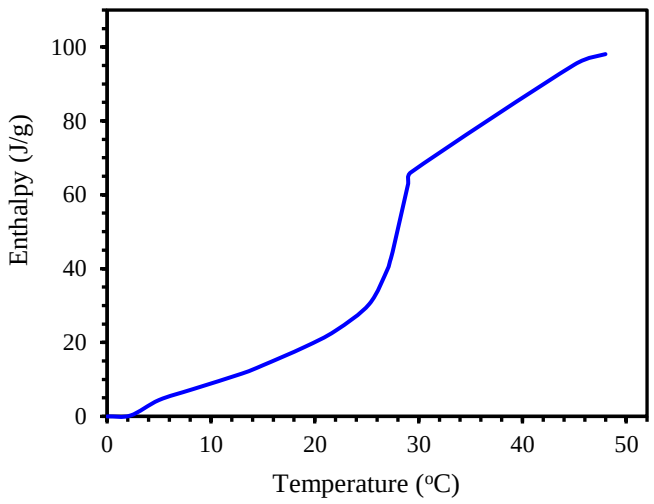

Fig. 5.6. Enthalpy curves as a function of temperature for FSPCM board.

The experimental test data was used to produce the boundary conditions for the simulation including thermo-physical properties of EPS, steel, FSPCM board, solar radiation, dry-bulb temperature and humidity. The house is closed and directly exposed to outdoor environment. The window is single glazed with a U value of 5.68 W/(m^2 °C). The solar heat gain coefficient and visible

transmittance of the window are taken as 0.855 and 0.901, respectively [172]. These values are used in the EnergyPlus simulation. In the parametric analysis of PCM with a different melting temperature, the enthalpy–temperature graph is shifted according to the melting temperature.

5.3.2. Validation of the model

To verify the simulation model's accuracy, the experimental data in the literature [95] were selected for validation. The building geometry and operating conditions were selected according to their experimental study. Fig. 5.7 shows that the simulation results are in very good agreement with the experimental data.

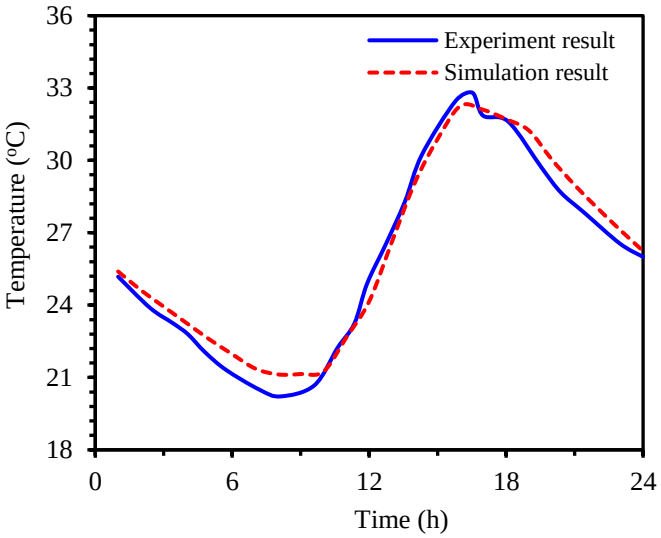

Fig. 5.7. Experimental and simulated zone air temperature.

The entire multi-layered construction capacity of EnergyPlus is held so that simulations can be performed with the FSPCM boards' placement in any location within the building envelope [173]. The CondFD algorithm for simulation of PCM has been validated again with our experimental results. The results for simulation and experimentation are shown in Fig. 5.8. A good agreement was obtained between the experimental data and simulated indoor air temperature results for two successive days in summer. Additionally, statistical indices, namely percentage of root-mean-square error (PRMSE) were used for error analysis of the simulated results. The definitions of PRMSE are given by Eq. (5.4) [174].

$$PRMSE = \sqrt{\frac{1}{n}\sum_{i=1}^{n}\left(\frac{S_i - E_i}{E_i}\right)^2} \quad (5.4)$$

where E_i and S_i are the experimental and simulated temperature values at hour i, respectively. By using the hourly temperature data, the obtained PRMSE value is 5.2% for walls case, 5.3% for ceiling case and 3.5% for combined case. These PRMSE values are within the limit of ±30% specified by the ASHRAE Guideline 14 for indoor air temperature [175]. Therefore, the simulation model has acceptable accuracy for simulation of PCM's.

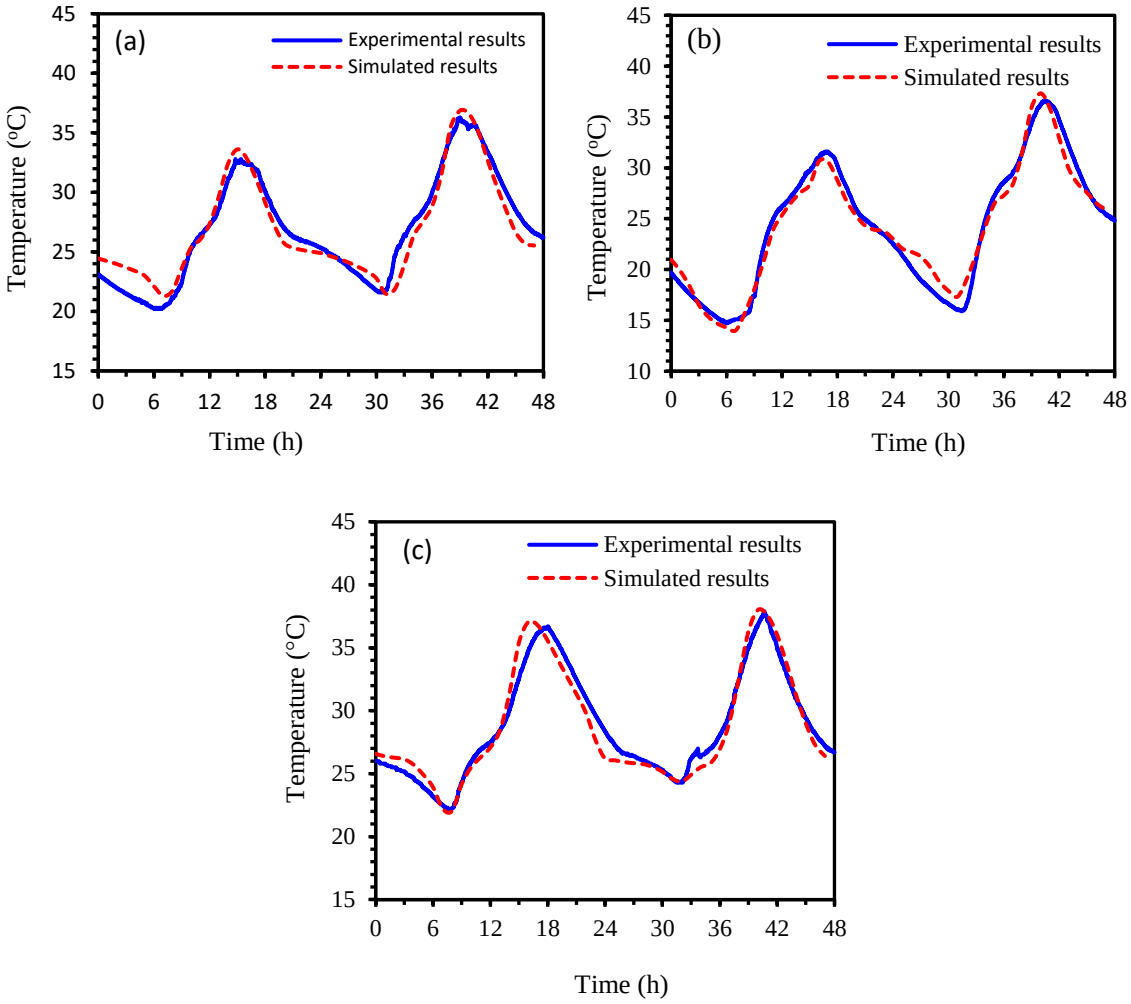

Fig. 5.8. Hourly indoor air temperatures of the experimental and simulated models: (a) walls case (24-25 February 2020), (b) ceilings case (18-19 March 2020) and (c) combined case (01-02 March 2020).

5.3.3. Parametric analysis

Parametric studies were performed to show the influential factors that govern FSPCM boards' performance for peak temperature reduction and improve thermal comfort during summer periods. The same model house and simulation period (one day on 24 February 2020) were adopted to conduct

the parametric analysis. The ambient air temperature and solar irradiations on this day are illustrated in Fig. 5.9. To evaluate the influence of PCM melting temperature on thermal performance, PCMs with melting temperatures between 23 °C and 29 °C at 1 °C interval was selected. Since the latent heat of PCM can be characterised by FSPCM board thickness [102], the FSPCM board thickness range of 10-30 mm was considered in this parametric study. Natural night ventilation by opening windows was also introduced from 19:00 to 7:00 to check its impact on improving the heat discharge efficiency of the FSPCM board.

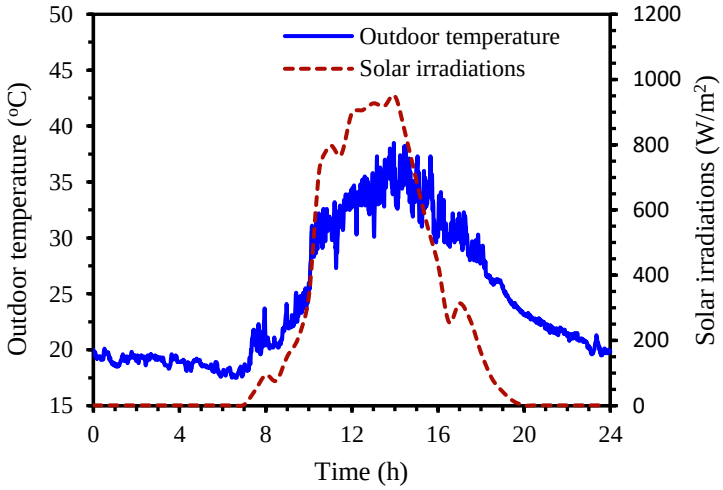

Fig. 5.9. Outdoor air temperature and solar irradiations in selected test day **(**24 February 2020).

5.3.4. Numerical results analysis

5.3.4.1. Effect of PCM melting temperature

When enthalpy of PCM is fixed, the most influencing factor is the melting temperature of PCM. One-day (24 February 2020) simulation results of the indoor air temperature of the model house gained by using 15 mm of FSPCM boards with melting temperature of PCM within 23-29 °C range are shown in Fig. 5.10. In all cases, the use of PCM with a melting temperature of 23 °C (T_m = 23 °C) for this specific day provided the maximum peak indoor air temperature. The reason may be that this PCM melted earlier than other PCMs during the daytime, leading to more sensible heat accumulation [176]. Consequently, the heat storage rate of FSPCM board at T_m = 23 °C was decreased, which resulted in a lower reduction in indoor air temperature than that of the other PCMs with higher melting temperatures.

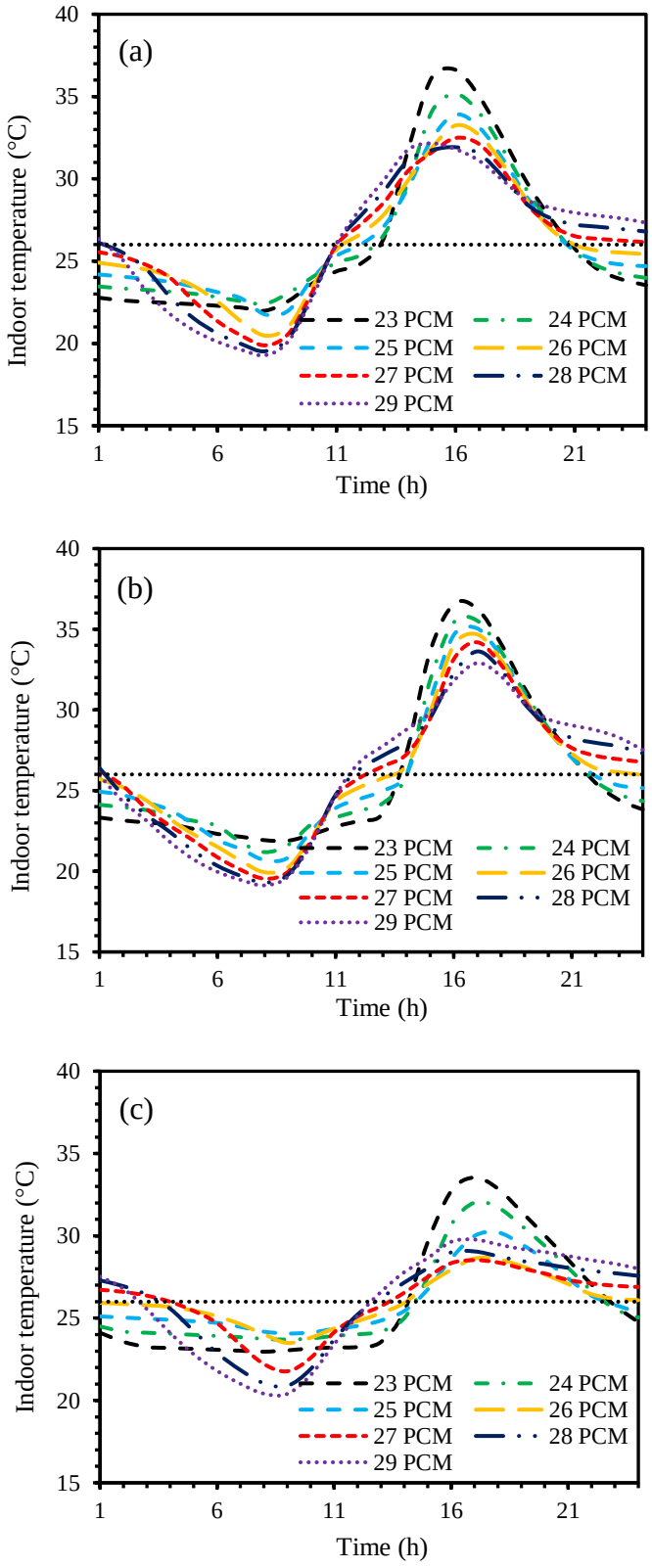

Fig. 5.10. The effect of PCM melting temperatures on indoor air temperature of PCM house: (a) walls case, (b) ceilings case and (c) combined case.

Fig. 5.10 (a) shows that the peak temperature decreases when increasing the PCM melting temperature up to 28 °C for the wall case. With a further increase in melting temperature (T_m = 29

°C), the peak temperature increased and shifted to on-peak hours in mid to late afternoon [177]. However, for the ceiling case (Fig. 5.10b), it can be observed that the use of PCM with a higher melting temperature improved the indoor thermal environment and comfort conditions as measured by the indoor temperature, and that T_m = 29 °C considerably decreased the peak temperature in the daytime compared to that of other low melting PCMs. During the nighttime, the indoor air temperature of the house with FSPCM boards with melting temperatures of 27-29 °C is higher than the comfort level temperature of 26 °C specified by Australian Building Codes Board [178], This will make occupants experiencing thermal discomfort, as the solidification of such PCMs occurs at temperatures higher than 26 °C. Hence, an air conditioner would need to be used to maintain a comfortable level, resulting in a higher level of energy consumption. By applying FSPCM boards on the walls and ceiling of the studied model house, it is observed that the peak temperature reduced to as low as 29 °C for T_m =26 °C while further increase in the PCM melting temperature resulted in an increase of peak temperature and discomfort level (Fig. 5.10c). Therefore, it can be concluded that the FSPCM board with T_m = 26 °C performed better compared to others during the studied period for all cases.

5.3.4.2. Effect of FSPCM board thickness

Apart from the phase change temperature, latent heat is another important parameter that has a significant affinity for the thermal storage performance of PCM. As the FSPCM contained in the boards is uniform (Fig. 5.3), the thickness can characterise the latent heat of FSPCM boards. This means a greater thickness of FSPCM board can have more latent heat [102], resulting in an increased operating period, which leads to a reduction in the peak indoor air temperature. However, due to the increased FSPCM board thickness, the charging and discharging ability can be declined due to the inferior heat transfer rate in PCM material. Thus, in the interest of determining the optimum thickness of the FSPCM board, the investigation was repeated with a board thickness range of 10-30 mm (5 mm intervals) in all cases, and the results are shown in Fig. 5.11. This study was performed for T_m = 26 °C, the optimum melting point of PCM obtained in the previous section. As can be seen, the indoor

air temperature reduces as a higher FSPCM board thickness is used. This is because the higher FSPCM board thickness causes an increase in the overall thermal resistance and heat storage capacity, thus absorbing increasing amounts of incoming heat. As can be seen from Fig. 5.11 (a), up to 20 mm of FSPCM board thickness, a reduction of indoor peak temperature can be observed for the wall case.

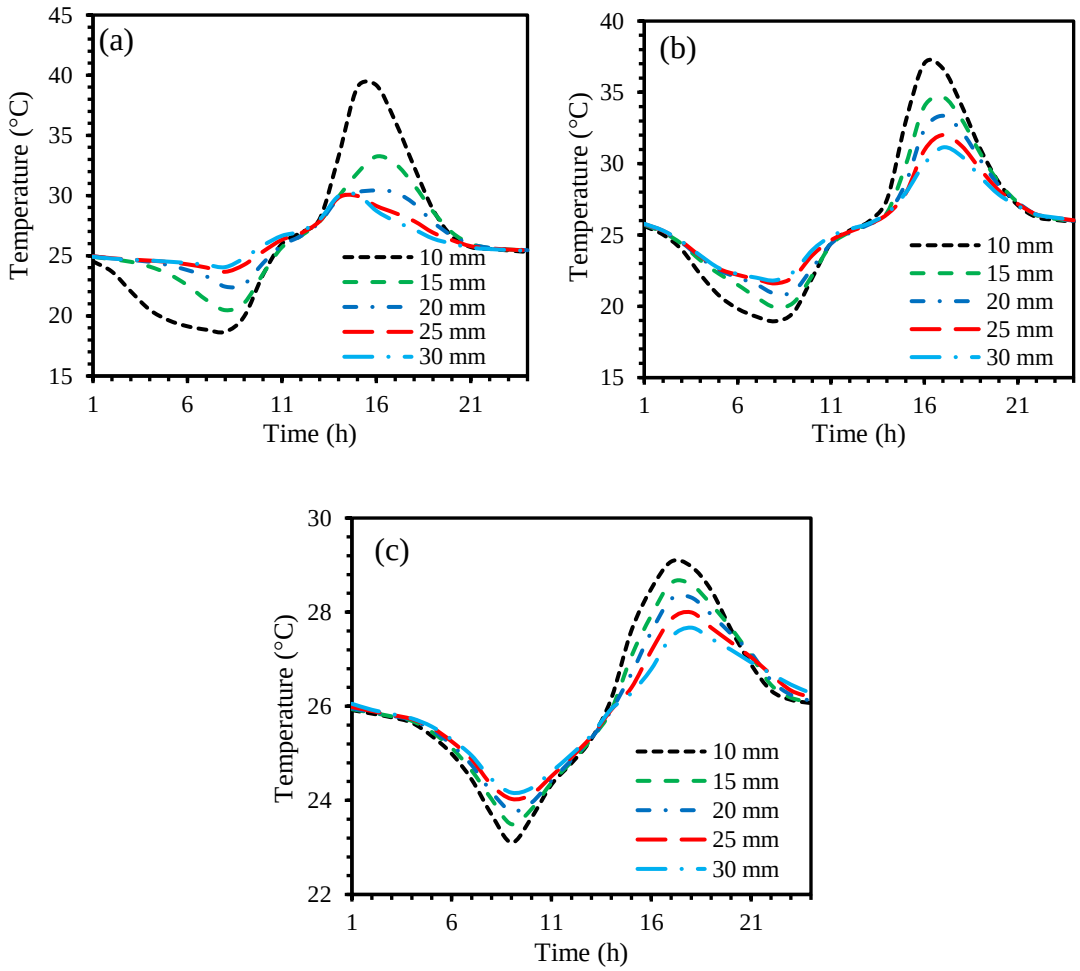

Fig. 5.11. The effect of FSPCM board thickness (latent heat) on indoor air temperature of PCM house: (a) walls case, (b) ceilings case and (c) combined case.

A further increase of FSPCM board thickness does not affect the peak temperature while a minor impact on the indoor air temperature is seen. By looking at the relative reduction in peak temperature and economic point of view, the FSPCM board with thickness of 20 mm is the best option. In contrast with the walls case, a sharp decrease of peak indoor air temperature can be observed for up to 30 mm of board thickness, reaching as low as 31.1 °C and 27.7 °C for the ceiling and combined cases (Fig. 5.11 (b,c)). It is relevant to mention here that for the ceiling and combined cases, the efficiency of 30

mm thick of FSPCM board was found to be the best. It should be mentioned that the temperature gradient (ΔT) between the PCM and surrounding environment performs a significant role in the PCM melting and freezing. The larger the temperature gradient, the faster the heat transfer rate between the PCM and surrounding environment. This leads to higher PCM melting or freezing rate [179]. In summer, solar heating through roof is the primary source of heat gain for a house. During the daytime, the attic temperature can be significantly higher (15-20 °C) than the outdoor air temperature [124, 180], resulting in a large temperature gradient in the ceiling. Hence, PCM is more likely to fully melt in a thick FSPCM board when used in ceilings. However, the walls experience less solar heating than the roofs. Thus, there is a smaller temperature gradient between the walls and surrounding environment. This explains the low efficacy of thick FSPCM board when used wall linings [181]. In comparison to using an FSPCM board-only ceiling, a significant decrease in peak temperature was obtained by applying the FSPCM board on both walls and ceilings. However, further research is required to study the economic factors combined with the performance of FSPCM board applications in both the walls and ceiling.

5.3.4.3. Effect of thermal conductivity

In general, the thermal conductivity (k) is a crucial parameter that directly affects the performance of PCM installed in a building envelope. Typically, to be fully effective in building applications, PCM needs to go through a complete phase transition during a day. The overall k and heat capacity of PCM has a strong effect on its thermal performance in building applications. They also have a relative impact on each other [182]. In this section, the effect of k on the thermal performance of the FSPCM board without changing the heat capacity is addressed. Fig. 5.12 shows the indoor air temperature at different k values of the FSPCM board. As seen in Fig. 5.12 (a) from the wall case, the k of 0.05 W/(m.K) displays enormous temperature fluctuation, and when increasing the k value the temperature curves are right-shifted, while the peak indoor air temperature decreases. However, when k is above 0.3 W/(m.K), the indoor air temperature curves are almost identical, indicating that

increasing *k* cannot further improve thermal comfort and save energy. In contrast to the wall case, the opposite trend is observed when the FSPCM board is installed in ceilings.

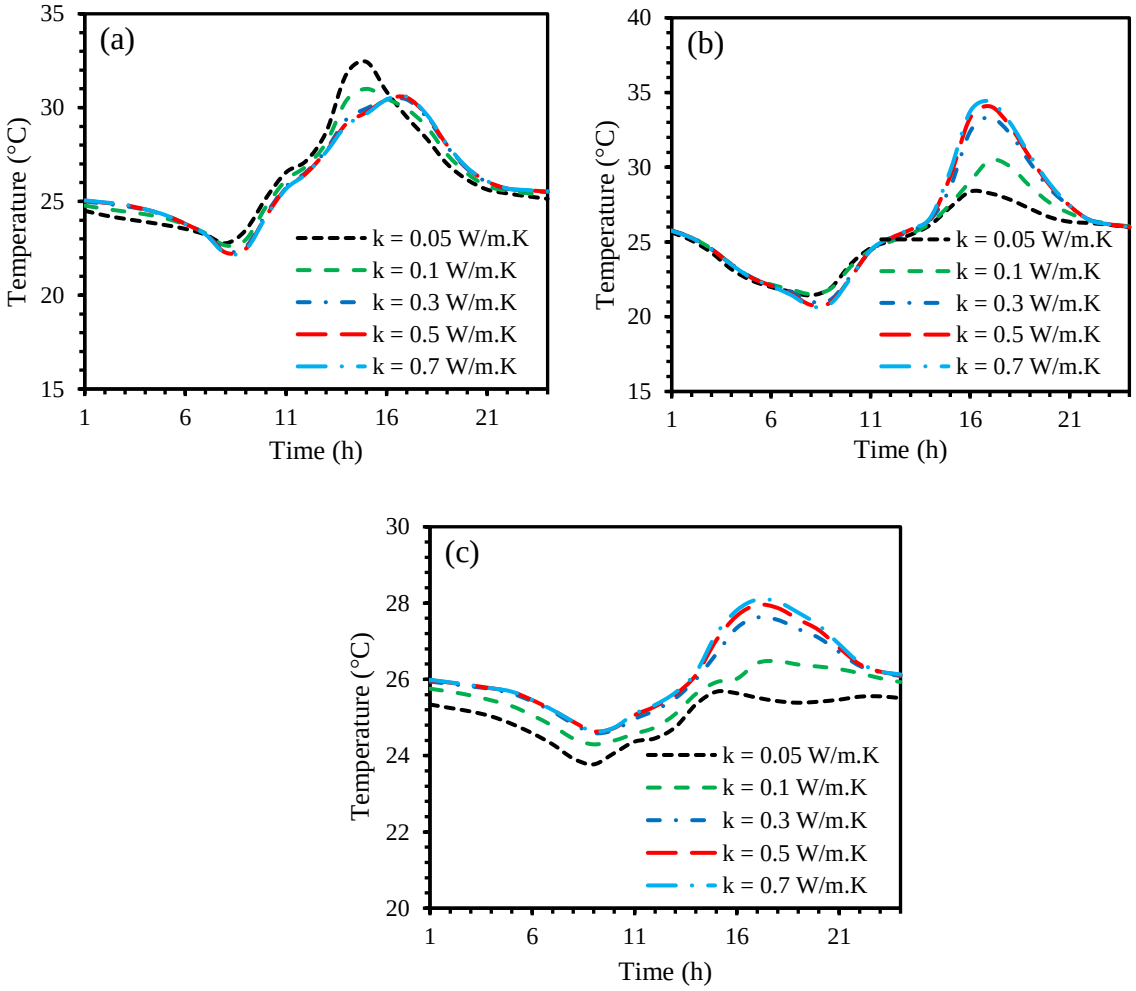

Fig. 5.12. Indoor air temperature of FSPCM board different thermal conductivity.

As can be seen in Fig. 5.12 (b), increasing the *k* of the FSPCM board causes a higher peak indoor air temperature, and when *k* is >0.5 W/(m.K), the temperature curves of the room are almost the same as each other, which is consistent with the study of Ye et al. [183]. The thermal performance of PCM incorporation is highly dependent on their heat storage and release rates, as well as the indoor and outdoor temperatures [184, 185]. When the *k* is < 0.3 W/(m.K), as the *k* is decreased, the peak indoor air temperature is significantly reduced. As the roof ceiling is the primary source of heat gain and the attic temperature is always considerably higher (15-20 °C) than the outdoor air temperature [22], a lower *k* is better for the ceiling as it reduces the heat transmission in the room. Therefore, in

this situation, the FSPCM board can use the latent heat to absorb the heat and utilise the higher thermal resistance to block the heat transfer. A similar result is found when the FSPCM board is installed in both the walls and ceiling (Fig. 5.12c).

5.3.4.4. Effect of night ventilation

To maximise the PCM's thermal storage, natural ventilation (NV) at night-time is introduced in the PCM house. The ventilation was applied from 19:00 pm to 7:00 am by opening 40% of the total area of the sliding windows. The NV should provide an advantage if the outside air temperature during the night is lower than that of the PCM's melting temperature. Note that this analysis was conducted using an optimum FSPCM board thickness with T_m = 26 °C for the specific case.

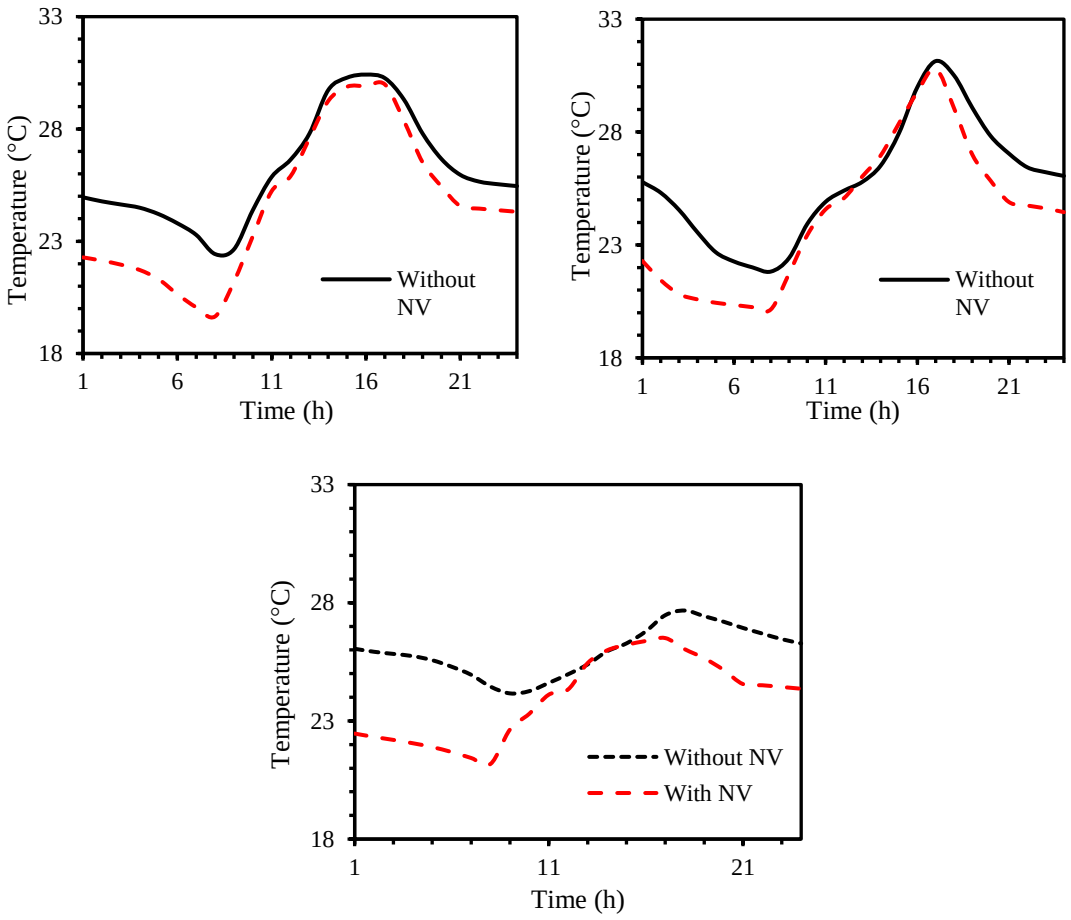

Fig. 5. 13. The effect of night ventilation on indoor air temperature of PCM house: (a) walls case, (b) ceilings case and (c) combined case.

Fig. 5.13 shows the simulated results of the studied PCM model house with and without NV. It is demonstrated that the cooling performance of the FSPCM board was increased with the operation of NV, as it further decreased the indoor peak temperature by 0.44 °C for the wall case, 0.34 °C for the ceiling case, and 1.2 °C for the combined case.

5.4. Economic analysis

5.4.1. Energy saving cost analysis

In Sections 5.2 and 5.3, the impact of the FSPCM board on reducing indoor air temperature and improving thermal comfort was studied. The results also confirmed that the application of FSPCM board in both the walls and ceiling has a significant effect on energy saving. This section aims to verify the most effective use of the FSPCM board with a thickness of 20 mm through economic evaluation. The energy consumption for heating and cooling of the model house was measured using EnergyPlus Representative Meteorological Years (RMY) weather files for Sydney. The heating and cooling set-point temperatures were taken as 18 °C and 26 °C, respectively. Energy cost (EC) is the energy intake multiplied by the cost of cooling and heating energy. To convert the energy savings into cost, the energy used in heating and cooling is electric and taken as 33.33 c/kWh [22]. Energy-saving cost (ESC) through the FSPCM board's usage in the model house for each case was calculated compared to the reference case (without FSPCM). Fig. 5.14 shows the EC and ESC for each case of the house. The energy cost savings for using the FSPCM board in the walls (wall case) of the test house was AU$11.2/y. However, when the FSPCM board was applied to only the ceiling (ceiling case), the energy cost was enhanced by 19.0% compared to the wall case. The test house showed the most significant savings when the FSPCM board was applied on both walls and ceiling and the energy cost was reduced by AU$ 12.9/y (73.6%) compared to the reference house.

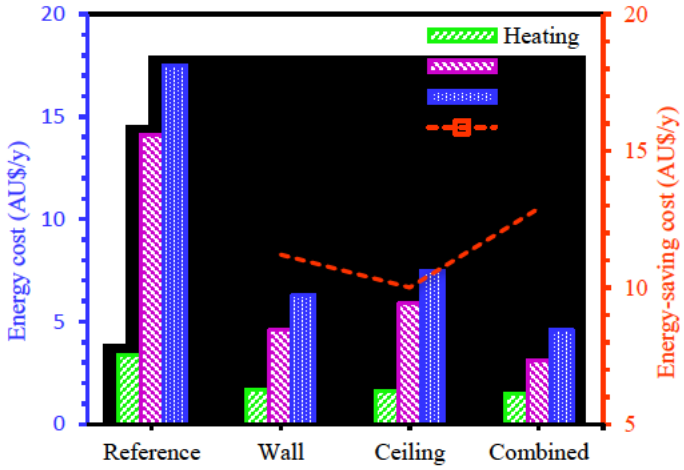

Fig. 5.14. Energy cost (left y-axis) and energy-saving cost (right y-axis) for different cases

5.4.2. Life cycle cost analysis

In the previous section, the energy-saving cost of different cases compared to the reference house was evaluated based on the house's one-year heating and cooling energy requirements. In this section, a life cycle cost (LCC) analysis is used to evaluate the economic benefits of different installation cases of FSPCM board in the house, as reported in section 5.2.1. A detailed description of the LCC analysis is given in Chapter 4. The economic benefits are evaluated based on the year-round energy consumption (heating and cooling) measured by EnergyPlus for different cases presented in Table 5.5

Table 5.5 Life cycle cost savings and payback periods for different cases.

	Energy consumption (kWh/y)	LCC saving (AU$)	Payback period (years)
Reference house	52.5	-	-
Wall case	19.0	90.2	1.8
Ceiling case	22.6	84.3	1.3
Combined case	13.8	99.8	2.3

The maximum cost savings are calculated corresponding to a minimum payback period of the FSPCM board cost over its expected lifetime. LCC is typically used for an investment calculation to compare different options to choose the best one. Through Chapter 4, FSPCM board application to roof ceiling was economically analysed using LCC analysis based on a small-scale chamber's tested results for three days in the real environment. The study in this chapter aims to determine the

economic feasibility of using FSPCM boards in the walls, ceiling, and both walls and ceiling of lightweight model houses by LCC analysis as reported in Chapter 4. Taking into account the simulation results in section 5.4.1, the life cycle cost savings calculated for different cases are presented in Table 5.5. The LCC savings in AU$ are found to be 90.2, 84.3, and 99.8 for the scenarios of using FSPCM board in the walls, ceiling, and both wall and ceiling, respectively. The maximum LCC saving is found by using the FSPCM board in the walls and ceiling. As a result of the energy performance, the performance of using the FSPCM board in the ceiling is lower than the other two cases. However, LCC analysis showed that the FSPCM board in the ceiling had a shorter payback period (1.3 years) compared to the FSPCM board in walls (1.8 years) or the FSPCM board in both walls and ceilings (2.3 years). This result is due to the difference in the initial cost of installing FSPCM boards. Since the initial cost for installing the FSPCM board in the ceiling is much lower than the other two cases, the use of the FSPCM board in ceilings is economically more viable despite relatively low LCC savings.

5.5. Conclusions

The integration of PCM into traditional building envelopes provides numerous advantages. For example, the PCM can not only store thermal energy in the daytime to reduce indoor temperature fluctuations but also shift the peak energy demand to the off-peak hour. Reductions in energy demands for heating and cooling are confirmed by the FSPCM board application. The results of the experimental study can be summarised as follows:

- FSPCM board applied to the walls, ceilings, and both walls and ceilings in the lightweight building were experimentally tested using two identical model houses at Penrith Campus, Western Sydney University, Australia. A maximum reduction of peak indoor air-temperature of 5.8 °C is found by applying the FSPCM board to the walls and ceiling. Under these conditions, the peak load can be shifted by up to 71 min to the off-peak period.

However, the performance and selection of PCMs are highly subject to the weather conditions where they are applied. For the FSPCM board's strategic application, parametric analysis was conducted using a validated simulation model (EnergyPlus) of the model house to optimise the PCM melting temperature and board thickness. The content of the simulation study can be summarised as follows:

- The FSPCM board with a melting temperature of 26 °C is the optimum for all cases. The maximum reduction of peak air temperature is achieved by applying 30 mm FSPCM board in both the ceiling and combined cases, while the efficiency of a 20 mm board thickness is found to be the best in the wall case. The use of NV has an impact on further reducing the maximum peak indoor air temperature by 1.2 °C for the combined case.
- The EnergyPlus simulation model was also used to analyse the energy-saving cost and economic efficiency. The analysed result for energy-saving cost is a maximum of AU$ 12.9 (73.6%) in a year when compared to the reference house. Moreover, through LCC analysis, the FSPCM board investment recovery period was confirmed for each case. LCC saving's economic benefits using the FSPCM board in each case were confirmed by showing a lower payback period from 1.3-2.3 years compared to the service lifetime (10 years) of the FSPCM board.

In this study, the energy cost of heating and cooling is decreased when the FSPCM board is applied to the inside surface of the walls, ceiling, and both walls and ceiling in a house. The simulation model in this study was used to evaluate the effects FSPCM board in a lightweight model house in Sydney rather than in a real house. Meanwhile, further studies should be conducted to use the FSPCM board with insulation materials in a real house for energy conservation. Analysis can then be conducted to evaluate the life-cycle cost and energy-savings cost, as well as payback periods for retrofitting houses using FSPCM board and insulation material in different weather conditions.

CHAPTER 6

Combined use of phase change material and thermal insulation to improve energy efficiency of residential buildings

6.1. Introduction

As concluded in Chapter 5, diatomite based FSPCM is highly compatible with gypsum board and has significantly enhanced thermal inertia and TES capacity. Hence, indoor thermal comfort and energy efficiency could be improved when the FSPCM-enhanced gypsum board (FSPCM board) is incorporated into building envelopes. However, the use of thermal insulation within building envelopes is common practice for improving a building's energy performance. It is not economical to fully replace thermal insulation with an FSPCM board for improving the energy rating of existing buildings. However, the combined use of FSPCM board and thermal insulation in building envelopes could provide an economical solution for improving energy efficiency while avoiding overheating issues. Therefore, it is necessary to evaluate the potential benefits in improving energy efficiency using the FSPCM board and thermal insulation in building envelopes. The FSPCM board using RT-26 instead of methyl stearate was adopted in this study. However, for different climates such as Darwin, Alice Springs, and Sydney, the ideal melting temperatures of PCM may be different. This will be studied in section 6.4.1. This research study is the first attempt to quantify the benefits of using FSPCM board together with thermal insulation to improve the energy rating of a typical standalone house in different Australian climates (Darwin, Alice Springs, and Sydney) through life-cycle cost analysis. An EnergyPlus numerical model is used to evaluate the influence of different parameters, such as the PCM melting temperature, board thickness, occupancy profile, and climate zone on energy performance. In the evaluation of energy performance, the star rating system in NatHERS is adopted. To further understand the potential economic benefits of the combined use of FSPCM board and insulation, an economic and environmental feasibility analysis is also conducted in this chapter.

6.2. Development and characterisation of FSPCM board

6.2.1. Fabrication of FSPCM board

In our published article [22], methyl stearate was used to develop the FSPCM board. However, methyl stearate has a relatively high phase transition temperature (36.8 °C) and is therefore not suitable for use in indoor applications. In this study, RT-26 supplied by APACI Pty Ltd in Australia was used as PCM to produce FSPCM board instead of methyl stearate. RT-26 with a melting temperature of 26 °C is suitable for interior surface applications. In developing the form-stable PCM, diatomite was still used as the supporting material. Details of the preparation of the FSPCM can be found in Chapter 3.

6.2.2. Properties of FSPCM board

The FSPCM board was prepared by incorporating a total of 40 wt.% of FSPCM into gypsum. Details of the preparation process can be found in Chapter 4. Fig. 6.1a shows the produced FSPCM board. The specific heat capacity and enthalpy of the FSPCM board were conducted by using the differential scanning calorimeter (DSC; Netzsch 204 F1 Phoenix). The DSC measurement was conducted in an inert Ar gas atmosphere at a flow rate of 25 mL/min and a heating-cooling rate of 5 °C/min. The specific heat capacity of the FSPCM board is shown in Fig. 6.1b, as a function of temperature up to 50 °C. It can be seen that the specific heat capacity is significantly increased during the melting process of the PCM, where a peak value of 4.67 J/g·K occurs at 28.5 °C. By integrating the area under the parabolic curve (22–35 °C) shown in Fig. 6.2b as suggested in [121], the latent heat of the FSPCM board is estimated to be 19.9 J/g, which proves that the developed FSPCM board has a high heat storage capacity and is suitable to be used for building applications.

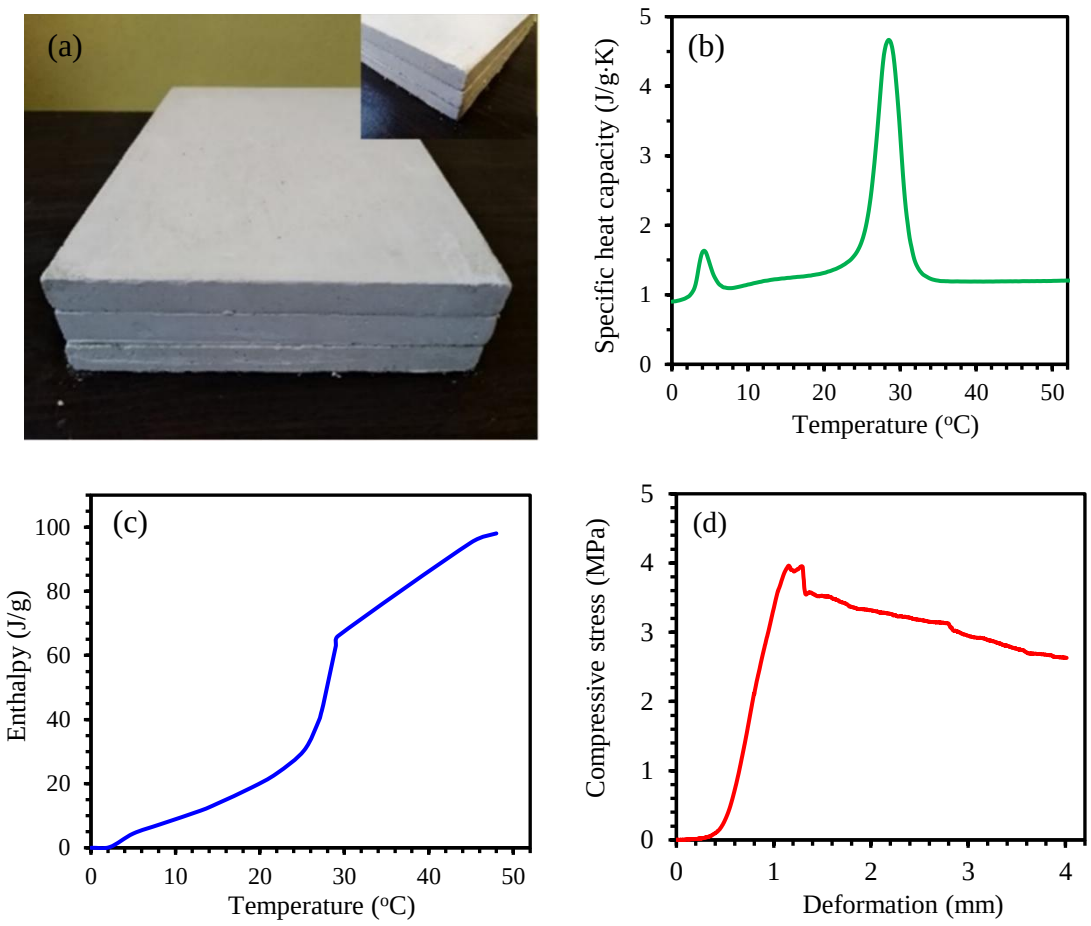

Fig. 6.1. Thermal and mechanical properties of FSPCM board: (a) produced FSPCM board, (b) specific heat capacity, (c) enthalpy-temperature curve, and (d) compressive strength.

The thermal performance of the FSPCM board can be evaluated from the enthalpy–temperature curve shown in Fig. 6.1c. The enthalpy increases slowly with the temperature until it reaches the melting temperature of 26 °C. During the phase transition of PCM, the enthalpy increases dramatically. This is due to the absorption of a large amount of thermal energy during the phase change of PCM [186]. Once the PCM fully melts, the enthalpy once again increases slowly with the temperature. Table 6.1 shows the thermo-physical and mechanical properties of the FSPCM board, where the thermal conductivity of the FSPCM board has been measured by a hot-disc thermal constant analyser (TPS 2500 S) [22]. The thermal conductivity of the FSPCM board is found to be 0.43 W/mK, which is about two times that of the pure RT-26 PCM (0.2 W/mK). The result is consistent with our previous findings in Chapter 3.

Table 6.1 Thermo-physical and mechanical properties of RT-26, FSPCM and FSPCM board.

Material	Apparent density (kg/m^3)	Heat storage capacity (J/g)	Specific heat capacity (J/kgK)	Thermal conductivity (W/mK)	Compressive strength (MPa)
RT-26	880	180.0	–	0.2	–
FSPCM	–	76.84	–	–	–
FSPCM board	530	19.88	1984	0.43	3.9

It has been widely reported that the addition of PCM may significantly decrease the strength of the gypsum board [187]. Accordingly, the compressive strength of the developed FSPCM board was evaluated. Cylindrical samples (ϕ50 × 100 mm) were prepared and tested using a universal testing machine at a crosshead speed of 0.5 mm/min [159]. Fig. 6.1d shows a typical compressive stress versus deformation curve for the FSPCM board. It was found that the compressive strength of the FSPCM board is 3.9 MPa, which is 62.5% higher than the required strength of 2.4 MPa for regular gypsum board [188]. Therefore, the developed FSPCM board is suitable for non-structural interior applications in buildings [189].

6.3. Evaluation of the combined use of PCM and thermal insulation

6.3.1. Description of the house used in simulation

The simulation was carried out on a typical residential house in Australia, as shown in Fig. 6.2. The house is one of the eight sample houses used by the Australian Building Codes Board for the accreditation of energy rating software [190]. As shown in Fig. 6.2a, the house has four bedrooms, a living/dining area, a kids' TV room, a separate toilet and bathroom, a rumpus room and a double garage. This house has a gross floor area of 289.6 m^2, where a net area of 207.4 m^2 is air-conditioned. The windows of the house are single glazed with aluminium frames and the doors are made of wood. The solid concrete slab floor covered with carpets is in direct contact with the ground.

This house has also been adopted by Ramakrishnan et al. [191] in their parametric analysis to optimise PCM configurations to improve indoor thermal comfort during summer. Construction details and thermo-physical properties of the construction materials have been reported in [31], and some key information is summarised in Table 6.2.

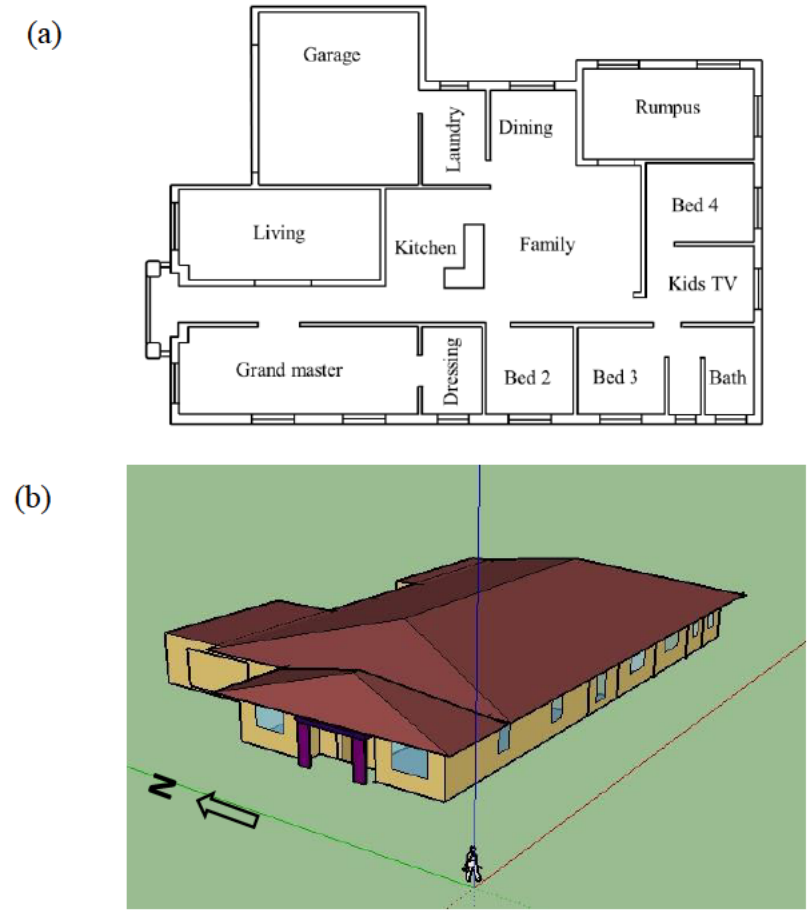

Fig. 6.2. Typical standalone single-storey residential house: (a) floor plan, and (b) 3D view.

Table 6.2 Details of house design and thermo-physical properties of building materials [191].

Component	Thickness (mm)	Thermal conductivity (W/m.K)	Density (kg/m^3)	Specific heat capacity (J/kg.K)
Exterior wall				
Brick	110	0.61	1690	878
EPS insulation[a]	–	0.035	25	1400
Plasterboard[b]	13	0.17	847	1090
FSPCM board[c]	–	0.43	530	1984
Internal partition				
Plasterboard	13	0.17	847	1090
Pitched roof				
Concrete roof tiles	20	1.42	2400	880
Flat ceilings				
EPS insulation[a]	–	0.035	25	1400
Plasterboard[b]	13	0.17	847	1090
FSPCM board[c]	–	0.43	530	1984
Floor				
Carpet	20	0.0465	104	1420
Concrete slab	100	1.42	2400	880
Door				
Timber	50	0.16	1122	1260

[a] Values suggested in [157].
[b] Either plasterboard or FSPCM board is used.
[c] Properties reported in Table 1.

6.3.2. Numerical model

The residential house described in Section 6.3.1 was simulated using the EnergyPlus software to evaluate its energy-saving potential and environmental performance. This software is widely used for the assessment of thermal and energy performance of houses integrated with PCM [20]. In EnergyPlus, a PCM module is available using a one-dimensional conduction finite-difference (CondFD) solution algorithm, which has been verified previously by many studies [192-195]. For example, it has been verified by test/analytical results of drywall/fibrous insulation with distributed PCM or concentrated PCM layers [171, 196].

EnergyPlus permits the modelling of PCM using an implicit finite difference scheme, where Crank-Nicholson's second-order or fully implicit first-order scheme can be chosen. In this study, the fully-implicit first-order scheme expressed by Eq. (6.2) is selected according to [197].

$$C_p \rho \Delta x \frac{T_i^{j+1} - T_i^j}{\Delta t} = \lambda_w \frac{T_{i+1}^{j+1} - T_i^{j+1}}{\Delta x} + \lambda_E \frac{T_{i-1}^{j+1} - T_i^{j+1}}{\Delta x} \quad (6.2)$$

where $\lambda_{\mathrm{w}} = \frac{\left(\lambda_{i+1}^{j+1} + \lambda_i^{j+1}\right)}{2}$, $\lambda_{\mathrm{E}} = \frac{\left(\lambda_{i-1}^{j+1} + \lambda_i^{j+1}\right)}{2}$, and $\lambda_i = \lambda\left(T_i^{j+1}\right)$ if thermal conductivity is variable. In Eq. (2), T is the temperature of a node; i is the node being modelled; i+1 and i–1 are adjacent nodes to the interior and exterior of the construction, respectively; j+1 and j represent new and previous time steps, respectively; Δt is the time step; Δx is the finite difference layer thickness; and C_{p} and ρ are the specific heat and density of the material, respectively.

Since PCM has temperature-dependent C_{p}, EnergyPlus updates the value at every iteration according to Eq. (6.3). The user defines the specific enthalpy (h) value with respect to the temperature (T) [197].

$$C_{\mathrm{p}} = \frac{h_i^j - h_i^{j-1}}{T_i^j - T_i^{j-1}} \quad (6.3)$$

The iteration ensures that accurate enthalpy and C_{p} are used in each time step. The time step for the simulation was set to 180 s as recommended by Alam et al. [198]. In the base model, the enthalpy–temperature graph shown in Fig. 6.2c is used for FSPCM board with RT-26. In the

parametric analysis of PCM with a different melting temperature, the enthalpy–temperature graph is simply shifted according to the melting temperature.

6.3.3. Verification of the EnergyPlus model

Rigorous verification has been performed by the EnergyPlus developers and many other researchers to evaluate the accuracy of the EnergyPlus CondFD algorithm. It is found that the PCM's behaviour can be simulated with good accuracy [171]. To ensure the simulation's accuracy, Tabares-Velasco et al. [171] provided a few suggestions in developing EnergyPlus models. For example, they suggested that the time step should be equal to or shorter than 180 s. Meanwhile, a small node space (1/3 of the default value in EnergyPlus) should be used to obtain accurate hourly results.

In this study, the above suggestions were followed in developing the simulation model for the selected house. It should be pointed out that Ramakrishnan et al. [191] also simulated the same house shown in Fig. 6.2 using EnergyPlus to evaluate the thermal performance of PCM during two consecutive summer days in Melbourne. To validate our EnergyPlus model, we adopted the same operating conditions as specified in [191]. Fig. 6.3 compares the air temperature in Bedroom 4 between our results and those previously reported in [191], which shows very good agreement between them. The very minor deviation could be caused by the difference in specified time step, node space and/or other parameters, which were not reported in [191]. This comparison verifies the accuracy of the developed EnergyPlus model for conducting further parametric studies.

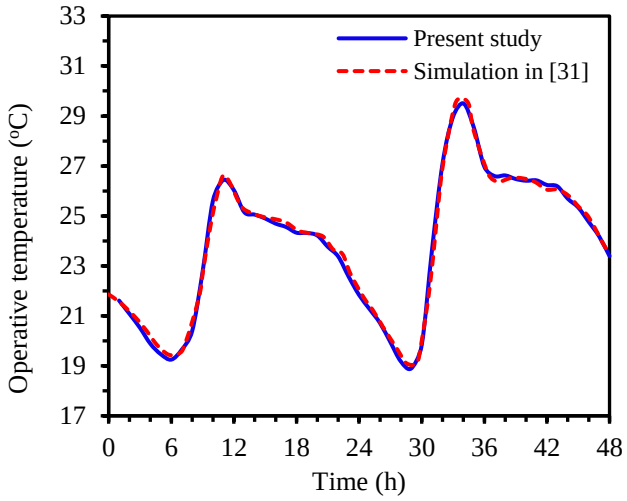

Fig. 6.3. Verification of the EnergyPlus model (air temperature in Bedroom 4).

6.3.4. Description of parametric analysis

It has been widely reported that the efficiency of PCM is highly dependent on climate conditions [199, 200]. One type of PCM that has the prospect of reducing the cooling energy consumption in a particular climate zone may increase the household cooling energy use in another climate zone [71]. As a consequence, there is a need to consider the influence of weather conditions when evaluating the energy efficiency of a passive house with PCM. Australia has a varied climate, and the present study only focuses on relatively hot climate regions. Accordingly, three cities, namely Darwin, Alice Springs, and Sydney have been selected to represent three different climate zones (i.e., tropical savanna, hot semi-arid, and humid subtropical), respectively. Some climate information of the three cities is summarised in Table 6.3. It is worth noting that the analysis conducted in this paper can be easily implemented for other climate zones in Australia or other countries.

To demonstrate the potential benefits of the combined use of PCM and thermal insultation, four cases (Cases 1-4) were simulated to compare the results. Case 1 is the base case, where the house is not refurbished. Case 2 represents the refurbished of the exterior walls and ceilings using EPS and plasterboard finish (13 mm in thickness). Case 3 represents the refurbished of the exterior walls and/or ceilings using FSPCM board only. In Case 4, the exterior walls and ceilings are refurbished using EPS and FSPCM board finish.

Table 6.3 Climate information of Darwin, Alice Springs, and Sydney.

City	Darwin	Alice Springs	Sydney
Climate zone	Tropical savanna (wet and dry)	Hot semi-arid	Humid subtropical
Latitude	12° 27' 46.18" S	23°41'50.9" S	33° 51' 54.51" S
Longitude	130° 50' 30.41" E	133°53'1" E	151° 12' 35.64" E
Elevation (m)	31	545	19
Mean annual maximum temperature (°C)	32	28	22
Mean annual minimum temperature (°C)	23	13	13.5
Solar radiation ($kWh/m^2 \cdot y$)	2117	2248	1862

The simulation was carried out over a period of one year to estimate the total energy consumption (TEC) for heating and cooling based on the typical meteorological year weather data available in EnergyPlus. In the simulation, the essential settings were chosen as follows:

- The cooling set-point temperature was taken as 26 °C according to the Australian standard [178].
- For the heating thermostat setting, 18 °C was specified from 7:00 am to 9:00 am and 16:00 pm to 24:00 am and 15 °C was used from 24:00 am to 7:00 am for sleeping spaces (bedrooms including the bathroom and dressing room). Meanwhile, 20 °C was specified for living spaces (kitchen and living/dining room) according to NatHERS [201].
- The value of TEC was obtained by using the "Ideal Load Air System" module in EnergyPlus [198].
- Natural night ventilation was introduced from 19:00 pm to 7:00 am by opening 40% of the total area of the sliding windows to improve the heat discharge efficiency of the FSPCM board.

The general expectation was that the energy rating of a house will increase with the increasing thickness of the insulation layer or the FSPCM board. However, this may not be cost-effective if the chosen thickness is too high. In this study, the optimal thickness of the insulation layer/FSPCM board was determined based on a life cycle cost analysis to compare the life cycle savings and payback period of the investment. Details of the life cycle cost analysis are given in Section 6.3.5.

The following parameters were studied in the parametric analysis for houses with different refurbishment strategies (Case 1-4) in three different climates (Darwin, Alice Springs, and Sydney):

- Thickness of the EPS insulation (50, 80, 110, 140, 170, and 200 mm)
- Thickness of the FSPCM board (10, 15, 20, 25, 30 mm)
- Installation of the FSPCM board for (i) all exterior walls and ceilings, (ii) only the exterior walls, and (c) only the ceilings

- A trial study was conducted to determine the optimal melting temperature of PCM in the range of 18–30 °C at 1 °C intervals. Based on the total energy consumption for heating and cooling, it was found that the optimal melting temperature is always around the cooling set-point temperature (26 °C) specified for different climate conditions. Hence, only a narrower range between 24–29 °C was considered for the PCM melting temperature in the following parametric study.
- The occupancy schedule was also an important parameter affecting the energy consumption for space heating and cooling. In Australia, a total of seven occupancy patterns were specified based on the household nature [202]. In this study, we choose two major occupancy patterns to study the house energy consumption and star rating: (1) the house is occupied all day (the occupants may be aged or have an infant to look after), which is the default and worst scenario; and (2) the house is unoccupied from 9:00 am to 17:00 pm (the dwellers may have full-time employment). To simplify the simulation, the first occupancy pattern was adopted throughout the analysis except for the parametric analysis conducted in Section 6.4.4,

After conducting the EnergyPlus simulation, the value of TEC for heating and cooling could be determined for each scenario. The information could then be used to determine the house star rating according to Fig. 6.4 [203] for a specific house location.

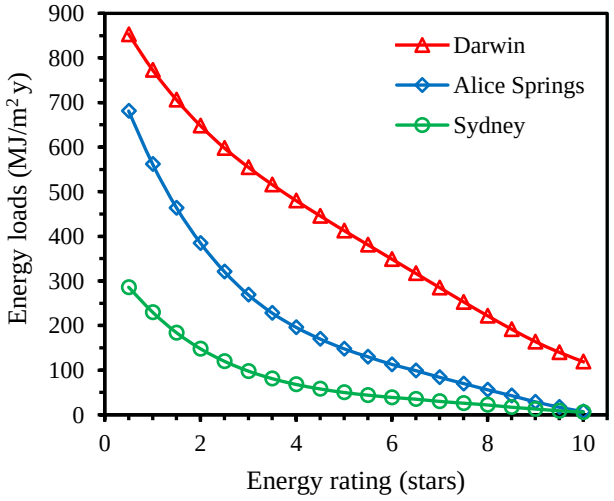

Fig. 6.4. Classification of star bands based on the annual heating and cooling requirements.

The maximum energy loads corresponding to the NatHERS star bands in 0.5 star increments are shown in Table 6.4 for each city. The annual energy consumptions for heating and cooling in megajoules (MJ) per unit area (MJ/m^2.year) of the designated house were calculated using EnergyPlus software and compared with the star rating criteria given in Table 6.4 to determine the house's energy rating. For the base house without renovation in Sydney, it requires a total heating and cooling energy of 165.1 MJ/m^2·y to maintain the indoor temperature within a comfortable range. According to Table 6.4, the base house in Sydney has a star rating of 1.8. Similarly, the base house is estimated to have 3.7 and 2.2 stars in Darwin and Alice Springs, respectively. Apparently, there is a need to take suitable measures to improve the energy efficiency of the base house in each city. It is expected that a minimum six-star rating should be met after renovation.

Table 6.4 Maximum allowable energy consumptions corresponding to the NatHERS energy star ratings in each climate zone [203].

Location	Energy rating (stars)																			
	0.5	1	1.5	2	2.5	3	3.5	4	4.5	5	5.5	6	6.5	7	7.5	8	8.5	9	9.5	10
	Energy consumptions (MJ/m^2.year)																			
Darwin	853	773	706	648	598	555	516	480	446	413	381	349	317	285	253	222	192	164	140	119
Alice Springs	681	562	464	385	321	269	228	196	170	148	130	113	99	84	70	56	43	29	17	7
Sydney	286	230	184	148	120	98	81	68	58	50	44	39	35	30	26	22	17	13	9	6

6.3.5. Life cycle cost analysis for economic evaluation

The life cycle cost analysis (LCCA) approach is applied in evaluating the economic and environmental benefits of energy related building renovation. The life cycle cost is the total expense over the lifetime of the used materials. In calculating the life cycle cost, the present value of all expenses must be determined to include the initial cost (materials and installation costs) and future operation costs (energy cost for heating and cooling). In this study, the costs of EPS, plasterboard and FSPCM board are taken as \$133, \$308 and \$705 per m^3, respectively, which are estimated based upon wholesale material prices obtained from suppliers. The installation costs for walls and ceilings are taken as \$4.6 and \$6.75 per m^2, respectively, based on quotes obtained from Insulation Australia. The present value of the future energy cost depends upon the lifetime period, as the inflation rate varies with time. In this study, a life cycle of 10 years is considered. Hence, the energy cost over the lifetime

is converted to the present value by multiplying it by the present worth factor (*PWF*). *PWF* is calculated from Eq. (6.4) based on the interest rate (i) and inflation rate (φ) [22].

$$PWF = \frac{(1+\tau)^n - 1}{\tau(1+\tau)^n} \tag{6.4}$$

where n is the number of operating years, taken as 10 years; and τ is a factor related to the values of i and φ, taken as 1.5% and 2.25%, respectively [22]. The τ–factor is given by Eq. (6.5) [22].

$$\tau = \frac{i-\varphi}{1+\varphi} \quad (\text{if } i > \varphi) \tag{6.5a}$$

$$\tau = \frac{\varphi-i}{1+i} \quad (\text{if } i \leq \varphi) \tag{6.5b}$$

According to the LCCA approach, the total cost (C_{T}) is the sum of the initial cost and the present value of future energy costs for the operating period. Hence, the value of C_{T} can be calculated based on Eq. (6.6) [22, 204].

$$C_{\mathrm{T}} = C_i \chi + C_{\mathrm{E}} \times PWF \tag{6.6}$$

where C_i is the initial cost or actual cost (\$/m^3); χ in the material volume (m^3); C_{E} is the energy cost in the first year, which is calculated based on an electricity price of \$33.33 c/kWh.

The life cycle savings (*LCS*) is the difference between the saved energy cost over the lifetime ($C_{\mathrm{T,Ref}}$) and the total cost (C_{T}). Hence, the value of *LCS* is calculated by using Eq. (6.7) [22].

$$LCS = C_{\mathrm{T,Ref}} - C_{\mathrm{T}} \tag{6.7}$$

where $C_{\mathrm{T,Ref}}$ is the difference in life cycle energy cost between the base house and the refurbished house. It is desirable to have higher life cycle savings, which often means a shorter payback period. The payback period of investment is calculated by using Eq. (6.8) [22].

$$Payback\ period\ (PP) = \frac{C_i}{LCS} \times PWF \tag{6.8}$$

where C_i is the initial investment for materials and installation.

6.3.6. Evaluation of indoor thermal comfort

It has been widely reported that highly insulated and air-tight building envelopes lead to overheating in summer [8]. The use of the FSPCM board can mitigate this effect and increase indoor

thermal comfort during this period. To prove this, the indoor thermal comfort was analysed first for the refurbished house with EPS insulation (with an optimised thickness) and plasterboard finish. The simulation was run again for the house with optimised combinations of EPS insulation and FSPCM board. It should be noted that air-conditioning was not considered in these simulations. After this the intensity of thermal discomfort (*ITD*) due to overheating could be calculated for each case and compared with each other. *ITD* is defined as the time integral of the difference between the indoor operative temperature and the upper limit of comfort temperature (26 °C). Accordingly, *ITD* can be determined according to Eq. (6.9) [205]:

$$ITD = \int_P \Delta T^+ (\tau).d\tau \tag{6.9}$$

$$\Delta T^+(\tau) = \begin{cases} T_{op}(\tau) - T_{\text{over}} & \text{if } T_{op}(\tau) \geq T_{\text{over}} \\ 0 & \text{if } T_{op}(\tau) < T_{\text{over}} \end{cases} \tag{6.10}$$

where *P* is the period over which the integration is performed, taken as one year in this study; and $T_{op}(\tau)$ is the indoor operative temperature taking as the average of the indoor air dry-bulb temperature and the mean radiant temperature [191, 206] and T_{over} is the upper limit of comfort temperature (26 °C). The operative temperature was determined by using the EnergyPlus software.

6.4. Results and discussion

6.4.1. Influence of phase change materials on house star rating

In this section, the effects of installation location, thickness and melting temperature of the FSPCM board on the annual heating, cooling and total energy consumption (TEC) of the house have been evaluated. It should be noted that the evaluation was conducted without considering natural ventilation, as the focus is on the year-round thermal performance of PCM. The impact of natural ventilation will be addressed in Section 6.4.2. The analysis was conducted for Case 3 where only the FSPCM board was used for renovation. Based on the annual energy consumption per square metre, the house star rating could then be determined. Fig. 6.5 shows the annual energy performance after installing FSPCM board with a thickness of 10 mm (t_b = 10 mm) and a PCM melting temperature of 26 °C (T_m = 26 °C). The FSPCM board was considered to be applied to either the inner surface of

the exterior walls, bottom surface of the ceilings, or both. According to the results shown in Fig. 6.5, the highest reduction in TEC was found in the application of FSPCM board to both walls and ceilings for all three cities. For this scenario, the energy rating of the refurbished house was improved by 0.7 stars in Darwin (from 3.7 to 4.4 stars), 0.4 stars in Alice Springs (from 2.2 to 2.6 stars) and 0.5 stars in Sydney (from 1.8 to 2.3 stars) when compared with the base house without renovation (Case 1). In the following analysis, FSPCM board is considered to be applied to both the exterior walls and ceilings in Case 3, unless otherwise specified.

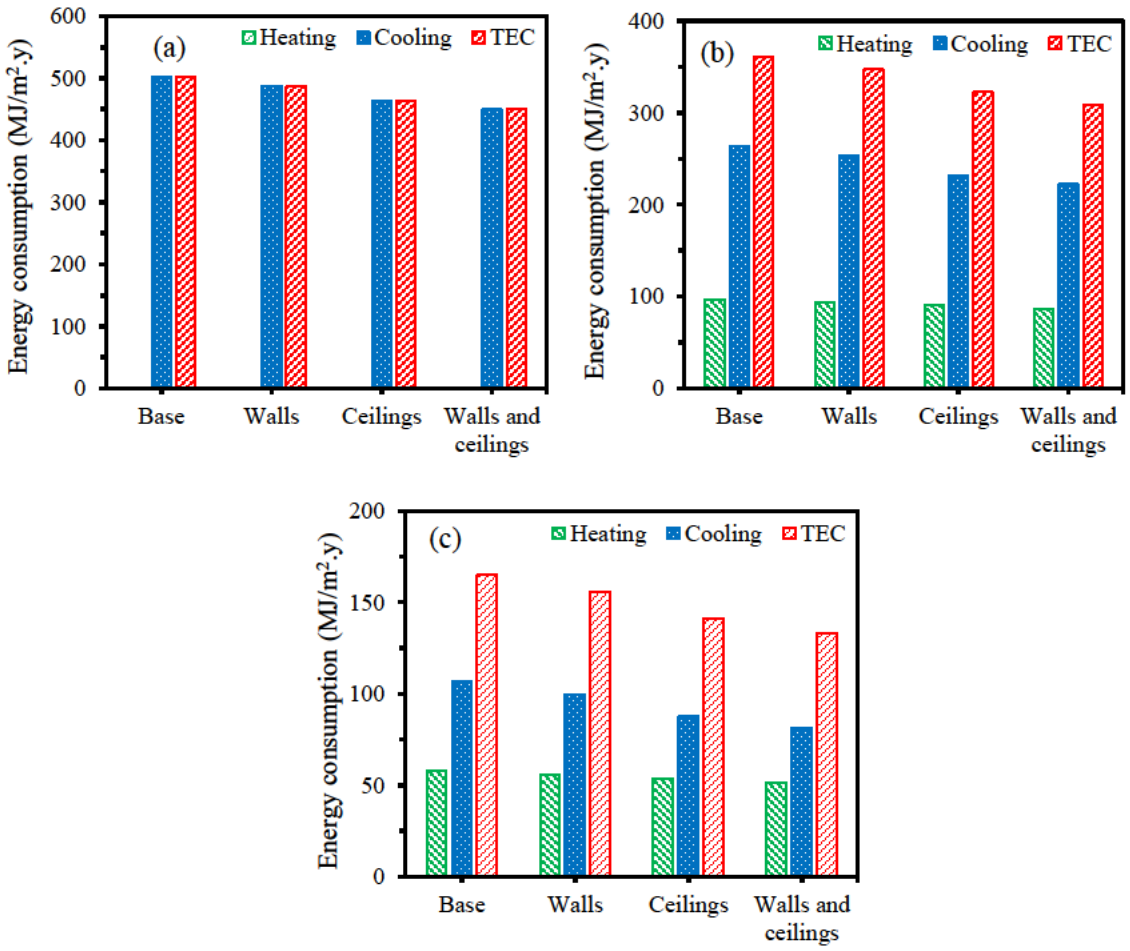

Fig. 6.5. Impact of FSPCM board (using RT-26) location on the energy consumption: (a) Darwin, (b) Alice Springs, and (c) Sydney

The PCM melting temperature should be carefully selected based on weather conditions to minimise annual energy consumption. To check the influence, the annual heating and cooling energy loads of the house were determined for Case 3 using FSPCM board only (t_b = 10 mm), where the

PCM melting temperature varies from 18 to 30 °C without enthalpy change. Fig. 6.6 shows the energy demand as a function of PCM melting temperature for the house in the three Australian cities. It can be observed that the optimal melting temperature of PCM depends on the climate conditions of a city.

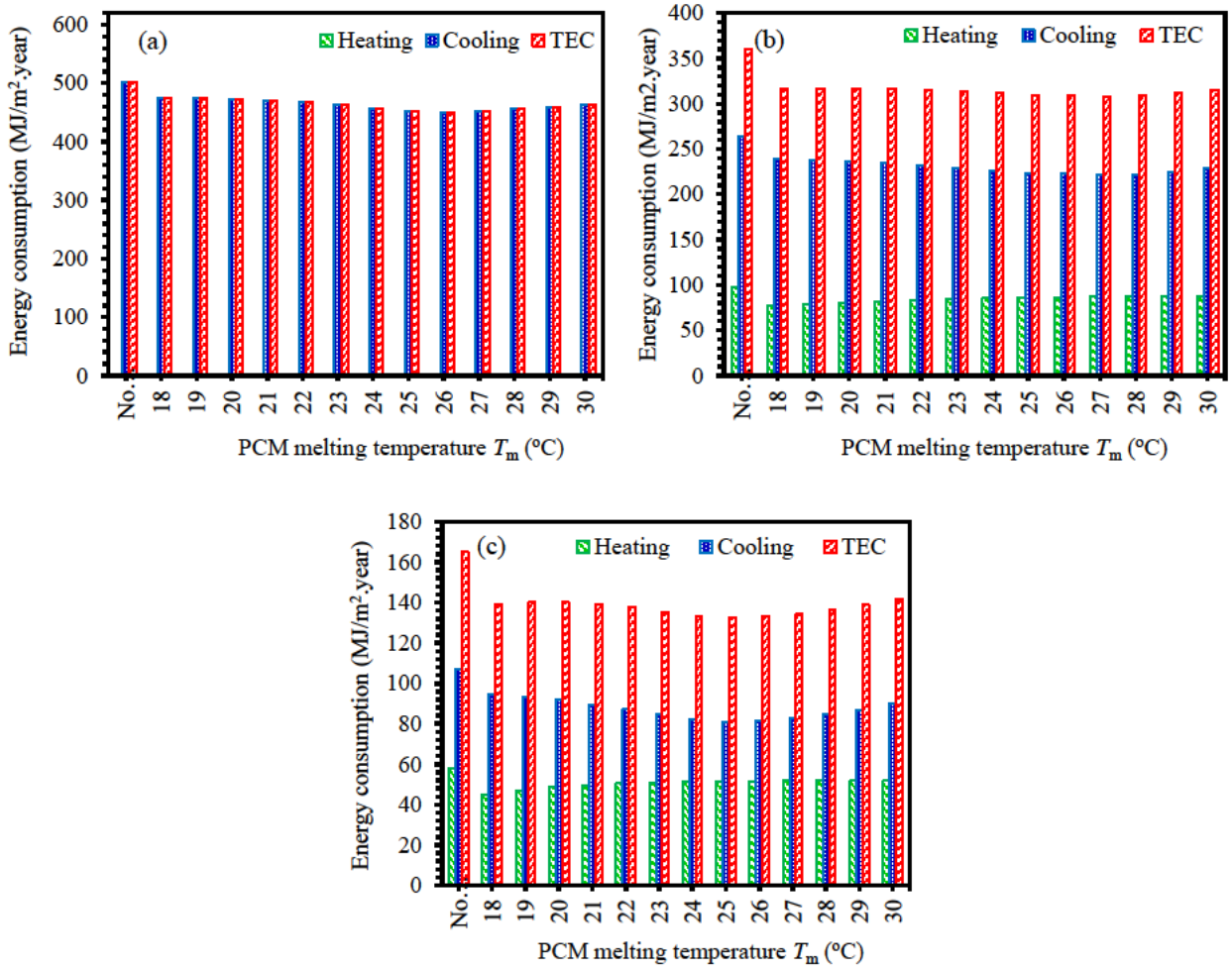

Fig. 6.6. Annual energy demand for using PCMs with different melting temperatures in: (a) Darwin, (b) Alice Springs, and (c) Sydney.

In Darwin, with a tropical climate, a negligible amount of energy is required for heating, as shown in Fig. 6.6a. The use of FSPCM board reduces the cooling energy consumption or TEC in Darwin by 10.3% (from 501.7 to 449.8 MJ/m^2.y) at an optimal PCM melting temperature (T_m) of 26 °C (Fig. 6.6a), which led to an increase in energy rating from 3.7 to 4.5 stars for the test house. Under the arid climate conditions of Alice Springs, the use of PCM can reduce both the cooling and heating energy consumption (Fig. 6.6b). However, the heating demand in Alice Springs is only about 28% of the annual TEC. It was found that the optimal T_m is 27 °C in Alice Springs, and the use of FSPCM board

can reduce the TEC by 14.6% (from 360.8 to 308.0 MJ/m^2.y), which increased the house's energy rating by ~0.4 stars (from 2.2 to 2.6 stars). For Sydney with a humid subtropical climate, the application of PCM can reduce energy consumption for both cooling and heating. The optimal T_m is 18 °C when considering the reduction in heating energy only, but the optimal T_m is 25 °C to minimise the cooling energy consumption (Fig. 6.6c). Since the cooling energy consumption is about two times the heating energy consumption in this city, the optimal T_m should be taken as 25 °C to maximise savings in TEC. Using FSPCM board with this melting temperature, the TEC in Sydney is reduced by 19.6% (from 165.0 to 132.6 MJ/m^2.y) and the house's energy rating was increased by ~0.5 stars (from 1.8 to 2.3 stars).

Apart from the melting temperature, another important parameter is the quantity of PCM used for improving the energy rating of the house. In this study, the quantity of PCM was changed by increasing the thickness of the FSPCM board (t_b) from 10 to 30 mm. It is not economical to use FSPCM board with a thickness greater than 30 mm in practice. It should be mentioned that the optimal PCM melting temperature T_m determined from Fig. 6.6 is only applicable to the scenario with a fixed FSPCM board thickness of 10 mm. The value of T_m changes slightly when t_b increases. Therefore, further analysis was conducted on the total annual energy consumption in Case 3 by considering different combinations of T_m (24–29 °C) and t_b. As shown in Fig. 6.7, TEC decreases with increases in t_b, and this tendency is independent of the climate conditions and the PCM melting temperature. However, the optimal value of t_b should be determined based on life-cycle economic analysis, which will be discussed in Section 6.4.4. It was also found that the optimal T_m varies slightly when t_b changes. For example, in Darwin with a tropical climate, the optimal T_m is 26 °C when t_b is in the range of 10–20 mm and increases to 27 °C when t_b increases to 25 or 30 mm (Fig. 6.7a). However, for Alice Springs with a hot semi-arid climate, the optimal T_m is 27 °C for FSPCM board with t_b of 10–15 mm, then increases to 28 °C for FSPCM board with t_b of 20–30 mm (Fig. 6.7b). In Sydney with a humid subtropical climate, the optimal T_m is 25 °C for FSPCM board with t_b of 10–15 mm, and 26 °C for FSPCM board with t_b of 20–30 mm (Fig. 6.7c). By applying FSPCM board with t_b of

30 mm, the maximum reduction in energy consumption is 20.3% in Darwin, 36.2% in Alice Springs and 43.6% in Sydney (Fig. 6.7d). It seems that the use of FSPCM board achieves the highest energy performance in Sydney due to the large diurnal temperature fluctuations. On the other hand, Darwin has the least percentage reduction in TEC by using FSPCM board. This is because Darwin has a tropical climate with a mean annual minimum temperature of 23 °C (Table 6.3). Therefore, thermal energy storage capacity of the PCM is not fully exploited in hot climate conditions.

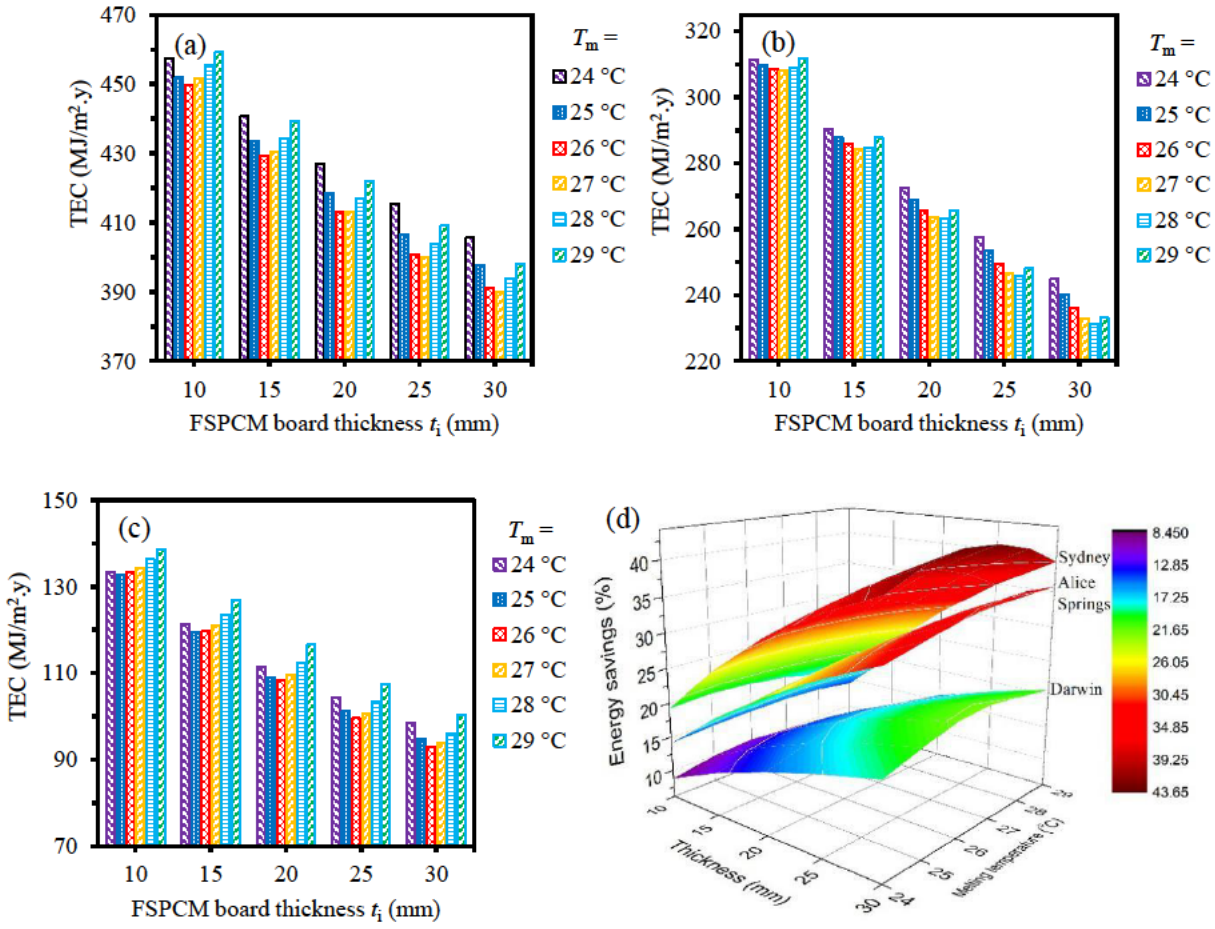

Fig. 6.7. Effects of FSPCM board thickness and PCM melting temperature on: (a-c) total energy consumption, and (d) energy savings in the three cities: Darwin, Alice Springs and Sydney.

According to the optimal results shown in Fig. 6.7, the use of 30-mm-thick FSPCM board can improve the house's energy rating by 1.7 stars (from 3.7 to 5.4 stars) in Darwin, 1.3 stars in Alice Springs (from 2.2 to 3.5 stars) and 1.3 stars (from 1.8 to 3.1 stars) in Sydney. However, the minimum six-star target for renovations has not been achieved in any cases when only the FSPCM board with a maximum thickness of 30 mm is used for renovation. Therefore, conventional thermal insulation

may be required in combination with FSPCM board to achieve the minimum energy rating of 6 stars after renovation.

6.4.2. Impact of natural ventilation on FSPCM board performance

Previous studies have confirmed that natural ventilation (NV) during the night-time could potentially increase the proportion of PCM effectively changing phase [207]. In this regard, the impact of NV on FSPCM board performance was studied by repeating the analysis conducted in Section 6.4.1 with controlled ventilation. The analysis was conducted for the case with t_b = 30 mm in combination with the optimum PCM melting temperature according to section 6.4.1. NV was performed from 19:00 to 7:00 if the outdoor temperature was in the range of 18–26 °C. The base house without PCM (Case-1) was also evaluated for comparison.

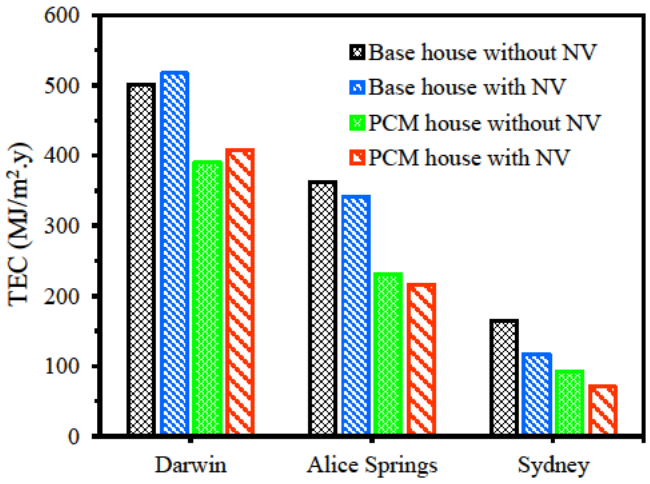

Fig. 6.8. Impact of NV on house energy performance in three different cities using FSPCM board with optimum melting temperatures.

Fig. 6.8 shows the influence of NV on the test house's energy performance in three different cities. It can be seen that NV had a slightly negative impact on energy performance in the tropical climate of Darwin due to the hot and humid weather and high night-time temperatures throughout the year. NV led to an increase of 3.1% in TEC for the base house; the corresponding increase was 4.5% for the refurbished house with FSPCM board (denoted as PCM house). Apparently, such climate conditions prevent the outdoor environment playing a role as a heat sink when NV is applied at night-time. However, NV did indeed improve the thermal performance of both the base house and PCM

house in Alice Springs and Sydney. The values of TEC reduced by 5.6% and 6.8% due to natural ventilation for the base house and PCM house in Alice Springs, respectively. NV had an even more significant effect on thermal performance of houses in Sydney; the corresponding reductions in TEC were 28.8% and 24.3% for the base house and PCM house, respectively. Although both Alice Springs and Sydney have hot summer days, the large diurnal temperature fluctuations help to reduce the indoor temperature at night-time through NV. This is especially true for Sydney. For the PCM house, NV led to an increase in star rating by 0.2 stars (from 3.5 to 3.7) in Alice Springs and 0.8 stars (from 3.1 to 3.9 stars) in Sydney. In the following analysis, natural ventilation was not considered for Darwin, but applied to the studied house in Alice Springs and Sydney.

6.4.3. Combined use of FSPCM board and thermal insulation on energy performance

Since it is not cost-effective to only use the FSPCM board to achieve the desired energy rating, the feasibility of using the FSPCM board in combination with conventional thermal insulation to improve the house energy performance is evaluated in this section. It should be noted that the optimal PCM melting temperature determined in Section 6.4.1 is used in the analysis based on t_b and the relevant climate conditions.

The calculated values of TEC are shown in Table 6.5 for the house refurbished with different thicknesses of FSPCM board (t_b) and EPS insulation (t_{EPS}). In general, TEC decreases with increasing t_b or t_{EPS}. It was found that the use of EPS insulation is very effective in reducing TEC. For instance, the use of 50-mm-thick EPS with a 13-mm-thick plasterboard finish can significantly reduce TEC from 501.7 to 331.9 MJ/m^2.y in Darwin. However, further increasing t_{EPS} only slightly reduces TEC. For example, the TEC of the house reduces from 331.9 to 298.6 MJ/m^2.y in Darwin when t_{EPS} increases from 50 to 140 mm. In contrast, the combined use of FSPCM board and thermal insulation can be more effective in reducing TEC. The TEC of the same house is only 292.8 MJ/m^2.y when 10-mm-thick FSPCM board is used in combination with 50-mm-thick EPS.

From Table 6.5, it can be postulated that the combined use of FSPCM board and thermal insulation can significantly improve the energy rating. In Darwin, an energy rating of 7.1 stars can be

achieved for the house refurbished with 30-mm-thick FSPCM board in combination with 50-mm-thick EPS. Similarly, energy ratings of 6.1 and 6.4 stars are achieved in Alice Springs and Sydney, respectively, when the house is refurbished with 25-mm-thick FSPCM board in combination with 80-mm-thick EPS.

Table 6.5 Effect of combined use of FSPCM board and thermal insulation on the TEC.

		TEC (MJ/m^2.y)					
	t_{EPS} (mm)	t_b =0 (mm)	t_b =10 (mm)	t_b =15 (mm)	t_b =20 (mm)	t_b =25 (mm)	t_b =30 (mm)
Darwin	0	501.7	449.8	429.3	413.1	400.0	389.8
	50	331.9	292.8	285.6	282.7	281.3	279.6
	80	314.4	276.9	270.7	268.1	267.0	266.0
	110	304.9	268.7	263.2	260.6	259.2	258.8
	140	298.6	263.2	257.8	255.5	254.2	254.0
	170	294.5	259.2	254.3	252.4	251.6	251.0
	200	291.2	256.5	251.9	249.5	249.4	248.6
Alice Springs	0	342.3	294.1	270.5	249.1	230.9	215.5
	50	181.1	145.8	133.2	125.8	120.6	116.7
	80	165.7	131.9	121.3	115.1	110.7	107.6
	110	157.4	124.8	115.0	109.3	105.5	102.7
	140	152.2	120.3	111.1	105.7	102.2	99.5
	170	148.5	116.9	108.4	103.3	99.8	97.6
	200	145.6	114.4	106.2	101.4	98.2	96.0
Sydney	0	117.6	99.4	90.6	82.7	76.0	70.5
	50	63.0	47.4	42.8	39.8	37.6	36.1
	80	58.4	42.9	38.7	36.1	34.3	33.0
	110	56.0	40.5	36.6	34.2	32.6	31.3
	140	54.4	38.9	35.3	33.0	31.4	30.3
	170	53.3	37.9	34.3	32.2	30.7	29.7
	200	52.3	37.0	33.6	31.6	30.2	29.1

6.4.4. Thickness optimisation of EPS insulation and FSPCM board

It has been reported in the previous section that the energy rating of a house increases with increasing t_b or t_{EPS}, leading to reduced energy consumption. However, the material cost will also increase with increasing thickness, which eventually outweighs the energy savings. Therefore, it is necessary to find out the optimal thicknesses of the EPS and FSPCM board based on the LCCA approach described in Section 6.3.5.

Fig. 6.9 shows the method to determine the optimal thickness of the EPS insulation/FSPCM board. For example, the thickness of the EPS insulation can be established first. Then the thickness

of the FSPCM board can be changed from 0 to 30 mm. Based on the selected t_b and t_{EPS}, the initial cost C_i can be determined. EnergyPlus simulation is then conducted to determine the annual energy cost (C_E), followed by the calculation of the total cost (C_T) based on Eq. (6.6). C_T can be depicted in Fig. 6.9 as a function of t_b. Initially, C_T decreases with increasing t_b, but increases again after reaching a minimum value. Obviously, t_b corresponding to the minimum C_T provides the optimal thickness of FSPCM board to achieve the maximum economic benefit at a certain t_{EPS} [208]. The optimisation can be further conducted to find out the optimal value of t_b corresponding to different values of t_{EPS}. Then the best combination of t_b and t_{EPS} can be found to achieve the overall maximum economic benefits.

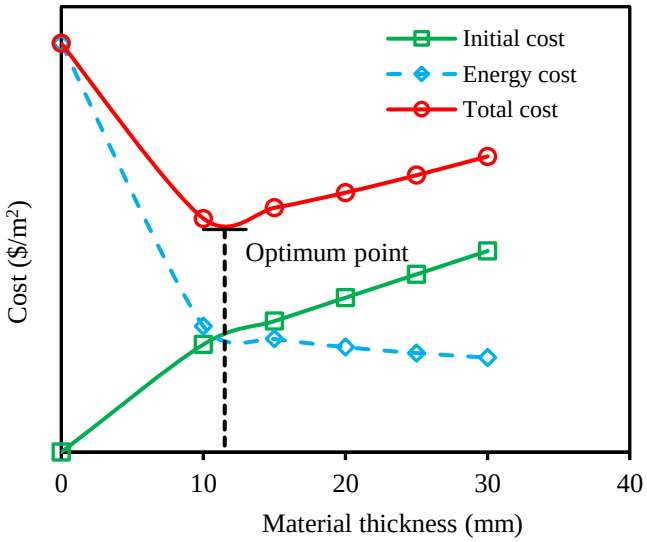

Fig. 6.9. Method to determine optimal thickness of EPS insulation/FSPCM board.

Table 6.6 Optimal thicknesses of EPS insulation and FSPCM board for different cities.

City	Optimal thickness (mm)			
	EPS only	FSPCM only	Combined use	
			EPS	FSPCM board
Darwin	65	25	65	25
Alice Spring	70	30	62	30
Sydney	65	20	60	20

The optimal thicknesses of EPS insulation and FSPCM board are shown in Table 6.6 for the house in Darwin, Alice Springs and Sydney. For comparison purposes, the optimal thickness is also presented for the cases with EPS or FSPCM board only. The optimal value of t_{EPS} is in the range of 65-70 mm for using EPS only. When only the FSPCM board is used, the optimal thicknesses of the

board are 25, 30 and 20 mm in Darwin, Alice Springs and Sydney, respectively. For the combined use of EPS insulation and FSPCM board, the optimal thicknesses of the two layers do not change greatly compared with the sole use of EPS insulation or FSPCM board.

The payback period (*PP*) was calculated using Eq. (6.8) based on the predicted life cycle savings (*LCS*) from Eq. (6.7). Table 6.7 shows the values of *PP* and *LCS* when adopting the optimal thicknesses of EPS and FSPCM board presented in Table 6.6. The energy rating results are also shown in the table for the house after renovation. It was found that the sole use of EPS is more economical and effective in improving the star rating of the house than the sole use of FSPCM board. However, an energy rating of 6.4 stars was only achieved in Darwin when using EPS only. In other cases, the minimum energy rating of six stars was not achieved by using EPS or FSPCM board only. In contrast, obvious benefits could be found for the combined use of EPS and FSPCM board. In general, the value of *PP* for the combined scenario is shorter than that of the scenario using FSPCM board only, and close to that of the scenario using EPS only. Meanwhile, the energy rating of the house can be significantly improved in the combined scenario; the minimum six-star target can be met in all three cities. It should be noted that it is not economically and technically viable to only increase the thickness of EPS to meet the minimum six-star target in Alice Springs and Sydney. Even if the EPS thickness is increased to 200 mm, the energy ratings of the house can only be increased to 5.1 and 4.9 stars in the two cities, respectively. Using such significant insulation thickness, the usable space of the house will be significantly reduced.

Table 6.7 Results of LCCA in different climate zones.

City	EPS only			FSPCM only			Combined use		
	LCS (AU$/m^2)	*PP* (yrs)	Stars	*LCS* (AU$/m^2)	*PP* (yrs)	Stars	*LCS* (AU$/m^2)	*PP* (yrs)	Stars
Darwin	137.3	1.6	6.4	66.7	3.4	5.2	167.0	2.2	7.2
Alice Springs	129.4	1.8	4.5	83.4	3.4	3.7	162.3	2.5	6.0
Sydney	27.9	8.0	4.4	12.8	13.7	3.4	39.7	7.5	6.1

Because of the benefits resulting from the combined use of EPS and FSPCM board, further enviro-economic analysis was conducted for this scenario. Currently, the electricity generation in

Australia is still heavily reliant on fossil fuels such as coal. Statistics show that electricity generation from coal in Australia accounted for 58% of total generation in 2019 [209]. In this analysis, we assumed that the energy saving from house renovation could reduce the consumption of electricity generated from coal. According to [210], around 0.81 kg of CO_2 is emitted per kWh for Sydney and 0.62 kg of CO_2 is emitted per kWh for both Darwin and Alice Springs. A carbon pricing scheme was implemented in Australia in 2012 only to be repealed in 2014. As the Northern Territory government did not impose any carbon price separately in 2014, there is no carbon price available in the open literature for Darwin and Alice Springs. Therefore, we have taken the 2014 carbon price AU$25.40/t$CO_2$ based on the Australian government policy for analysis [211]. The results of the enviro-economic analysis for the combined case are shown in Table 6.8. In the enviro-economic analysis, we first determined the energy savings (E_{savings}) from renovation in the life cycle. Then the CO_2 savings (ϕ_{CO_2}) were calculated as E_{savings} × kg CO_2/kWh. Finally, the environmental cost savings were determined as ϕ_{CO_2} × AU$25.40/t$CO_2$.

The results of the enviro-economic analysis found that significant reduction in carbon emissions can be achieved through the combined use of EPS and FSPCM board. The environmental cost savings are more significant in Darwin and Alice Springs than in Sydney. This is because relative less thermal energy consumption is required in Sydney than in the other two cities. Therefore, the relative energy savings in Sydney is also lessened. In general, it can be concluded that the combined use of EPS and FSPCM board is environmentally viable for renovating Australian houses in the three selected cities.

Table 6.8 Results of enviro-economic analysis.

City	Energy savings in life cycle (kWh)	Savings in CO_2-eq (kg/m^2)	Environmental cost savings (AU$/m^2)
Darwin	613.65	380.5	9.7
Alice Springs	614.45	380.9	9.7
Sydney	212.0	171.7	4.4

6.4.5. Impact of occupancy profiles

In the previous sections, we only considered the worst scenario (Scenario 1), i.e., the house is occupied for 24 hours a day. In this section, we study the effect of the occupancy schedule on the

energy consumption of the house. The second scenario (Scenario 2) is further considered, where the house is unoccupied from 9:00 am to 17:00 pm, and so the heating, ventilation and air-conditioning system are not used during that period, potentially saving on energy consumption. This analysis was conducted on the house refurbished with the optimal thicknesses of EPS and FSPCM board as described in the last section.

Table 6.9 shows the energy consumption for the two occupancy schedules in the three cities. Compared with Scenario 1, Scenario 2 led to significant reduction in energy consumption and an increase in life-cycle savings (40.3–50.3%). Meanwhile, the star rating of the house increased further. Because of the change in occupancy schedules, the energy rating of the house was improved by 1.9 stars (from 7.2 to 9.1 stars) in Darwin, 1.6 stars (from 6.0 to 7.6 stars) in Alice Springs and 2.2 stars (from 6.1 to 8.3 stars) in Sydney. The analysis highlights the need to establish a realistic occupancy schedule in determining energy consumption and the energy rating for a house.

Table 6.9 Impact of occupancy schedule on annual energy consumption.

City	Energy consumption ($MJ/m^2.y$)		Life-cycle savings (LCS)	
	Scenario 1	Scenario 2	$AU\$/m^2$	%
Darwin	271.9	159.9	99.7	41.2
Alice Springs	112.2	67.0	40.3	40.3
Sydney	38.2	19.0	17.1	50.3

6.4.6. Indoor environment characteristics

Indoor thermal comfort was analysed following the method described in Section 6.3.6, where two consecutive summer days (16–17 December) were chosen for the analysis. One of the bedrooms in the house (Bed 2) was chosen to demonstrate the simulation results, as shown in Fig. 6.10. Fig. 6.10 (a-c) shows the temperature variations in the selected bedroom of the house in Darwin, Alice Springs, and Sydney. The average maximum and minimum peak temperatures in the two days are shown in Table 6.10. Without the use of air-conditioning, the indoor temperature was always higher than that of the outdoor temperature when only the EPS was used with a plasterboard finish. This would lead to significant overheating in summer. When FSPCM board was used in combination with EPS, it is not surprising that the indoor temperatures were reduced in the daytime but increased at

night. This is due to the ability of the PCM to absorb heat energy during the daytime and then release it at night. Accordingly, the variation in the indoor temperature and potential overheating could be reduced using PCM on hot summer days.

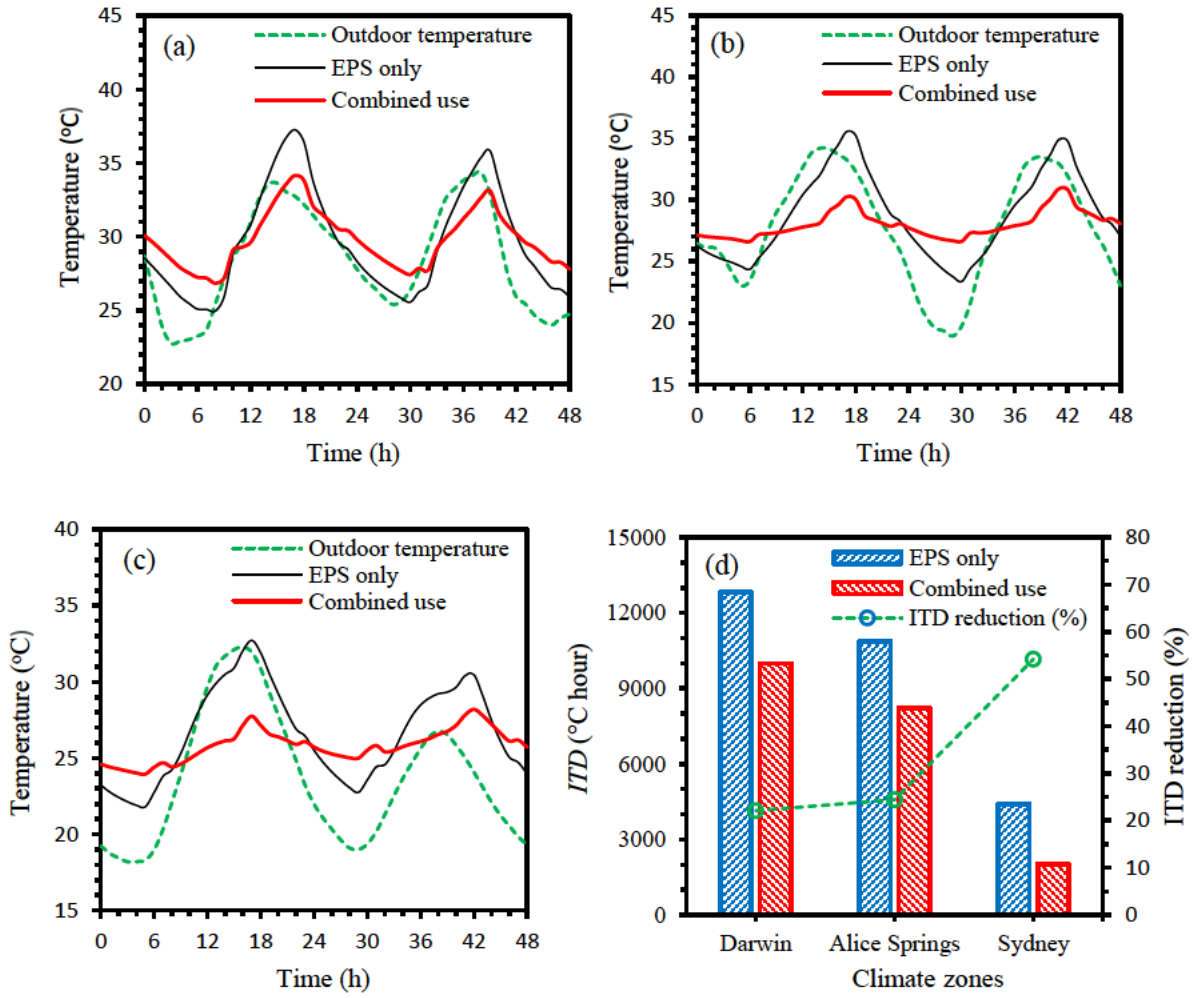

Fig. 6.10. Analysis results of indoor thermal comfort: (a-c) temperature variations in the selected bedroom in Darwin, Alice Springs, and Sydney; and (d) comparison of *ITD*.

Table 6.10 Average maximum and minimum temperatures.

City		Darwin	Alice Springs	Sydney
EPS only	Average maximum temperature (°C)	36.6	35.2	31.6
	Average minimum temperature (°C)	25.2	23.9	22.3
Combined use	Average maximum temperature (°C)	33.6	30.6	28.0
	Average minimum temperature (°C)	27.1	26.6	24.5

The intensity of thermal discomfort (*ITD*) was determined based on Eq. (9) for a whole year and the results are compared in Fig. 6.10d. Compared with the sole use of EPS, the combined use of EPS and FSPCM board could reduce the value of *ITD* by 22.1% in Darwin, 24.4% in Alice Springs, and

54.2% in Sydney. The results confirm that the combined use of EPS and FSPCM board is superior to the sole use of EPS in improving the indoor thermal comfort by reducing the overheating.

6.5. Conclusions

Australia requires a minimum of six stars for the energy rating of all new houses or renovations of existing houses. In particular, there is a need to improve the poor energy efficiency of many existing old houses. Although providing thermal insulation to the external walls and ceilings is a common practice for this purpose, the combined use of phase change materials (PCM) and thermal insulation in building envelopes could potentially provide some additional benefits. Accordingly, the EnergyPlus software has been used to evaluate the energy performance of a typical standalone house in Australia retrofitted with expanded polystyrene (EPS) insulation in combination with form-stable PCM (FSPCM) board. The conclusions from this study include:

(1) The FSPCM board can be effectively applied to both the exterior walls and ceilings. The optimal melting temperature of PCM varies from 25 to 28 °C in Darwin, Alice Springs, and Sydney, depending on the climate conditions and the thickness of the FSPCM board. The natural ventilation at night improves the house's energy performance in Alice Springs and Sydney, but reduces its energy performance in Darwin

(2) The use of EPS insulation is very effective in reducing thermal energy consumption (TEC), but further increasing the insulation thickness only slightly reduces TEC. On the other hand, it is not cost-effective to only use FSPCM board to achieve a desired energy rating. The combined use of FSPCM board and thermal insulation can be more effective in reducing TEC and achieving a minimum six-star rating.

(3) Optimal thicknesses of EPS insulation and FSPCM board have been suggested for the analysed house in Darwin, Alice Springs and Sydney. The optimal thickness of insulation is in the range of 60–65 mm, whereas that of the board ranges from 20 to 30 mm.

(4) In a life cycle of 10 years, the total savings for the optimal combination of PCM board and insulation in Darwin, Alice Springs and Sydney are AU$167.0, $162.3 and $39.7 /$m^2$,

respectively. Meanwhile, the energy ratings of the house are increased by 3.5, 3.8 and 4.3 stars in the three cities, respectively. The combined use of PCM and thermal insulation in the life cycle can generate an annual carbon credit potential ranging between AU$ 4.4 and AU$ 9.7 /m^2. The payback periods of the renovation range between 2.2 and 7.5 years, depending on the climate conditions.

In this study, the impact of the local outdoor climatic condition on the performance of FSPCM board with insulation materials was evaluated for three different Australian cities (Darwin, Alice Springs and Sydney), aiming to achieve minimum six-star rating house requirements and suggest their optimum design parameter of thickness value through a life cycle cost analysis. Nevertheless, to build an energy-efficient house, the design variables and construction parameters directly connected to heat transfer processes need to be optimised. Therefore, further studies should be conducted to optimise the different design variables and construction parameters to that may lead to a high-energy efficiency house.

CHAPTER 7

Sensitivity analysis for house energy efficiency and their cost effectiveness

7.1. Introduction

Energy efficiency within houses is an idea that seeks to develop strategies in reducing energy demand for heating and cooling while still achieving the required thermal comfort levels. An analysis was made in the previous chapter that assessed the benefits of using FSPCM board together with thermal insulation in improving house energy efficiency. In Chapter 6, we evaluated the impact of local outdoor climatic conditions on the performance of FSPCM board with insulation materials for three different Australian cities (Darwin, Alice Springs and Sydney) in achieving minimum six-star rating house requirements and suggested their optimum design parameter of thickness value through a life cycle cost analysis. However, to build an energy efficient house, the design variables and construction parameters connected to heat transfer processes need to be optimised [5, 212, 213]. This chapter outlines some standards developed for improving the energy efficiency of houses by reducing the energy consumption for heating and cooling. These standards are based on adopting proper parameters for thermal insulation, orientation, FSPCM board (thermal mass), ventilation, window shading coefficient, and glazing type. Finally, the house model is optimised relating to life cycle cost, and the set of design variables required to a minimum energy rating standard in PCM-enhanced residential houses in Sydney are presented. Since Sydney's climate is humid subtropical, shifting from mild and cool in winter to warm and hot in the summer, a house’s energy consumption is required for both heating and cooling. Thus, the house design optimisation adopted in this study focuses on Sydney.

7.2. House modelling

The base-case in this study was a typical residential house in Sydney with a 289.6 m^2 floor area, as reported in Chapter 6 where all design variables were applied and examined. The house was modelled using EnergyPlus 8.4.0. The fixed parameters of the house were its floor area and height. The thermostat setting for cooling and heating systems was adjusted according to the Australian standard, as reported in Chapter 6 (section 6.3.4). The house models were provided with boundless electric heating and cooling energy to determine the space energy need for each set of design variables. All windows were single glazed with aluminium frames (U = 5.68 W/(m^2 °C)), one of the most commonly used window types for a new house in Sydney. The design variables' primary setting was an air infiltration rate of 0.6 ACH, with walls and roof fully exposed to sun, and internal blinds that provided the window with a shading coefficient of 0.9. For energy efficient building design, a large series of alternative designs of such residential houses should be considered in seeking an optimal solution in the design space. For the studied house, we pre-defined 8 design variables and their different values as shown in Table 7.1. Premised on these investigations, the suggested value for every design variable was fixed to gain a high energy efficiency performance residential house.

Table 7.1 House parameters for simulations

Variable	Parameter description	Parametric set
V01	Ceiling insulation (resistance; m^2.K/W)	0, 0.571, 1.143, 1.714, 2.286, 2.857
V02	Wall insulation (resistance; m^2.K/W)	0, 0.571, 1.143, 1.714, 2.286, 2.857
V03	Orientation	North, East, South and West
V04	FSPCM board's location in walls and ceiling	Inside, outside in the insulation
V05	Natural ventilation (air changes per hour)	0, 2, 5
V06	Infiltration (air changes per hour)	0.6, 2, 5, 10, 15.5
V07	Window shading coefficient	0.1, 0.3, 0.5, 0.7, 0.9
V08	Window glazing (U-value)	Single (U = 5.68), Double (air-filled; U = 2.83), Double (Ar-filled; U = 1.4)

The different values for each of the design variables in the above Table 7.1 were selected based on the following:

- Wall and ceiling insulation (resistance; m^2.K/W): The insulation level or *R*-value (m^2.K/W) is a measure of resistance to heat flow through a given thickness of the material. The *R*-value of a material can be calculated by dividing its thickness by its thermal conductivity. Here, the *R*-value is considered based on the insulation thickness from 0 to 100 mm (R = 2.857 m^2.K/W) in an interval of 20 mm.
- Natural ventilation rate (ACH): A maximum ventilation rate of 5 ACH is realistic and achievable for a typical air-conditioned house [214].
- Infiltration (ACH): The average infiltration air charge rate of homes constructed in Australia is 15.5 at a pressure difference of 50 Pa, while a low air infiltration of 0.6 ACH is recommended for a passive house [215].
- Shading coefficient: The shading coefficient is a measure of the heat gain through the glass from solar radiation. The shading coefficient for window shades is expressed as a number between 0 and 1. The lower a shading coefficient, the less solar heat it transmits.
- Window glazing: Single glazed with a aluminium frame is the most commonly used windows type in Australia. However, double glazing (air and gas fill) can contribute significantly to a six-star or higher energy-efficient house and is now widely available [216].

7.3. Research method

The sensitivity analysis plays a crucial role in house energy analysis. It provides a ranking of influential design variables that are significant in improving the house's energy performance. The sensitivity analysis for this study was performed on a set of design variables identified during the house's conceptual design stage, as listed in Table 7.1. This chapter aims to guide residential house designers on the impact various design variables have on energy efficiency performance. At first, each individual design variable was checked in the studied house while keeping other variables constant and evaluated the effect of different reasonable values on its energy demand for heating and

cooling, as shown in the investigation diagram in Fig. 7.1. Based on the results, the optimum value for all of the design variables was determined. Fig. 7.2-7.9 show the annual energy consumption results required for heating and cooling per square meter of the house for the analysed design variables.

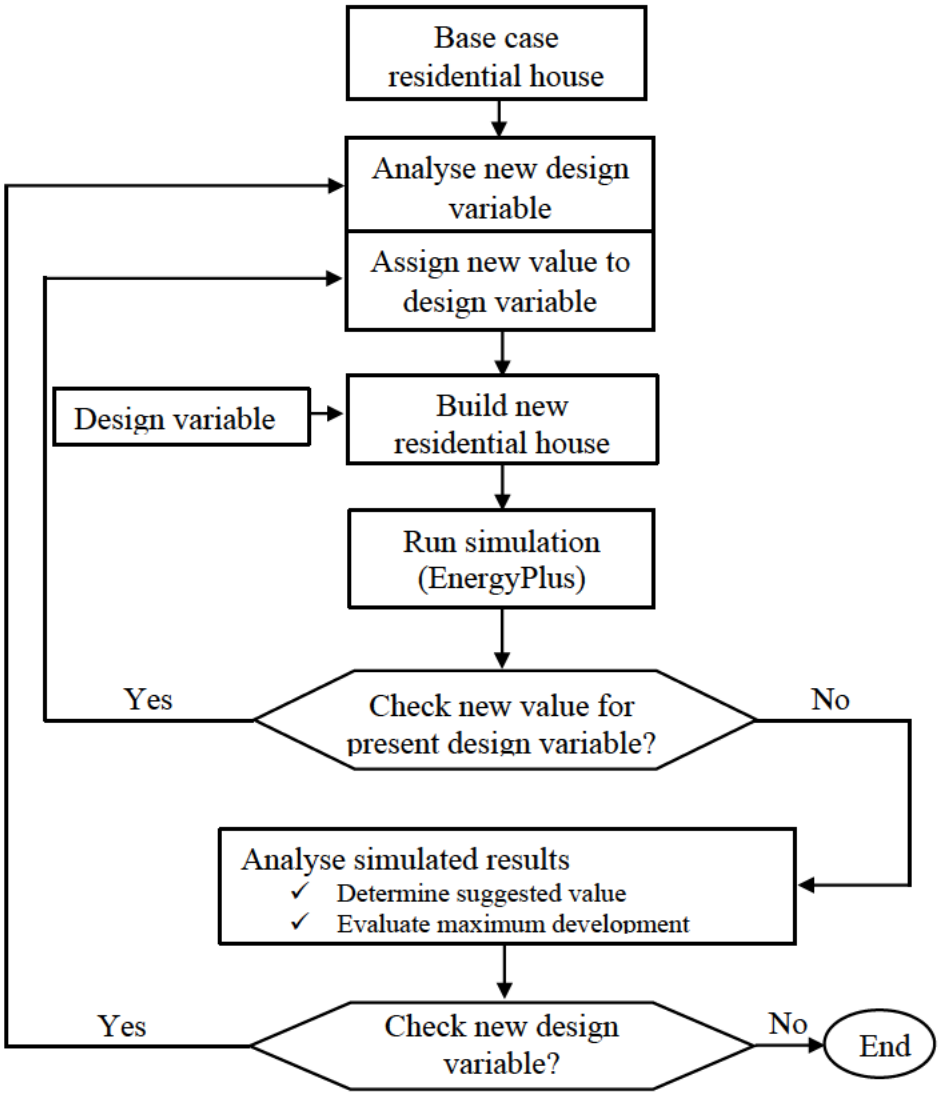

Fig. 7.1. Determining the recommended value of design variables.

7.4. Results and discussion

7.4.1. Effect of thermal insulation on the energy consumption

A combination of insulation materials in the walls and ceilings is a practical approach to improving houses' energy efficiency [9]. In a real house, walls and ceilings are fabricated by many different material layers. A series of simulations were performed to determine the most suitable insulation (*R*-value) layers for both the walls and ceiling. Fig. 7.2 shows the impact of the *R*-value

for insulation material on energy consumption in the house. As shown in Fig. 7.2 (a), increasing the *R*-value of the ceiling insulation material caused reduced energy consumption, and when *R* was >1.714 m^2.K/W, the energy consumption was almost the same at each tested R-value, which is consistent with the previous study in Chapter 6. Based on the results, it is suggested that the ceiling should have an insulation material with an *R*-value of 1.714 m^2.K/W. However, the residential house's external walls, as shown in Fig. 7.2 (b), should have an *R*-value of 0.571 m^2.K/W. By applying the proposed *R*-values, the energy demand for cooling and heating of the ventilated house was reduced by 53.9% for the ceiling and 11.2% for the walls compared to the house without any applyied insulation material. These insulation levels (*R*-values) for walls and ceilings were used for optimising other design variables.

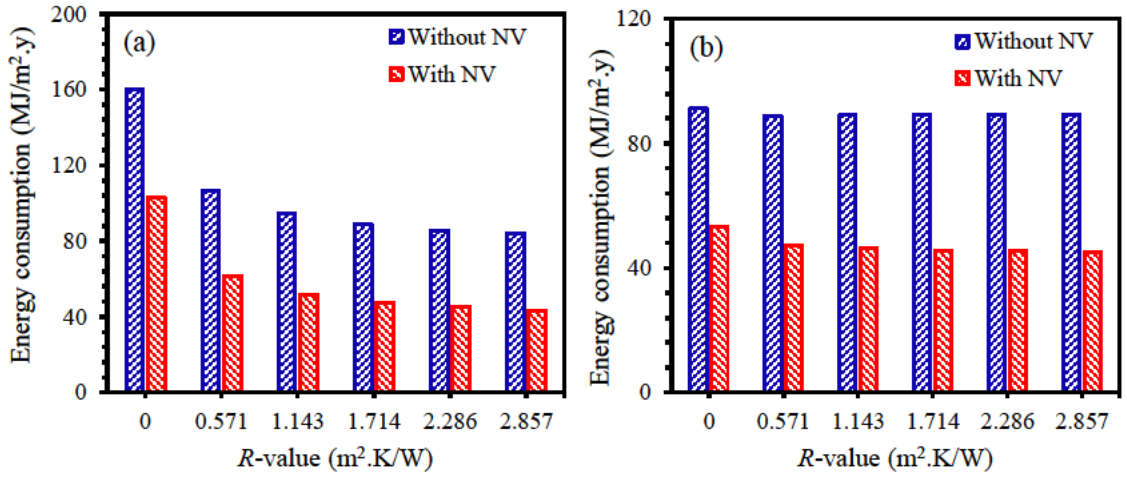

Fig. 7.2. Effect of insulation material's *R*-value on energy consumption, (a) ceiling insulation and (b) wall insulation.

7.4.2. Effect of building orientation on energy consumption

Among various structural parameters that determine energy requirements [217], building orientation is the most important one [213]. Determining the appropriate direction is the most effective approach to lowering energy consumption. If planned at the early stages in the design process, it could be inexpensive and straightforward to execute. To prevent summer overheating, the building should avoid east and west glazing. Fig. 7.3 provides an overview of energy consumption concerning four orientations, specifically North, East, South, and West (0, 90, 180 and 270°) for the

houses. The results show that the minimum energy consumption is achieved at 90°, because at this position the east wall area, which has the largest load contribution, is minimised. Although the orientation is not a major determining factor in the design of a building because of low energy savings, a reduction in the annual energy consumption of 5.3 MJ/m^2 (10.8%) can result, compared to the opposite at 270° from its maximum load direction for this house. Of course, practically the house cannot always orient to the best location since orientation is mostly driven by the plot shape and position with respect to roads.

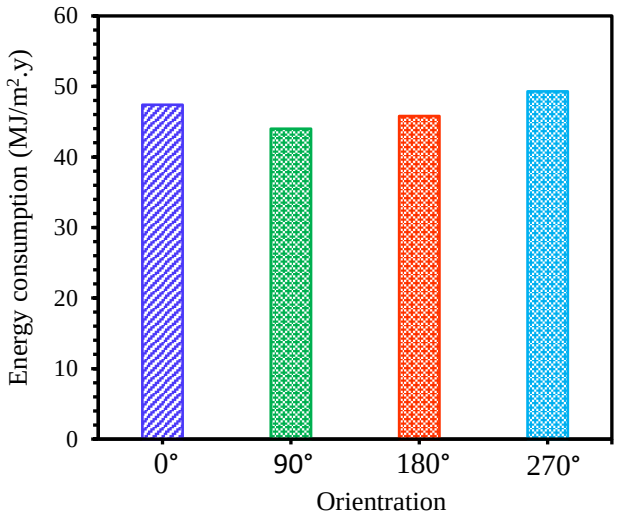

Fig. 7.3. Effect of building orientation on energy consumption.

7.4.3. Impact of FSPCM board location on energy consumption

With the rapid rise of summer temperatures in Australia and an increasing number of extreme heat events, the high insulation and airtight houses' effect comes down to increased overheating (reported in Chapter 6), resulting in an increased cooling energy demand for air conditioning. In Chapter 6, it has been demonstrated that the combined use of FSPCM board and insulation in building envelopes is effective in controlling the issue of overheating while improving the indoor thermal comfort. PCM thus helps to improve thermal comfort in summer while reducing the cooling energy consumption [218]. In winter, it is also useful for reducing energy demand for heating. The effect of the FSPCM board on house energy consumption for different thicknesses of the FSPCM board (t_b = 10-30 mm) inside the insulation layer in the walls and ceilings was evaluated in Chapter 6. The FSPCM board's location in the external walls and ceiling, either outside (position 1) or inside

(position 2) of the insulation layer (Fig. 7.4), affects its capacity to store thermal energy and release it inside the house when required.

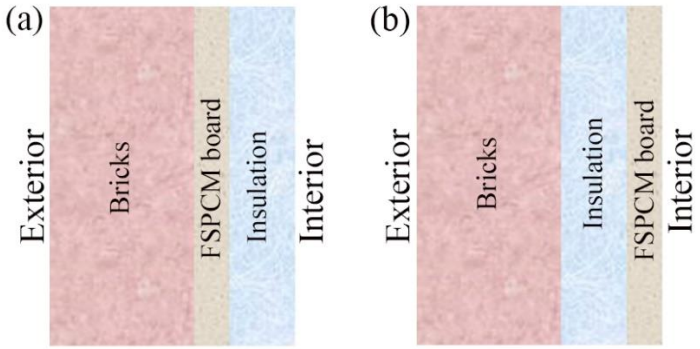

Fig. 7.4. Location allocation of FSPCM board in the building envelope: (a) position-1, and (b) position-2.

Based on this understanding, house energy efficiency was tested using an FSPCM board with a thickness of 20 mm in these locations for the walls and ceiling. As can be seen from Fig. 7.5, the walls and ceiling with the FSPCM board at position-2 (inside of the insulation board) had a higher energy reduction than at position-1 (outer side of the insulation layer). This result is consistent with the findings reported by Wang et al. [184] and Li et al. [219], where reduction in heat transfer to the interior of the building was achieved by installing PCM near the inner wall surface. This is because, at position 1 (outer surface of the insulation board), the PCM can melt quickly at daytime and remain in the liquid phase longer than the PCM at position 2 (inner surface of the insulation board). The thermal storage potential of PCM is reduced if the PCM remains in the melted state for a longer time, as demonstrated in a previous study [192]. The FSPCM board at position-1 could not absorb heat from the inside of the room, and it only reduced the heat flow to the indoors from the outdoors. From the prospect of balance between sufficient heat absorbed from the indoors and released to the outdoors, position-2 could attain more benefits. This study is consistent with previous studies [105, 181], where the optimum position for the PCM layer was closed to the interior surface. Since up to 40% of solar heat gain and loss is through the roof alone, installing the FSPCM board in the ceiling has a greater impact on reducing total energy use than in the external walls. It can be seen from Fig.

7.5 that using t_b = 20 mm inside the insulation layer of the walls can save energy consumption of 5.8 MJ/m^2.y, which is much lower than the energy-saving of 8.1 MJ/m^2.y for use of an FSPCM board inside the ceiling. Thus, it is more advantageous in terms of energy savings to use an FSPCM board within the ceiling.

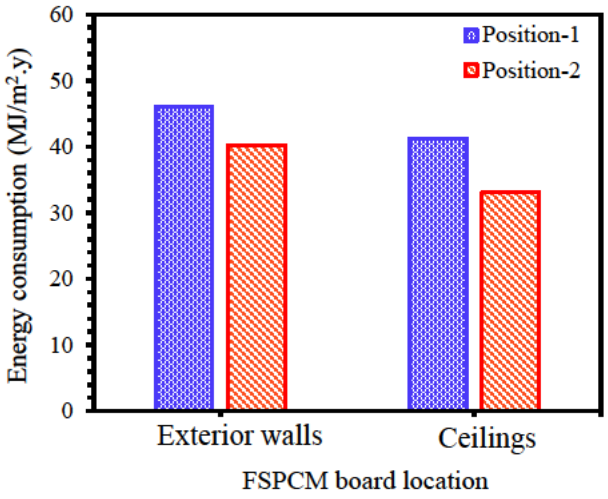

Fig. 7.5. Effect of FSPCM board location

7.4.4. Effect of NV and FSPCM board on energy consumption

While the beneficial use of natural ventilation (NV) with the FSPCM board at night-time was demonstrated in the previous chapter, it should also be worth noting that an appropriate NV design with the PCM system is critical for enhancing PCM efficiency performance by increasing the possibility of a full charging and discharging process. Coupling the PCM passive system with NV at night could be a perfect choice to enhance the house's energy efficiency. However, the temperature profile and amount of ventilation are important factors for the proper and effective functioning of PCM. In this study, the air temperature profile provided by the ventilation system was controlled with a set point temperature (T_{set}) of 18 and 26 °C. The T_{set} denotes that ventilation operation happens excepting when the outdoor temperature either exceeds 26 °C or is below 18 °C. The amount of NV can also be controlled with variable airflow rates of ventilation for a specific operation period. Solgi et al. [220] studied the impact of using PCMs with night ventilation in various Australian cities and reported that the amount of ventilation does not influence the PCM's melting point while it affects the energy demand for cooling. The effect of NV was evaluated in this section, determining how its

addition improves the performance of FSPCM board with an optimum PCM melting temperature when compared to the non-ventilated house. Hence, the variables tested in this section were the amount of night ventilation, which can be controlled by ventilation airflow rates for an operation period of 19:00 to 7:00. To understand the effect of the ventilation airflow rate, we conducted a sensitivity analysis for 2.0 ACH and 5.0 ACH airflow rates for two passive systems by installing different FSPCM boards' thicknesses only in the ceiling and the same board within the walls. The results showed that a combination of FSPCM board coupled with NV could increase PCM's effectiveness for passive systems and reduce energy consumption by up to 9.2% (with t_b =20 mm only in walls) and 17.9% (with t_b =20 mm in ceilings) compared to the consumption of the house without NV (Fig. 7.6). Overall, the highest efficiency is achieved with greater airflow (5 ACH) and 20 mm of FSPCM board thickness.

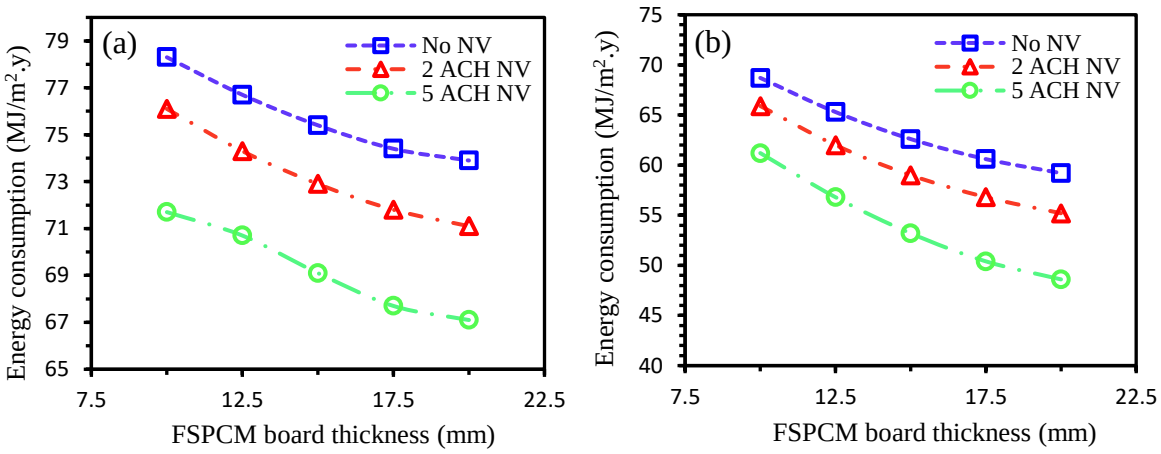

Fig. 7.6. Effect of NV and FSPCM board on energy consumption: (a) FSPCM board only in walls, (b) FSPCM board only in the ceiling.

7.4.5. Effect of infiltration on energy consumption

A residential house's airtightness depends on the types of windows and doors, materials, and the construction process' quality. The air infiltration through and around windows and doors, in joints and floor/ceiling to wall connections are major problems within conventional residential houses. Previous studies reported that the average infiltration air charge rate of homes constructed in Australia is 15.5 at a pressure difference of 50 Pa (15.5-ACH@50Pa) [221], a lower performance in energy efficiency than expected. For homes without a mechanical ventilation system, an infiltration rate

lower than 3.0-ACH@50Pa is required, and for places with mechanical ventilation, an infiltration rate of 1.5-ACH@50Pa is needed [222]. An airtight building envelope ensures minimal gaps, which is essential for thermal comfort, especially in Passive House buildings. A Passive House requires the air infiltration to be as low as 0.6 air changes per hour (ACH) at a pressure of 50 Pa [215].

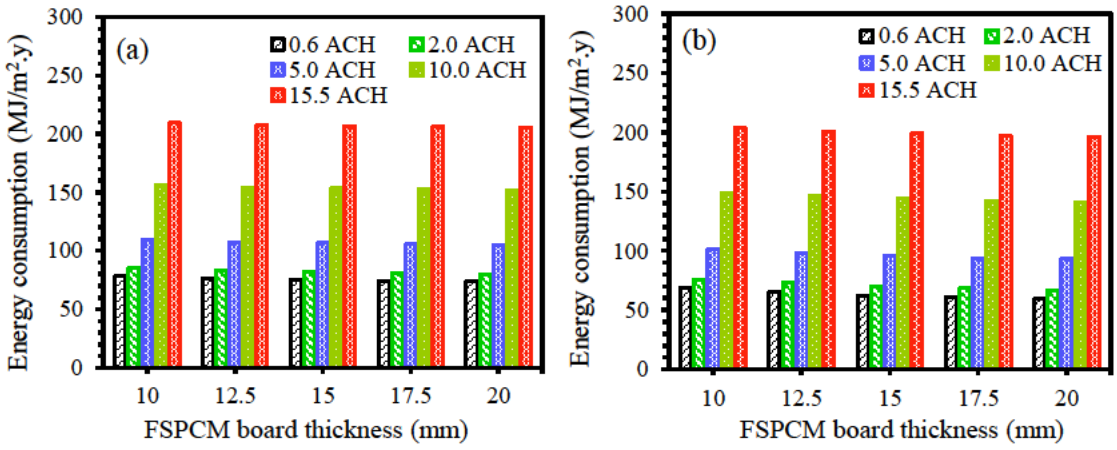

Fig. 7.7. Effect of infiltration and FSPCM board on house energy consumption: (a) FSPCM installation within walls (b) FSPCM installation within ceiling.

Fig. 7.7 shows the impact of air infiltration on energy performance with the FSPCM board installed in walls and ceilings. The infiltration rate has a significant influence on the energy efficiency of the house retrofitted with FSPCM board. When the infiltration rate is very high, the FSPCM board has little impact on the energy consumption of the house (Fig. 7.7). In contrast, if the house is well sealed against air leakage, the use of FSPCM board could significantly reduce the energy consumption of the house. The results show that an air infiltration rate of 0.6 ACH is necessary to realise the energy-saving potential of a PCM integrated house.

7.4.6. Effect of window shading on energy consumption

Solar heat gains through windows are one of the most common reasons for indoor air-conditioning cooling energy consumption. That makes controlling the entrance of solar heat crucially important in improving energy efficiency management. Roughly 40% of the solar heat that builds up in a house comes in through windows [223]. The shading coefficient (SC) is a measure of how well a window blocks heat caused by sunlight. Thus, effective shading design in the window can limit heat gains, regulate swings in temperature, and reduce cooling requirements. In this section, an analysis

of the influence of a window's shading coefficient on a house's energy consumption for different FSPCM board thickness in walls and ceilings is presented. SC is expressed as a number between 0 and 1. The higher a window's SC, the more solar heat it transmits. The result in Fig. 7.8 shows the effect of different values of SC on house energy consumption.

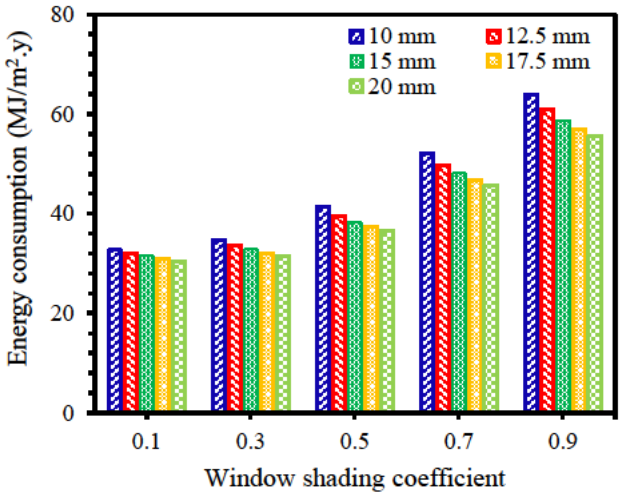

Fig. 7.8. Effect of window shading and FSPCM board on house energy consumption.

As shown in Fig. 7.8, decreasing SC causes a reduction in energy consumption, and when SC<0.3, the energy consumptions recorded are almost the same. However, further reduction of SC has a negligible impact on the decrease in house energy consumption. This result confirms that a maximum SC of 0.3 (30% of incoming solar energy being transmitted inside the house) should be maintained for an energy-efficient home.

7.4.7. Effect of window glazing on energy consumption

While windows and glazing are essential architectural and functional components of a building for daylighting and ventilation, glazing areas are affected by heat loss, discomfort, and condensation problems. However, a high-performance, energy-efficient glazing system is now available to reduce energy demands for heating and cooling. Windows utilising this system have low heat loss and warmer window surfaces that improve thermal comfort and minimise condensation. In this section, an analysis of the impact of window glazing such as single and double glazing (air and argon filled) on the house's energy consumption with FSPCM board in the walls and ceilings is presented. The characteristic features of different glazing systems are shown in Table 7.2.

Table 7.2 Characteristics of different glazing types [172]

Glazing type	*U* value (W/m^2°C)	Solar heat gain coefficient (*SHGC*)	Visible transmittance (*VT*)
Single	5.68	0.855	0.901
Double (air-filled)	2.83	0.775	0.817
Double (Ar-filled)	1.4	0.589	0.706

The simulation results presented in Fig. 7.9 show that a significant energy saving of 13.7-14.7% can result for the house with different FSPCM board thicknesses for air-filled double-glazed windows when compared to the construction with single-glazed windows. Double glazing Ar-filled windows perform with significant energy efficiency to further reduce energy consumption by an average of ~32.3% compared to air-filled double-glazed windows. Although energy-efficient double glazing with Ar-filled windows may initially be expensive, ~10% compared to double glazing with air-filled windows [216], their long-term energy saving benefits may be worth it.

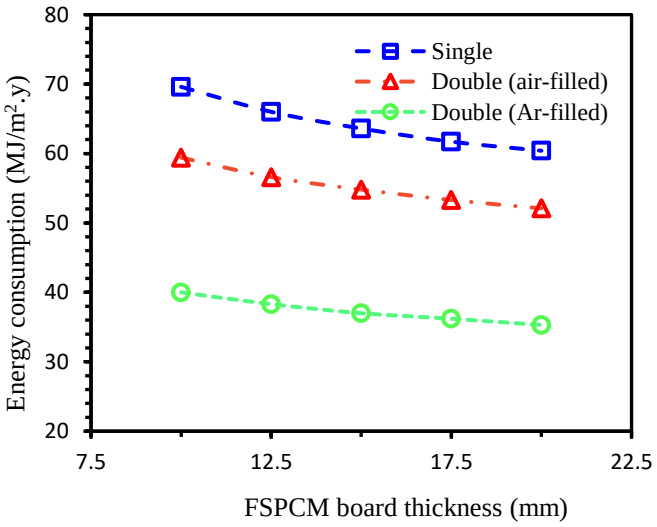

Fig. 7.9. Effect of window glazing and FSPCM board on house energy consumption.

A minimum 6-star requirement for house energy ratings provides an easy means of associating windows for house energy-efficiency, allowing users to make a more educated purchase decision. It is clear that with the increase of FSPCM board thickness, the energy consumption for all glazing systems decreases. However, it is essential to mention that the amount of energy saving with changing the FSPCM board thickness is different. For example, in the case of double glazing (Ar-filled), the energy-saving is 4.7 MJ/m^2.y, which is less in comparison with 9.2 MJ/m^2.y for single glazing and

7.3 MJ/m^2.y for double glazing (air-filled) when FSPCM board thickness increases from 10 mm to 20 mm. Thus, in practical applications, the suitable thickness of the FSPCM board should be selected considering both effectiveness and the cost of the FSPCM board.

The main principle of this study was to create a building envelope to optimally control solar heat gains and reduce energy demand for heating and cooling while maintaining a comfortable indoor environment. Detailed energy simulations were then conducted as shown in Fig. 7.2-7.9 to present recommendations on the choice of insulation, glazing, shading, infiltration, FSPCM board (thermal mass) and natural ventilation of a house in Sydney. Based on the above simulation results on house energy consumption, the optimum value for each design variable is summarised in Table 7.3.

Table 7.3 Optimum value of each design variable based on energy consumption.

Design variable	Value
Orientation	East
Ceiling insulation (resistance)	R 1.714 m^2.K/W (60 mm thickness)
Wall insulation (resistance)	R 0.571 m^2.K/W (20 mm thickness)
FSPCM board ceiling	Inside (20 mm thickness)
FSPCM board walls	Inside (20 mm thickness)
Night ventilation	5 ACH
Infiltration rate	0.6 ACH
Window shading coefficient	0.3
Window glazing	Double glazed-high: U = 1.4; $SHGC$ = 0.589, VT = 0.706

7.4.8. Economic and enviro-economic analysis

In Chapter 6, an economic analysis of using FSPCM board and insulation in both walls and ceilings was performed. According to the results, the most attractive solution for improving houses' energy performance in different Australian cities is using FSPCM board together with thermal insulation rather than the use of insulation or FSPCM board only. In this section, three various case studies have been performed, those being installing an FSPCM board with insulation on the external walls only, ceiling only, and both the walls and ceiling using the optimum design parameters. A life cycle cost (LCC) analysis, which compares different design alternatives for the house in Sydney considering the cost and savings associated with each design option, is considered as reported in

Chapter 6. For economic analysis, the various cases (Scenarios 1-3) examined in the simulation are as follows:

- Reference case (optimised house) – No insulation and FSPCM board
- Scenario-1 (wall case) – Insulation and FSPCM board used in exterior walls only
- Scenario-2 (ceiling case) – Insulation and FSPCM board used in ceiling only
- Scenario-3 (wall and ceiling case) – Insulation and FSPCM board used in exterior walls and ceilings

Table 7.4 shows the values of life cycle savings *(LCS)* and payback periods *(PP)* when adopting the value for different design variables are presented in Table 7.3. The *PP* was calculated by taking into account the *LCS* for electricity as an energy source. The *LCS* of AU$5.1/m^2 was calculated for installing FSPCM board and insulation in the walls only (wall case), which is much lower than the *LCS* values of AU$36.7/m^2 and AU$39.5/m^2 for installing in the ceiling only and both the walls and ceiling. The results show that using the FSPCM board and insulation in the walls is not economically viable as the estimated payback period for this case is 13.9 years, which is higher than their service life of 10 years. In contrast, a shorter payback of 4.7 and 6.2 years is found for the scenarios in using FSPCM board with insulation in the ceiling only and both the walls and ceiling, which is 1.3 years lower than the payback period found in Chapter 6 for installing FSPCM board and insulation material with a thickness of 20 mm and 60 mm in both the walls and ceiling. Table 7.4 shows that the optimum thickness of the FSPCM board and insulation materials were found to be similar to the value reported in Chapter 6, except for the insulation materials in walls. It can be seen that the optimum thickness of insulation materials for walls is 20 mm, which is 40 mm lower than the value reported in Chapter 6, thus resulting in a lower payback period. These results would be useful for selecting economic installation options of FSPCM board with insulation material in the envelope for residential building; it has important potential when carrying out energy conservation and sustainable building designs.

Table 7.4 Results of life cycle cost and enviro-economic analysis

	Energy consumption ($MJ/m^2.y$)	*LCS* ($AU\$/m^2$)	*PP* (yrs)	Stars	Savings in CO_2-eq (kg/m^2)	Environmental cost savings ($AU\$/m^2$)
Reference case	89.4	-	-	3.3	-	-
Scenario-1	75.3	5.1	13.9	3.7	30.5	0.8
Scenario-2	27.8	36.7	4.7	7.3	133.2	3.8
Scenario-3	16.4	39.5	6.2	8.5	157.9	4.0

It is important to note that a higher energy rating (3.3 stars) residential house (Table 7.4) can be achieved in Sydney by using an optimum orientation, infiltration, window glazing and shading coefficient (Table 7.3) compared to the typical 1.8-star rating house as reported in Chapter 6. However, the minimum energy rating of six stars has not been achieved without using insulation and the FSPCM board. Meanwhile, the house's energy ratings increase by 0.4, 4.0, and 5.2 stars when the FSPCM board is used together with insulation in the walls only, ceiling only, and both the walls and ceiling, respectively. The result shows that installing the FSPCM board with insulation material in the ceiling is more economically and technically viable to meet the minimum energy efficiency (six-star) target in Sydney (Table 7.4).

The growing awareness of environmental issues requires reporting of environmental impacts in addition to an economic analysis. This evaluation is conducted depending on the cost of carbon dioxide (CO_2) emissions to the environment from generating electricity using coal as per section 6.4.4. The results show (Table 7.4) that the reduction of CO_2 emissions to the environment vary between 30.5 kg/m^2 and 157.9 kg/m^2 over a lifetime of 10 years based on the scenarios. The environmental cost savings related to carbon emissions in $AU\$/m^2$ is found to be 0.8, 3.8 and 4.0 for the scenarios of installing FSPCM board with insulation material in the walls, ceiling, and both the walls and ceiling.

7.5. Conclusions and recommendations

In this study, the energy efficiency performance of a residential house for Sydney was optimised using EnergyPlus 8.4.0, which is useful in the early-stage design phase when different building designs are being considered. A set of design variables was taken, and a range of variation was given

for each variable. The simulation results show that the load for house energy demand can be significantly reduced by adopting energy efficiency strategies (optimisation processes). The main conclusions and recommendations are as follows:

- Referring to orientation, the best position for a house is to have its unglazed side facing east with the most significant load contribution. Locating the unglazed wall at 90° (east) resulted in an annual load reduction of 5.3 MJ/m^2 (10.8%) compared to the opposite at 270° (west) from its maximum load direction for this house.
- The best performing optimisation models had insulation levels of 0.571 and 1.714 m^2.K/W for the exterior walls and ceiling, a natural ventilation rate of 5 ACH, and argon-filled double-glazed windows with a U-value of 1.4 W/m^2°C, and shading coefficient of 0.3.
- The ceiling insulation and infiltration air charge rate are the most influential design variables on energy efficiency of the house. The house energy rating can be achieved by adopting an infiltration rate of 0.6 ACH.
- A 20 mm thick layer of FSPCM integrated into the house's exterior walls and ceiling was found to be the optimum option. The best performance of the FSPCM board is achieved by placing it inside the surface of the thermal insulation.
- The life cycle cost analysis has shown that installing the FSPCM board with insulation material in the ceiling is more economically and technically viable to meet the minimum energy efficiency (six-star) target in Sydney.

Regarding the fast economic growth and building development in Australia, the proposed design optimisation would be of great interest to building designers concerned about energy efficiency in houses and the environment.

CHAPTER 8

Conclusions and recommendations for future research

8.1. Conclusions

An idea regarding the improvement of energy efficiency in residential houses using PCM in passive manners directed researchers in recent years to develop PCM-based composite materials and utilise them to increase TES capacity in houses. Gypsum board integrated with PCM has excellent potential to be used as an interior finishing material for improving indoor thermal comfort while reducing energy use. This research has aimed to overcome the main issues with the inclusion of PCM into gypsum board, including their shape instability or leakage during the phase change process and poor heat transfer rate related to PCM's low thermal conductivity, that acts as a block upon the effective utilisation of its enormous TES capacity benefits. Hence, a form-stable PCM was developed by containing PCM into porous diatomite material to address these issues and study the impact of using them in maximising the TES capacity of gypsum board to improve the energy efficiency performance of houses. Besides, no research has been conducted to study the energy performance of using FSPCM-based gypsum board in real houses, especially in combination with thermal insulation. This thesis presented an experimental evaluation of thermal performance improvement using the FSPCM-enhanced gypsum board within a house and compared it with a traditional one without FSPCM. EnergyPlus was also used to validate the experimental results of a model house, and other parametric studies to optimise FSPCM board performance were carried out. The simulation using the validated EnergyPlus model was performed to develop a framework for the cost-benefit assessment of retrofitting strategies (using insulation, FSPCM-enhanced gypsum board, and FSPCM-enhanced gypsum board coupled with insulation) to achieve a minimum six-star energy rating performance of existing residential houses in Australia. The key conclusions of this research are as follows:

1. The development of FSPCM using diatomite resulted in higher PCM retention into diatomite pores with good thermal stability. The developed FSPCM has improved thermal conductivity

and excellent phase change properties, making it suitable for developing thermal energy storage building materials, such as PCM wallboard for reducing energy consumption and indoor temperature fluctuations

2. The main issue associated with integrating pure PCM into building materials was PCM leakage or instability which is effectively resolved by developing a diatomite supported FSPCM. Gypsum board containing FSPCM fabricated in this study was shown to have multifunctional properties, i.e., excellent TES capacity and energy performance with suitable mechanical performance.
3. The FSPCM integrated gypsum board is considered an internal furnishing material for utilizing passive latent heat storage in houses that can significantly reduce peak indoor air temperature and shift to off-peak period, as displayed from the thermal performance examinations carried on small test chambers and model houses.
4. FSPCM-enhanced gypsum board application in building envelopes was affected by inadequate solidification at night, leading to decreased TES efficiency at daytime. The use of natural ventilation at night-time enhanced the PCM solidification and further improved the indoor thermal performance.
5. FSPCM board's use, coupled with thermal insulation into walls and ceilings, could significantly reduce overheating while improving the houses' energy efficiency performance. Their combined use was found to be more effective in achieving a minimum six-star rating. However, the houses' star rating improvement is different for each of three different Australian cities (Darwin, Alice Springs, and Sydney), representing three different climate zones (tropical savanna, hot semi-arid, and humid subtropical).
6. From the economic evaluation of the FSPCM board and insulation into walls and ceilings of residential housing in Australia, the recovery or payback period was found to be between 2.2 and 7.5 years, depending on climate conditions. Since the payback period is smaller than the average life span (10 years) of the materials, their incorporation into walls and ceilings is

economically feasible. From environmental evaluation, a saving of 171.7–380.9 kg CO_2-eq/year/m^2 was achieved. Therefore, these reductions would contribute to mitigating emissions of Greenhouse Gases over the life span of houses.

7. The parametric sensitivity case study conducted in Sydney with the optimisation of different influential design variables revealed that the optimum variables helped maximise the house's energy efficiency performance.

8.2. Recommendations for future research

1. A hybrid FSPCM board system with two or more PCM melting temperatures can be an effective approach for year-round TES in buildings, particularly in climates with an extensive diurnal temperature range. Further study of the optimisation of FSPCM board with a multi-PCM system should be addressed.
2. Future work may focus on further improving thermal properties of the FSPCM by adding some nanoparticles. Other alternatives to supporting materials could be investigated to achieve a better cyclic performance of the FSPCM so that it can extend the lifetime of the PCMs as long as possible for building applications.
3. The present research work was limited to improving typical residential houses' thermal/energy efficiency by using energy simulation software. Implementing retrofits to existing residential dwellings and getting real-world energy loads measurements to determine the benefits is recommended.
4. This study was limited to the addition of FSPCM into gypsum board and its use as an internal finishing material in walls and ceilings to improve the energy efficiency performance of residential houses under three different Australian cities (Darwin, Alice Springs and Sydney). Future study should focus on how to utilise FSPCM more effectively in Australian homes under different climate zones. The selection of proper building materials is required to achieve higher PCM effectiveness. Analysing the performance of FSPCM with medium and

heavy construction materials such as plasterboard, mortar, and concrete would be valuable. Future study may also be needed to evaluate the effects of using FSPCM on roof tiles and PV panels, assessing performance for building applications.

5. In this work, we investigated the brick veneer residential houses with a fixed floor design. However, the effect of climate change on different types and sizes of residential building stock needs to be more extensively investigated. It is also important to realize how the occupants become adept in with the changing climate conditions.
6. The thermal performance of the FSPCM could reduce after many phase change cycles. The economic benefits of the FSPCM board were evaluated based on the year-round energy consumption (heating and cooling) measured by EnergyPlus for different cases in chapter 5 and Chapter 6 without considering the above issue. Therefore, further research should be conducted to check the long-term thermal performance of the FSPCM, which may be taken into account in the life cycle cost analysis

References

[1] X. Cao, X. Dai, J. Liu, Building energy-consumption status worldwide and the state-of-the-art technologies for zero-energy buildings during the past decade, Energy and Buildings 128 (2016) 198-213.

[2] World Business Council for Sustainable Development, Energy Efficiency in Buildings – Transforming the Market <https://docs.wbcsd.org/2009/08/EEB-TransformingTheMarket.pdf>, 2009 (accessed 11 March.2020).

[3] L. Pérez-Lombard, J. Ortiz, C. Pout, A review on buildings energy consumption information, Energy and Buildings 40(3) (2008) 394-398.

[4] Australia's national greenhouse gas inventory 1990, 1995, and 1999 : end use allocation of emissions : report to the Australian greenhouse office /George Wilkenfeld & Associates Pty Ltd and Energy Strategies. <https://trove.nla.gov.au/work/22963526?selectedversion=NBD24535903>, 2002).

[5] S.B. Sadineni, S. Madala, R.F. Boehm, Passive building energy savings: A review of building envelope components, Renewable and Sustainable Energy Reviews 15(8) (2011) 3617-3631.

[6] M. Saffari, A. de Gracia, S. Ushak, L.F. Cabeza, Passive cooling of buildings with phase change materials using whole-building energy simulation tools: A review, Renewable and Sustainable Energy Reviews 80 (2017) 1239-1255.

[7] Clean Energy News and Analysis, Top 10 technologies to double energy efficiency, deliver zero emissions. <https://reneweconomy.com.au/top-10-technologies-to-double-energy-efficiency-deliver-zero-emissions-65210/>, (accessed 11 March.2020).

[8] Standards Australia. Thermal insulation of dwellings, Part 1: Thermal insulation of roof/ceilings and walls in dwellings, AS 2627.1-1993. Australia: Sydney; 1993.).

[9] L. Aditya, T.M.I. Mahlia, B. Rismanchi, H.M. Ng, M.H. Hasan, H.S.C. Metselaar, O. Muraza, H.B. Aditiya, A review on insulation materials for energy conservation in buildings, Renewable and Sustainable Energy Reviews 73 (2017) 1352-1365.

[10] J. Kosny, N. Shukla, A. Fallahi, Cost analysis of simple phase change material-enhanced building envelopes in southern U.S. climates. U.S. Department of Energy, Oak Ridge, TN, USA, 2013.

[11] J. Mlakar, J. Štrancar, Overheating in residential passive house: Solution strategies revealed and confirmed through data analysis and simulations, Energy and Buildings 43(6) (2011) 1443-1451.

[12] M.K. Rathod, J. Banerjee, Thermal stability of phase change materials used in latent heat energy storage systems: a review, Renewable and Sustainable Energy Reviews 18 (2013) 246-258.

[13] K. Du, J. Calautit, Z. Wang, Y. Wu, H. Liu, A review of the applications of phase change materials in cooling, heating and power generation in different temperature ranges, Applied Energy 220 (2018) 242-273.

[14] C. Barreneche, M.E. Navarro, A.I. Fernández, L.F. Cabeza, Improvement of the thermal inertia of building materials incorporating PCM. Evaluation in the macroscale, Applied Energy 109 (2013) 428-432.

[15] T. Qian, J. Li, X. Min, W. Guan, Y. Deng, L. Ning, Enhanced thermal conductivity of PEG/diatomite shape-stabilized phase change materials with Ag nanoparticles for thermal energy storage, Journal of Material Chemistry A 3(16) (2015) 8526-8536.

[16] F. Ascione, N. Bianco, R.F. De Masi, F. de' Rossi, G.P. Vanoli, Energy refurbishment of existing buildings through the use of phase change materials: Energy savings and indoor comfort in the cooling season, Applied Energy 113 (2014) 990-1007.

[17] N. Zhu, Z. Ma, S. Wang, Dynamic characteristics and energy performance of buildings using phase change materials: A review, Energy Conversion and Management 50(12) (2009) 3169-3181.

[18] M. Sovetova, S.A. Memon, J. Kim, Thermal performance and energy efficiency of building integrated with PCMs in hot desert climate region, Solar Energy 189 (2019) 357-371.

[19] D. Zhou, C.Y. Zhao, Y. Tian, Review on thermal energy storage with phase change materials (PCMs) in building applications, Applied Energy 92 (2012) 593-605.

[20] N. Soares, J.J. Costa, A.R. Gaspar, P. Santos, Review of passive PCM latent heat thermal energy storage systems towards buildings' energy efficiency, Energy and Buildings 59 (2013) 82-103.

[21] G.P. Panayiotou, S.A. Kalogirou, S.A. Tassou, Evaluation of the application of Phase Change Materials (PCM) on the envelope of a typical dwelling in the Mediterranean region, Renewable Energy 97 (2016) 24-32.

[22] M.J. Abden, Z. Tao, Z. Pan, L. George, R. Wuhrer, Inclusion of methyl stearate/diatomite composite in gypsum board ceiling for building energy conservation, Applied Energy 259 (2020) Article 114113.

[23] X.W. Sun, Y.X. Zhang, D. Losic, Diatom silica, an emerging biomaterial for energy conversion and storage, Journal of Material Chemistry A 5(19) (2017) 8847-8859.

[24] C.Y. Zhao, W. Lu, Y. Tian, Heat transfer enhancement for thermal energy storage using metal foams embedded within phase change materials (PCMs), Solar Energy 84 (2010) 1402-1412.

[25] K. Lafdi, O. Mesalhy, S. Shaikh, Experimental study on the influence of foam porosity and pore size on the melting of phase change materials, Journal of Applied Physics 102 (2007) 083549.

[26] P. Lv, C. Liu, Z. Rao, Review on clay mineral-based form-stable phase change materials: Preparation, characterization and applications, Renewable and Sustainable Energy Reviews 68 (2017) 707-726.

[27] T.F. Huang, Z. Peng, S.Q. Liao, Y.Y. Luo, Y.Z. Li, Properties of diatomite reinforced NR composites China Rubber Industry 38 (2011) 275–279.

[28] S.L. Hu, J. Lv, F.Y. Lu, Z. Zhang, H.S. Liu, Study on property of diatomite/unsaturated polyester composite, Plastic Science 41 (2013) 42–45.

[29] S.G. Jeong, J. Jeon, O. Chung, S. Kim, S. Kim, Evaluation of PCM/diatomite composites using exfoliated graphite nanoplatelets (xGnP) to improve thermal properties, Journal of Thermal Analysis and Calorimetry 114(2) (2013) 689-698.

[30] M. Zhang, Y. Xu, S.I. Wang, J.Y. Shi, C.Y. Liu, C.Y. Wang, Improvement of wood properties by composite of diatomite and "phenol-melamine-formaldehyde" co-condensed resin, Journal of Forestry Research 24(4) (2013) 741.

[31] A. Sharma, V.V. Tyagi, C. Chen, D. Buddhi, Review on thermal energy storage with phase change materials and applications, Renewable and Sustainable energy reviews 13(2) (2009) 318-345.

[32] A. Pasupathy, R. Velraj, R. Seeniraj, Phase change material-based building architecture for thermal management in residential and commercial establishments, Renewable and Sustainable Energy Reviews 12(1) (2008) 39-64.

[33] H. Mehling, L.F. Cabeza, Heat and cold storage with PCM, Springer2008.

[34] K. Pielichowska, K. Pielichowski, Phase change materials for thermal energy storage, Progress in materials science 65 (2014) 67-123.

[35] S. Jegadheeswaran, S.D. Pohekar, Performance enhancement in latent heat thermal storage system: A review, Renewable and Sustainable Energy Reviews 13(9) (2009) 2225-2244.

[36] A. Abhat, Low temperature latent heat thermal energy storage: heat storage materials, Solar energy 30(4) (1983) 313-332.

[37] F. Souayfane, F. Fardoun, P.-H. Biwole, Phase change materials (PCM) for cooling applications in buildings: A review, Energy and Buildings 129 (2016) 396-431.

[38] S.A. Memon, Phase change materials integrated in building walls: A state of the art review, Renewable and Sustainable Energy Reviews 31 (2014) 870-906.

[39] I. Sarbu, C. Sebarchievici, A Comprehensive Review of Thermal Energy Storage, Sustainability 10(2) (2018) 191.

[40] Z. Wang, Z. Tong, Q. Ye, H. Hu, X. Nie, C. Yan, W. Shang, C. Song, J. Wu, J. Wang, Dynamic tuning of optical absorbers for accelerated solar-thermal energy storage, Nature communications 8(1) (2017) Article 1478.

[41] A.S. Fleischer, Thermal energy storage using phase change materials: fundamentals and applications, Springer2015.

[42] R. Sharma, P. Ganesan, V. Tyagi, H. Metselaar, S. Sandaran, Developments in organic solid–liquid phase change materials and their applications in thermal energy storage, Energy Conversion and Management 95 (2015) 193-228.

[43] A. Waqas, Z.U. Din, Phase change material (PCM) storage for free cooling of buildings—a review, Renewable and sustainable energy reviews 18 (2013) 607-625.

[44] S. Kahwaji, M.B. Johnson, A.C. Kheirabadi, D. Groulx, M.A. White, Fatty acids and related phase change materials for reliable thermal energy storage at moderate temperatures, Solar Energy Materials and Solar Cells 167 (2017) 109-120.

[45] G. Alva, L. Liu, X. Huang, G. Fang, Thermal energy storage materials and systems for solar energy applications, Renewable and Sustainable Energy Reviews 68 (2017) 693-706.

[46] J.P. da Cunha, P. Eames, Thermal energy storage for low and medium temperature applications using phase change materials–a review, Applied Energy 177 (2016) 227-238.

[47] X. Huang, G. Alva, Y. Jia, G. Fang, Morphological characterization and applications of phase change materials in thermal energy storage: A review, Renewable and Sustainable Energy Reviews 72 (2017) 128-145.

[48] J. Pereira da Cunha, P. Eames, Thermal energy storage for low and medium temperature applications using phase change materials – A review, Applied Energy 177 (2016) 227-238.

[49] A. Solé, H. Neumann, S. Niedermaier, I. Martorell, P. Schossig, L.F. Cabeza, Stability of sugar alcohols as PCM for thermal energy storage, Solar Energy Materials and Solar Cells 126 (2014) 125-134.

[50] S.N. Gunasekara, R. Pan, J.N. Chiu, V. Martin, Polyols as phase change materials for surplus thermal energy storage, Applied Energy 162 (2016) 1439-1452.

[51] Y. Kang, S.G. Jeong, S. Wi, S. Kim, Energy efficient Bio-based PCM with silica fume composites to apply in concrete for energy saving in buildings, Solar Energy Materials and Solar Cells 143 (2015) 430-434.

[52] J. Kosny, E. Kossecka, A. Brzezinski, A. Tleoubaev, D. Yarbrough, Dynamic thermal performance analysis of fiber insulations containing bio-based phase change materials (PCMs), Energy and Buildings 52 (2012) 122-131.

[53] S.A. Mohamed, F.A. Al-Sulaiman, N.I. Ibrahim, M.H. Zahir, A. Al-Ahmed, R. Saidur, B. Yılbaş, A. Sahin, A review on current status and challenges of inorganic phase change materials for thermal energy storage systems, Renewable and Sustainable Energy Reviews 70 (2017) 1072-1089.

[54] L.F. Cabeza, G. Svensson, S. Hiebler, H. Mehling, Thermal performance of sodium acetate trihydrate thickened with different materials as phase change energy storage material, Applied Thermal Engineering 23(13) (2003) 1697-1704.

[55] S. Khare, M. Dell'Amico, C. Knight, S. McGarry, Selection of materials for high temperature latent heat energy storage, Solar Energy Materials and Solar Cells 107 (2012) 20-27.

[56] H. Ge, H. Li, S. Mei, J. Liu, Low melting point liquid metal as a new class of phase change material: An emerging frontier in energy area, Renewable and Sustainable Energy Reviews 21 (2013) 331-346.

[57] T.-C. Ling, C.-S. Poon, Use of phase change materials for thermal energy storage in concrete: An overview, Construction and Building Materials 46 (2013) 55-62.

[58] D.W. Hawes, D. Banu, D. Feldman, Latent heat storage in concrete, Solar Energy Materials 19(3) (1989) 335-348.

[59] H. Cui, W. Tang, Q. Qin, F. Xing, W. Liao, H. Wen, Development of structural-functional integrated energy storage concrete with innovative macro-encapsulated PCM by hollow steel ball, Applied Energy 185 (2017) 107-118.

[60] Q. Al-Yasiri, M. Szabó, Influential aspects on melting and solidification of PCM energy storage containers in building envelope applications, International Journal of Green Energy 18(9) (2021) 966-986.

[61] A. Adesina, Use of phase change materials in concrete: current challenges, Renewable Energy Environmental Sustainability 4 (2019) Article 9.

[62] S. Ramakrishnan, J. Sanjayan, X. Wang, M. Alam, J. Wilson, A novel paraffin/expanded perlite composite phase change material for prevention of PCM leakage in cementitious composites, Applied Energy 157 (2015) 85-94.

[63] D. Wu, W. Wen, S. Chen, H. Zhang, Preparation and properties of a novel form-stable phase change material based on a gelator, Journal of Materials Chemistry A 3(6) (2015) 2589-2600.

[64] A. Sivanathan, Q. Dou, Y. Wang, Y. Li, J. Corker, Y. Zhou, M. Fan, Phase change materials for building construction: An overview of nano-/micro-encapsulation, Nanotechnology Reviews 9(1) (2020) 896-921.

[65] M. Delgado, A. Lázaro, C. Peñalosa, B. Zalba, Experimental analysis of the influence of microcapsule mass fraction on the thermal and rheological behavior of a PCM slurry, Applied Thermal Engineering 63(1) (2014) 11-22.

[66] C.J. Ho, C.R. Siao, W.M. Yan, Thermal energy storage characteristics in an enclosure packed with MEPCM particles: An experimental and numerical study, International Journal of Heat and Mass Transfer 73 (2014) 88-96.

[67] A. Jamekhorshid, S. Sadrameli, M. Farid, A review of microencapsulation methods of phase change materials (PCMs) as a thermal energy storage (TES) medium, Renewable and Sustainable Energy Reviews 31 (2014) 531-542.

[68] C. Liu, Z. Rao, J. Zhao, Y. Huo, Y. Li, Review on nanoencapsulated phase change materials: Preparation, characterization and heat transfer enhancement, Nano Energy 13 (2015) 814-826.

[69] A.F. Regin, S.C. Solanki, J.S. Saini, Heat transfer characteristics of thermal energy storage system using PCM capsules: A review, Renewable and Sustainable Energy Reviews 12(9) (2008) 2438-2458.

[70] M. Kenisarin, K. Mahkamov, Solar energy storage using phase change materials, Renewable and Sustainable Energy Reviews 11(9) (2007) 1913-1965.

[71] V.A.A. Raj, R. Velraj, Review on free cooling of buildings using phase change materials, Renewable and Sustainable Energy Reviews 14(9) (2010) 2819-2829.

[72] B. Zalba, J.M. Marín, L.F. Cabeza, H. Mehling, Free-cooling of buildings with phase change materials, International Journal of Refrigeration 27(8) (2004) 839-849.

[73] V.V. Tyagi, S.C. Kaushik, S.K. Tyagi, T. Akiyama, Development of phase change materials based microencapsulated technology for buildings: A review, Renewable and Sustainable Energy Reviews 15(2) (2011) 1373-1391.

[74] J. Giro-Paloma, M. Martínez, L.F. Cabeza, A.I. Fernández, Types, methods, techniques, and applications for microencapsulated phase change materials (MPCM): A review, Renewable and Sustainable Energy Reviews 53 (2016) 1059-1075.

[75] Z. Chen, G. Fang, Preparation and heat transfer characteristics of microencapsulated phase change material slurry: A review, Renewable and Sustainable Energy Reviews 15(9) (2011) 4624-4632.

[76] Y. Yamagishi, T. Sugeno, T. Ishige, H. Takeuchi, A.T. Pyatenko, An evaluation of microencapsulated PCM for use in cold energy transportation medium, Institute of Electrical and Electronics Engineers, Piscataway, NJ (United States), Proceedings of the 31st Intersociety Energy Conversion Engineering Conference 1996.

[77] Z. Rao, S. Wang, F. Peng, Self diffusion of the nano-encapsulated phase change materials: A molecular dynamics study, Applied Energy 100 (2012) 303-308.

[78] Z.-H. Chen, F. Yu, X.-R. Zeng, Z.-G. Zhang, Preparation, characterization and thermal properties of nanocapsules containing phase change material n-dodecanol by miniemulsion polymerization with polymerizable emulsifier, Applied Energy 91(1) (2012) 7-12.

[79] E.M. Shchukina, M. Graham, Z. Zheng, D.G. Shchukin, Nanoencapsulation of phase change materials for advanced thermal energy storage systems, Chemical Society Reviews 47(11) (2018) 4156-4175.

[80] G.E. Fonseca, T.F. McKenna, M.A. Dubé, Miniemulsion vs. conventional emulsion polymerization for pressure-sensitive adhesives production, Chemical Engineering Science 65(9) (2010) 2797-2810.

[81] Z. Han, F. Cao, B. Yang, Synthesis and thermal characterization of phase-changeable indium/polyalphaolefin nanofluids, Applied Physics Letters 92(24) (2008) 243104.

[82] H. Inaba, P. Tu, Evaluation of thermophysical characteristics on shape-stabilized paraffin as a solid-liquid phase change material, Heat and Mass Transfer 32(4) (1997) 307-312.

[83] A. Fallahi, G. Guldentops, M. Tao, S. Granados-Focil, S. Van Dessel, Review on solid-solid phase change materials for thermal energy storage: Molecular structure and thermal properties, Applied Thermal Engineering 127 (2017) 1427-1441.

[84] Y.P. Zhang, K.P. Lin, R. Yang, H.F. Di, Y. Jiang, Preparation, thermal performance and application of shape-stabilized PCM in energy efficient buildings, Energy and Buildings 38(10) (2006) 1262-1269.

[85] G. Zhou, Y. Zhang, K. Lin, W. Xiao, Thermal analysis of a direct-gain room with shape-stabilized PCM plates, Renewable Energy 33(6) (2008) 1228-1236.

[86] D. Zhang, J. Zhou, K. Wu, Z. Li, Granular phase changing composites for thermal energy storage, Solar Energy 78(3) (2005) 471-480.

[87] C.Y. Zhao, W. Lu, Y. Tian, Heat transfer enhancement for thermal energy storage using metal foams embedded within phase change materials (PCMs), Solar Energy 84(8) (2010) 1402-1412.

[88] R. Velraj, R.V. Seeniraj, B. Hafner, C. Faber, K. Schwarzer, Heat transfer enhancement in a latent heat storage system, Solar Energy (65) (1999) 171-180.

[89] L.F. Cabeza, A. Castell, C. Barreneche, A. de Gracia, A.I. Fernández, Materials used as PCM in thermal energy storage in buildings: A review, Renewable and Sustainable Energy Reviews 15 (2011) 1675-1695.

[90] L. Shilei, F. Guohui, Z. Neng, D. Li, Experimental study and evaluation of latent heat storage in phase change materials wallboards, Energy & Buildings 39(10) (2007) 1088-1091.

[91] X. Wang, Y. Zhang, W. Xiao, R. Zeng, Q. Zhang, H. Di, Review on thermal performance of phase change energy storage building envelope, Science Bulletin 54(6) (2009) 920-928.

[92] W.A. Miller, J. Kosny, A. Zaltash, Dynamic thermally-disconnected building envelopes-a new paradigm for walls and roofs in low energy buildings, Thermal Performance of the Exterior Envelopes of Whole Buildings XI International Conference, EE USDOE - Office of Energy Efficiency and Renewable Energy (EE), United States, 2010.

[93] A.K. Athienitis, C. Liu, D. Hawes, D. Banu, D. Feldman, Investigation of the thermal performance of a passive solar test-room with wall latent heat storage, Building and Environment 32(5) (1997) 405-410.

[94] M. Zhang, M.A. Medina, J.B. King, Development of a thermally enhanced frame wall with phase-change materials for on-peak air conditioning demand reduction and energy savings in residential buildings, International Journal of Energy Research 29(9) (2005) 795-809.

[95] F. Kuznik, J. Virgone, Experimental assessment of a phase change material for wall building use, Applied Energy 86(10) (2009) 2038-2046.

[96] F. Kuznik, J. Virgone, Experimental investigation of wallboard containing phase change material: Data for validation of numerical modeling, Energy & Buildings 41(5) (2009) 561-570.

[97] G. Evola, L. Marletta, F. Sicurella, A methodology for investigating the effectiveness of PCM wallboards for summer thermal comfort in buildings, Building and Environment 59 (2013) 517-527.

[98] I. Mandilaras, M. Stamatiadou, D. Katsourinis, G. Zannis, M. Founti, Experimental thermal characterization of a Mediterranean residential building with PCM gypsum board walls, Building and Environment 61 (2013) 93-103.

[99] K. Biswas, J. Lu, P. Soroushian, S. Shrestha, Combined experimental and numerical evaluation of a prototype nano-PCM enhanced wallboard, Applied Energy 131 (2014) 517-529.

[100] X. Kong, C. Yao, P. Jie, Y. Liu, C. Qi, X. Rong, Development and thermal performance of an expanded perlite-based phase change material wallboard for passive cooling in building, Energy & Buildings 152 (2017) 547-557.

[101] J. Xie, W. Wang, J. Liu, S. Pan, Thermal performance analysis of PCM wallboards for building application based on numerical simulation, Solar Energy 162 (2018) 533-540.

[102] C. Yao, X. Kong, Y. Li, Y. Du, C. Qi, Numerical and experimental research of cold storage for a novel expanded perlite-based shape-stabilized phase change material wallboard used in building, Energy Conversion and Management 155 (2018) 20-31.

[103] F. Kuznik, J. Virgone, J. Noel, Optimization of a phase change material wallboard for building use, Applied Thermal Engineering 28(11) (2008) 1291-1298.

[104] F. Kuznik, J. Virgone, K. Johannes, In-situ study of thermal comfort enhancement in a renovated building equipped with phase change material wallboard, Renewable Energy 36(5) (2011) 1458-1462.

[105] X. Jin, M.A. Medina, X. Zhang, On the placement of a phase change material thermal shield within the cavity of buildings walls for heat transfer rate reduction, Energy 73 (2014) 780-786.

[106] T. Zhou, J. Darkwa, G. Kokogiannakis, Thermal evaluation of laminated composite phase change material gypsum board under dynamic conditions, Renewable Energy 78 (2015) 448-456.

[107] S.-G. Jeong, S.J. Chang, S. Wi, J. Lee, S. Kim, Energy performance evaluation of heat-storage gypsum board with hybrid SSPCM composite, Journal of Industrial and Engineering Chemistry 51 (2017) 237-243.

[108] S.P. Singh, V. Bhat, Performance evaluation of dual phase change material gypsum board for the reduction of temperature swings in a building prototype in composite climate, Energy & Buildings 159 (2018) 191-200.

[109] J. Kośny, D. Yarbrough, W. Miller, S. Shrestha, E. Kossecka, E. Lee, Numerical and experimental analysis of building envelopes containing blown fiberglass insulation thermally enhanced with phase change material (PCM) In: Therm. perform. exter. envel. whole Build. XI International Conference, 2010.

[110] D.S. Kapetanakis, E. Mangina, D.P. Finn, Input variable selection for thermal load predictive models of commercial buildings, Energy and Buildings 137 (2017) 13-26.

[111] V. Shabunko, C.M. Lim, S. Mathew, EnergyPlus models for the benchmarking of residential buildings in Brunei Darussalam, Energy and Buildings 169 (2018) 507-516.

[112] D.B. Crawley, J.W. Hand, M. Kummert, B.T. Griffith, Contrasting the capabilities of building energy performance simulation programs, Building and Environment 43(4) (2008) 661-673.

[113] D.B. Crawley, C.O. Pedersen, L.K. Lawrie, F.C. Winkelmann, EnergyPlus: Energy Simulation Program, ASHRAE 42 (2000) 49-56.

[114] S.A. Klein, TRNSYS 17: A transient system simulation program. <www.trnsys.com/>, 2010).

[115] I. Beausoleil-Morrison, F. Macdonald, M. Kummert, T. McDowell, R. Jost, Co-simulation between ESP-r and TRNSYS, Journal of Building Performance Simulation 7(2) (2014) 133-151.

[116] P.G. Ellis, P.A. Torcellini, D. Crawley, Simulation of Energy Management Systems in EnergyPlus, USDOE, United States.

[117] <https://github.com/nrgsim/EnergyPlus-Fortran/>, (accessed Nov. 15.2018).

[118] P. Zhang, X. Xiao, Z.W. Ma, A review of the composite phase change materials: Fabrication, characterization, mathematical modeling and application to performance enhancement, Applied Energy 165 (2016) 472-510.

[119] E. Jud Sierra, S.A. Miller, A.R. Sakulich, K. MacKenzie, M.W. Barsoum, Pozzolanic Activity of Diatomaceous Earth, Journal of the American Ceramic Society 93(10) (2010) 3406-3410.

[120] P.C.R.A. Abrão, F.A. Cardoso, V.M. John, Evaluation of Portland pozzolan blended cements containing diatomaceous earth, Cerâmica 65 (2019) 75-86.

[121] B. Xu, Z. Li, Paraffin/diatomite composite phase change material incorporated cement-based composite for thermal energy storage, Applied Energy 105 (2013) 229-237.

[122] K.S.W. Sing, D.H. Everett, R.A.W. Haul, L. Moscou, R.A. Pieroti, J. Rouquerol, T. Siemieniewska, Reporting physisorption data for gas/solid systems, Pure and Applied Chemistry 57 (1985) 603-619.

[123] J. Yang, G.Q. Qi, Y. Liu, R.Y. Bao, Z.Y. Liu, W. Yang, B.H. Xie, M.B. Yang, Hybrid graphene aerogels/phase change material composites: Thermal conductivity, shape-stabilization and light-to-thermal energy storage, Carbon 100 (2016) 693-702.

[124] A. Nielsen, M. Morelli, Measured temperature and moisture conditions in the roof attic of a one-and-a-half story house, Energy Procedia 132 (2017) 789-794.

[125] W. Liang, P. Chen, H. Sun, Z. Zhu, A. Li, Innovative spongy attapulgite loaded with n-carboxylic acids as composite phase change materials for thermal energy storage, RSC Advances 4(73) (2014).

[126] C. Wang, L. Feng, H. Yang, G. Xin, W. Li, J. Zheng, W. Tian, X. Li, Graphene oxide stabilized polyethylene glycol for heat storage, Phys Chem Chem Phys 14(38) (2012) 13233-8.

[127] L. Zhang, J. Zhu, W. Zhou, J. Wang, Y. Wang, Thermal and electrical conductivity enhancement of graphite nanoplatelets on form-stable polyethylene glycol/polymethyl methacrylate composite phase change materials, Energy 39(1) (2012) 294-302.

[128] S. Karaman, A. Karaipekli, A. Sarı, A. Biçer, Polyethylene glycol (PEG)/diatomite composite as a novel form-stable phase change material for thermal energy storage, Solar Energy Materials and Solar Cells 95(7) (2011) 1647-1653.

[129] S.G. Jeong, J. Jeon, J.H. Lee, S. Kim, Optimal preparation of PCM/diatomite composites for enhancing thermal properties, International Journal of Heat and Mass Transfer 62 (2013) 711-717.

[130] S. Song, L. Dong, Y. Zhang, S. Chen, Q. Li, Y. Guo, S. Deng, S. Si, C. Xiong, Lauric acid/intercalated kaolinite as form-stable phase change material for thermal energy storage, Energy 76 (2014) 385-389.

[131] T. Wei, B. Zheng, J. Liu, Y. Gao, W. Guo, Structures and thermal properties of fatty acid/expanded perlite composites as form-stable phase change materials, Energy and Buildings 68 (2014) 587-592.

[132] B. Xu, H. Ma, Z. Lu, Z. Li, Paraffin/expanded vermiculite composite phase change material as aggregate for developing lightweight thermal energy storage cement-based composites, Applied Energy 160 (2015) 358-367.

[133] A. Karaipekli, A. Sarı, Development and thermal performance of pumice/organic PCM/gypsum composite plasters for thermal energy storage in buildings, Solar Energy Materials and Solar Cells 149 (2016) 19-28.

[134] A. Sarı, Thermal energy storage characteristics of bentonite-based composite PCMs with enhanced thermal conductivity as novel thermal storage building materials, Energy Conversion and Management 117 (2016) 132-141.

[135] R. Wen, X. Zhang, Z. Huang, M. Fang, Y. Liu, X. Wu, X. Min, W. Gao, S. Huang, Preparation and thermal properties of fatty acid/diatomite form-stable composite phase change material for thermal energy storage, Solar Energy Materials and Solar Cells 178 (2018) 273-279.

[136] J. Han, S. Liu, Myristic acid-hybridized diatomite composite as a shape-stabilized phase change material for thermal energy storage, RSC Advances 7(36) (2017) 22170-22177.

[137] T. Qian, J. Li, X. Min, W. Guan, Y. Deng, L. Ning, Enhanced thermal conductivity of PEG/diatomite shape-stabilized phase change materials with Ag nanoparticles for thermal energy storage, Journal of Materials Chemistry A 3(16) (2015) 8526-8536.

[138] B. Xu, Z. Li, Performance of novel thermal energy storage engineered cementitious composites incorporating a paraffin/diatomite composite phase change material, Applied Energy 121 (2014) 114-122.

[139] N. Soares, A.R. Gaspar, P. Santos, J.J. Costa, Experimental evaluation of the heat transfer through small PCM-based thermal energy storage units for building applications, Energy and Buildings 116 (2016) 18-34.

[140] X. Li, J.G. Sanjayan, J.L. Wilson, Fabrication and stability of form-stable diatomite/paraffin phase change material composites, Energy and Buildings 76 (2014) 284-294.

[141] J. Zhang, X. Guan, X. Song, H. Hou, Z. Yang, J. Zhu, Preparation and properties of gypsum based energy storage materials with capric acid–palmitic acid/expanded perlite composite PCM, Energy and Buildings 92 (2015) 155-160.

[142] L. Fu, Q. Wang, R. Ye, X. Fang, Z. Zhang, A calcium chloride hexahydrate/expanded perlite composite with good heat storage and insulation properties for building energy conservation, Renewable Energy 114 (2017) 733-743.

[143] S. Hasanabadi, S.M. Sadrameli, H. Soheili, H. Moharrami, M.M. Heyhat, A cost-effective form-stable PCM composite with modified paraffin and expanded perlite for thermal energy storage in concrete, Journal of Thermal Analysis and Calorimetry 136(3) (2018) 1201-1216.

[144] S. Wi, S. Yang, J.H. Park, S.J. Chang, S. Kim, Climatic cycling assessment of red clay/perlite and vermiculite composite PCM for improving thermal inertia in buildings, Building and Environment 167 (2020) Article 106464.

[145] D. Li, Y. Wu, G. Zhang, M. Arıcı, C. Liu, F. Wang, Influence of glazed roof containing phase change material on indoor thermal environment and energy consumption, Applied Energy 222 (2018) 343-350.

[146] J. Le Dréau, P. Heiselberg, R.L. Jensen, Experimental investigation of convective heat transfer during night cooling with different ventilation systems and surface emissivities, Energy and Buildings 61 (2013) 308-317.

[147] S.R. Delaforce, E.R. Hitchin, D.M.T. Watson, Convective heat transfer at internal surfaces, Buildiny and Environment 28 (1993) 211-220.

[148] J. Li, X. Li, N. Wang, Y. Hu, R. Feng, Experimental research on indoor thermal environment of new rural residence with active solar water heating system and external wall insulation, Applied Thermal Engineering 95 (2016) 35-41.

[149] J. Yu, C. Yang, L. Tian, D. Liao, A study on optimum insulation thicknesses of external walls in hot summer and cold winter zone of China, Applied Energy 86(11) (2009) 2520-2529.

[150] E. Cuce, P.M. Cuce, C.J. Wood, S.B. Riffat, Optimizing insulation thickness and analysing environmental impacts of aerogel-based thermal superinsulation in buildings, Energy and Buildings 77 (2014) 28-39.

[151] N. Daouas, Z. Hassen, H.B. Aissia, Analytical periodic solution for the study of thermal performance and optimum insulation thickness of building walls in Tunisia, Applied Thermal Engineering 30(4) (2010) 319-326.

[152] A. Karaipekli, A. Sarı, Preparation and characterization of fatty acid ester/building material composites for thermal energy storage in buildings, Energy and Buildings 43(8) (2011) 1952-1959.

[153] A. Sarı, A. Karaipekli, K. Kaygusuz, Capric acid and stearic acid mixture impregnated with gypsum wallboard for low-temperature latent heat thermal energy storage, International Journal of Energy Research 32(2) (2008) 154-160.

[154] A. Karaipekli, A. Sarı, A. Biçer, Thermal regulating performance of gypsum/(C18–C24) composite phase change material (CPCM) for building energy storage applications, Applied Thermal Engineering 107 (2016) 55-62.

[155] A. Waqas, Z. Ud Din, Phase change material (PCM) storage for free cooling of buildings—A review, Renewable and Sustainable Energy Reviews 18 (2013) 607-625.

[156] E. Rodriguez-Ubinas, L. Ruiz-Valero, S. Vega, J. Neila, Applications of Phase Change Material in highly energy-efficient houses, Energy and Buildings 50 (2012) 49-62.

[157] Integrated Environmental Solutions Limited. Table 6 Thermal Conductivity, Specific Heat Capacity and Density. <https://help.iesve.com/ve2018/table_6_thermal_conductivity__specific_heat_capacity_and_density.htm#>, (accessed 13 September.2020).

[158] ASTM A514 Steel, grade P, plate thickness ≤ 19 mm <http://www.matweb.com/search/DataSheet.aspx?MatGUID=399f2dcfb1774f15a27c55978e2714f8>, (accessed 13 September.2020).

[159] J.D. Afroze, M.J. Abden, M.A. Islam, An efficient method to prepare magnetic hydroxyapatite-functionalized multi-walled carbon nanotubes nanocomposite for bone defects, Mater Sci Eng C Mater Biol Appl 86 (2018) 95-102.

[160] X. Kong, S. Lu, J. Huang, Z. Cai, S. Wei, Experimental research on the use of phase change materials in perforated brick rooms for cooling storage, Energy and Buildings 62 (2013) 597-604.

[161] L.F. Cabeza, C. Castellón, M. Nogués, M. Medrano, R. Leppers, O. Zubillaga, Use of microencapsulated PCM in concrete walls for energy savings, Energy and Buildings 39(2) (2007) 113-119.

[162] A.K. Athienitis, C. Liu, D. Hawes, D. Banu, D. Feldman, Investigation of the thermal performance of a passive solar test-room with wall latent heat storage, Building and Environment 32 (1997) 405-410.

[163] G. Zhou, Y. Zhang, X. Wang, K. Lin, W. Xiao, An assessment of mixed type PCM-gypsum and shape-stabilized PCM plates in a building for passive solar heating, Solar Energy 81(11) (2007) 1351-1360.

[164] M. Medina, J. King, M. Zhang, On the heat transfer rate reduction of structural insulated panels (SIPs) outfitted with phase change materials (PCMs), Energy 33(4) (2008) 667-678.

[165] G. Zhou, Y. Yang, X. Wang, S. Zhou, Numerical analysis of effect of shape-stabilized phase change material plates in a building combined with night ventilation, Applied Energy 86(1) (2009) 52-59.

[166] A. Castell, I. Martorell, M. Medrano, G. Pérez, L.F. Cabeza, Experimental study of using PCM in brick constructive solutions for passive cooling, Energy and Buildings 42(4) (2010) 534-540.

[167] X. Kong, C. Yao, P. Jie, Y. Liu, C. Qi, X. Rong, Development and thermal performance of an expanded perlite-based phase change material wallboard for passive cooling in building, Energy and Buildings 152 (2017) 547-557.

[168] L.F. Cabeza, L. Navarro, A.L. Pisello, L. Olivieri, C. Bartolomé, J. Sánchez, S. Álvarez, J.A. Tenorio, Behaviour of a concrete wall containing micro-encapsulated PCM after a decade of its construction, Solar Energy 200 (2020) 108-113.

[169] M.M. El Idi, M. Karkri, Heating and cooling conditions effects on the kinetic of phase change of PCM embedded in metal foam, Case Studies in Thermal Engineering 21 (2020) Article 100716.

[170] H. Jouhara, A. Żabnieńska-Góra, N. Khordehgah, D. Ahmad, T. Lipinski, Latent thermal energy storage technologies and applications: A review, International Journal of Thermofluids 5-6 (2020) Article 100039.

[171] P.C. Tabares-Velasco, C. Christensen, M. Bianchi, Verification and validation of EnergyPlus phase change material model for opaque wall assemblies, Building and Environment 54 (2012) 186-196.

[172] S. Jaber, S. Ajib, Thermal and economic windows design for different climate zones, Energy and Buildings 43(11) (2011) 3208-3215.

[173] C.O. Pedersen, Advanced zone simulation in EnergyPlus: incorporation of variable properties and phase change material (PCM) capability, Proceedings: Building Simulation, 2007, pp. 1341-1345.

[174] F. Souayfane, P.H. Biwole, F. Fardoun, P. Achard, Energy performance and economic analysis of a TIM-PCM wall under different climates, Energy 169 (2019) 1274-1291.

[175] ASHRAE Guideline 14-2002: Measurement of Energy and Demand Savings, ASHRAE, Atlanta (USA)

[176] R. Sirmelis, R. Vanaga, R. Freimanis, A. Blumberga, Solar Facade Module for Nearly Zero Energy Building. Optimization Strategies, Environmental and Climate Technologies 23(3) (2019) 170–181.

[177] S. Sultan, J. Hirschey, K.R. Gluesenkamp, S. Graham, Analysis of Residential Time-of-Use Utility Rate Structures and Economic Implications for Thermal Energy Storage, 6th International High Performance Buildings Conference at Purdue, 2021.

[178] Australian Building Codes Board, National Construction Code, Standards Australia, Canberra, Australia, 2015.

[179] A. Albury, Why thermal conductivity matters — and gel based products fail. <https://soothsoft.com/technology/thermal-conductivity-matters/>, 2013 (accessed August 25.2021).

[180] A. Fallahi, H. Durschlag, D. Elliott, J. Hartsough, N. Shukla, J. Kosny, Internal roof and attic thermal radiation control retrofit strategies for cooling-dominated climates, National Renewable Energy Lab.(NREL), Golden, CO (United States), 2013.

[181] L. Zhu, Y. Yang, S. Chen, Y. Sun, Numerical study on the thermal performance of lightweight temporary building integrated with phase change materials, Applied Thermal Engineering 138 (2018) 35-47.

[182] V.D. Cao, T.Q. Bui, A.-L. Kjøniksen, Thermal analysis of multi-layer walls containing geopolymer concrete and phase change materials for building applications, Energy 186 (2019) Article 115792.

[183] R. Ye, W. Lin, X. Fang, Z. Zhang, A numerical study of building integrated with $CaCl_2 \cdot 6H_2O$/expanded graphite composite phase change material, Applied Thermal Engineering 126 (2017) 480-488.

[184] Q. Wang, R. Wu, Y. Wu, C.Y. Zhao, Parametric analysis of using PCM walls for heating loads reduction, Energy and Buildings 172 (2018) 328-336.

[185] V.D. Cao, S. Pilehvar, C. Salas-Bringas, A.M. Szczotok, T.Q. Bui, M. Carmona, J.F. Rodriguez, A.-L. Kjøniksen, Thermal analysis of geopolymer concrete walls containing microencapsulated phase change materials for building applications, Solar Energy 178 (2019) 295-307.

[186] G. Peng, G. Dou, Y. Hu, Y. Sun, Z. Chen, Phase change material (PCM) microcapsules for thermal energy storage, Advances in polymer technology (2020) Article ID 9490873.

[187] J. Lee, S. Wi, B.Y. Yun, S. Yang, J.H. Park, S. Kim, Development and evaluation of gypsum/shape-stabilization phase change materials using large-capacity vacuum impregnator for thermal energy storage, Applied Energy 241 (2019) 278-290.

[188] Gypsum Association. Gypsum board typical mechanical and physical properties, GA-235, Washington, DC, USA, 2019.

[189] H. Zhang, Building Materials in Civil Engineering, Woodhead Publishing, 2011.

[190] X. Wang, D. Chen, Z. Ren, Assessment of climate change impact on residential building heating and cooling energy requirement in Australia, Building and Environment 45(7) (2010) 1663-1682.

[191] S. Ramakrishnan, X. Wang, M. Alam, J. Sanjayan, J. Wilson, Parametric analysis for performance enhancement of phase change materials in naturally ventilated buildings, Energy and Buildings 124 (2016) 35-45.

[192] J.S. Sage-Lauck, D.J. Sailor, Evaluation of phase change materials for improving thermal comfort in a super-insulated residential building, Energy and Buildings 79 (2014) 32-40.

[193] H. Jamil, M. Alam, J. Sanjayan, J. Wilson, Investigation of PCM as retrofitting option to enhance occupant thermal comfort in a modern residential building, Energy and Buildings 133 (2016) 217-229.

[194] N.M. Mateus, A. Pinto, G.C.d. Graça, Validation of EnergyPlus thermal simulation of a double skin naturally and mechanically ventilated test cell, Energy and Buildings 75 (2014) 511-522.

[195] C.L. Zhuang, A.Z. Deng, Y. Chen, S.B. Li, H.Y. Zhang, G.Z. Fan, Validation of veracity on simulating the indoor temperature in PCM light weight building by EnergyPlus, Life system modeling and intelligent computing, Springer, 2010, pp. 486-496.

[196] P.C. Tabares-Velasco, C. Christensen, M. Bianchi, Validation methodology to allow simulated peak reduction and energy performance analysis of residential building envelope with phase change materials, National Renewable Energy Lab, Golden, CO, USA, 2012.

[197] EnergyPlus Documentation, Engineering Reference – EnergyPlus 8.5. The Reference to EnergyPlus Calculation, 2016.

[198] M. Alam, H. Jamil, J. Sanjayan, J. Wilson, Energy saving potential of phase change materials in major Australian cities, Energy and Buildings 78 (2014) 192-201.

[199] M. Alam, P.X.W. Zou, J. Sanjayan, S. Ramakrishnan, Energy saving performance assessment and lessons learned from the operation of an active phase change materials system in a multi-storey building in Melbourne, Applied Energy 238 (2019) 1582-1595.

[200] A. de Gracia, Dynamic building envelope with PCM for cooling purposes – Proof of concept, Applied Energy 235 (2019) 1245-1253.

[201] Centre for International Economics. Energy efficiency: building code star ratings, Sydney & Canberra, Australia, 2010.

[202] Z. Ren, P. Paevere, C. McNamara, A local-community-level, physically-based model of end-use energy consumption by Australian housing stock, Energy Policy 49 (2012) 586-596.

[203] Australian National Wide House Energy Rating Scheme. How NatHERS star ratings are calculated. <https://www.nathers.gov.au/owners-and-builders/how-nathers-star-ratings-are-calculated>, 2019 (accessed 13 September.2020).

[204] Ö.A. Dombaycı, M. Gölcü, Y. Pancar, Optimization of insulation thickness for external walls using different energy-sources, Applied Energy 83(9) (2006) 921-928.

[205] F. Sicurella, G. Evola, E. Wurtz, A statistical approach for the evaluation of thermal and visual comfort in free-running buildings, Energy and Buildings 47 (2012) 402-410.

[206] B.W. Olesen, H. Wang, O.B. Kazanci, D. Coakley, The effect of room temperature control by air-or operative temperature on thermal comfort and energy use, Proceedings of Building Simulation, 2019, pp. 1-8.

[207] C. Piselli, M. Prabhakar, A. de Gracia, M. Saffari, A.L. Pisello, L.F. Cabeza, Optimal control of natural ventilation as passive cooling strategy for improving the energy performance of building envelope with PCM integration, Renewable Energy 162 (2020) 171-181.

[208] Ö.A. Dombayci, Ö. Atalay, Ş. Güven Acar, E. Yilmaz Ulu, H. Kemal Ozturk, Thermoeconomic method for determination of optimum insulation thickness of external walls for the houses: Case study for Turkey, Sustainable Energy Technologies and Assessments 22 (2017) 1-8.

[209] Australian Government, Department of Industry, Science, Energy and Resources, Electricity generation. <https://www.energy.gov.au/data/electricity-generation>, (accessed 13 September.2020).

[210] National Greenhouse Accounts Factors. <https://www.industry.gov.au/sites/default/files/2020-10/national-greenhouse-accounts-factors-2020.pdf>, 2020 (accessed 27 October 2021.).

[211] P. Maryniak, S. Trück, R. Weron, Carbon pricing and electricity markets — The case of the Australian Clean Energy Bill, Energy Economics 79 (2019) 45-58.

[212] G.A. Florides, S.A. Tassou, S.A. Kalogirou, L.C. Wrobel, Measures used to lower building energy consumption and their cost effectivene, Applied Energy 73 (2002) 299-328.

[213] R. Pacheco, J. Ordóñez, G. Martínez, Energy efficient design of building: A review, Renewable and Sustainable Energy Reviews 16(6) (2012) 3559-3573.

[214] M. Kolokotroni, A. Aronis, Cooling-energy reduction in air-conditioned offices by using night ventilation, Applied Energy 63 (1999) 241-253.

[215] Passive House Institute, Passive House Planning Package (PHPP), Passivhaus Institut, Darmstadt, Germany, 2007.

[216] C. Gibson, 2020 How much does double glazing cost? <https://hipages.com.au/article/how_much_does_double_glazing_cost>, (accessed 25 December.2020).

[217] J. Morrissey, T. Moore, R.E. Horne, Affordable passive solar design in a temperate climate: An experiment in residential building orientation, Renewable Energy 36(2) (2011) 568-577.

[218] F.H. Abanda, L. Byers, An investigation of the impact of building orientation on energy consumption in a domestic building using emerging BIM (Building Information Modelling), Energy 97 (2016) 517-527.

[219] Z.X. Li, A.A.A.A. Al-Rashed, M. Rostamzadeh, R. Kalbasi, A. Shahsavar, M. Afrand, Heat transfer reduction in buildings by embedding phase change material in multi-layer walls: Effects of repositioning, thermophysical properties and thickness of PCM, Energy Conversion and Management 195 (2019) 43-56.

[220] E. Solgi, Z. Hamedani, R. Fernando, B. Mohammad Kari, H. Skates, A parametric study of phase change material behaviour when used with night ventilation in different climatic zones, Building and Environment 147 (2019) 327-336.

[221] M. Ambrose, M. Syme, Air tightness of new Australian residential buildings, Procedia engineering 180 (2017) 33-40.

[222] Bundesministerium fuer Wirtschaft, Verordnung ueber energiesparenden Waermeschutz und energiesparende Anlagentechnik bei Gebaeuden: Energieeinsparverordnung – EnEV (Regulation for energy saving insulation and energy saving installations for buildings), Bonn, Germany, 2007.).

[223] Energy Efficiency and Renewable Energy, Cooling Your Home Naturally, 1994.